AD-A156 156 CERENKOV RADIATION FROM PERIODIC ELECTRON BUNCHES FOR FINITE EMISSION LENGTH IN AIR(U) NAVAL POSTGRADUATE SCHOOL MONTEREY CA M VUJAKLIJA DEC 84 1/2

UNCLASSIFIED F/G 2/0.30 NL

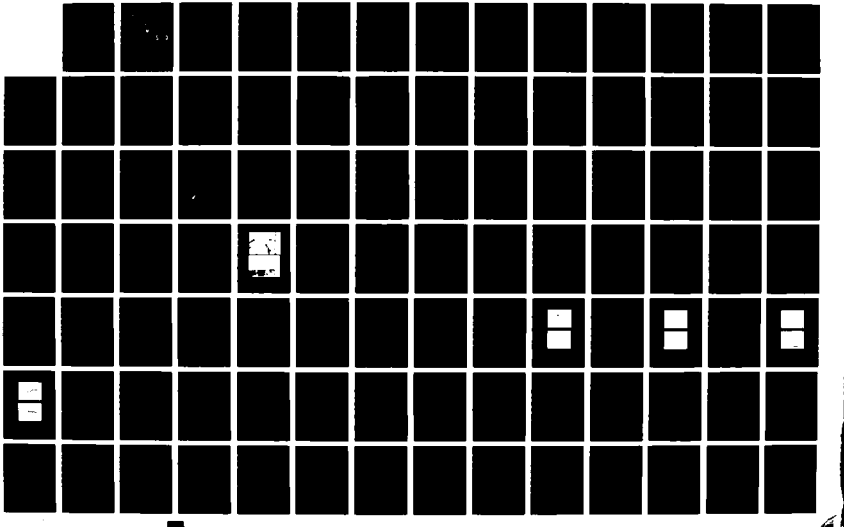

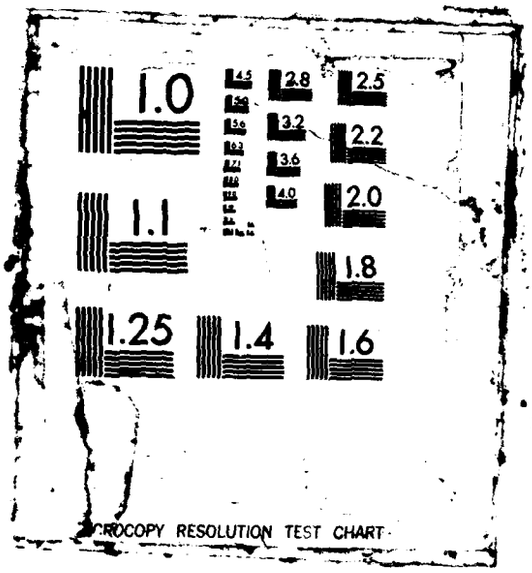
1.0
1.1
1.25
1.4
1.6
2.8
2.5
3.2
2.2
3.6
2.0
4.0
1.8
ROCOPY RESOLUTION TEST CHART

NAVAL POSTGRADUATE SCHOOL
Monterey, California

THESIS

G

CERENKOV RADIATION FROM PERIODIC ELECTRON BUNCHES FOR FINITE EMISSION LENGTH IN AIR

by

Vujaklija Milorad

December 1984

Thesis Advisor: J. R. Neighbours

Approved for public release: Distribution unlimited

UNCLASSIFIED

SECURITY CLASSIFICATION OF THIS PAGE *(When Data Entered)*

REPORT DOCUMENTATION PAGE	READ INSTRUCTIONS BEFORE COMPLETING FORM
1. REPORT NUMBER	2. GOVT ACCESSION NO. AD-A156 156 / 3. RECIPIENT'S CATALOG NUMBER
4. TITLE *(and Subtitle)* Cerenkov Radiation from Periodic Electron Bunches for Finite Emission Length in Air	5. TYPE OF REPORT & PERIOD COVERED Master's Thesis December 1984
	6. PERFORMING ORG. REPORT NUMBER
7. AUTHOR(s) Vujaklija, Milorad	8. CONTRACT OR GRANT NUMBER(s)
9. PERFORMING ORGANIZATION NAME AND ADDRESS Naval Postgraduate School Monterey, California 93943-5100	10. PROGRAM ELEMENT, PROJECT, TASK AREA & WORK UNIT NUMBERS
11. CONTROLLING OFFICE NAME AND ADDRESS Naval Postgraduate School Monterey, California 93943-5100	12. REPORT DATE December 1984
	13. NUMBER OF PAGES 116
14. MONITORING AGENCY NAME & ADDRESS*(if different from Controlling Office)*	15. SECURITY CLASS. *(of this report)* UNCLASSIFIED
	15a. DECLASSIFICATION/DOWNGRADING SCHEDULE

16. DISTRIBUTION STATEMENT *(of this Report)*

Approved for public release; Distribution unlimited

17. DISTRIBUTION STATEMENT *(of the abstract entered in Block 20, if different from Report)*

18. SUPPLEMENTARY NOTES

19. KEY WORDS *(Continue on reverse side if necessary and identify by block number)*

Microwave Cerenkov Radiation

20. ABSTRACT *(Continue on reverse side if necessary and identify by block number)*

The physical mechanism of Cerenkov radiation in air caused by the periodic electron bunches is presented here in a simplified and exact mathematical forms, as well, as some applications and evidence. The experiment is an effort to verify the theoretical prediction of the power increase and fall off with discrete harmonic frequency in the microwave region.

The radiation diagrams and absolute power measurements in the far field

DD FORM 1 JAN 73 1473 EDITION OF 1 NOV 65 IS OBSOLETE

S N 0102-LF-014-6601

UNCLASSIFIED

SECURITY CLASSIFICATION OF THIS PAGE *(When Data Entered)*

for the first four harmonics are provided by the improvements such as: frequency selection by the YIG filter, power amplification by the TWT amplifiers, high sensitivity of the signal detection by the oscilloscope vertical differential amplifier along with the noise reduction and radiation shielding. Suggested experimental method may be expanded to the higher harmonics with appropriate equipment.

The experimental data reveal the unexpected spikes in the radiation diagrams. The absolute power results are reasonably close to the theoretical ones. The experimental method satisfies this Cerenkov experiment and may be improved. Further research may provide usable information for the electron beam monitoring or Cerenkov source at higher microwave frequencies, for which a certain interest exists.

Accession For	
NTIS GRA&I	☒
DTIC TAB	☐
Unannounced	☐
Justification	
By	
Distribution/	
Availability Codes	
Dist	Avail and/or Special
A/1	

Approved for public release; distribution is unlimited.

Cerenkov Radiation from Periodic Electron Bunches for Finite Emission Length in Air

by

Milorad Vujaklija
Lieutenant, Yugoslav Navy
B.S., Naval Academy, Split, 1979

Submitted in partial fulfillment of the requirements for the degree of

MASTER OF SCIENCE IN PHYSICS

from the

NAVAL POSTGRADUATE SCHOOL
December 1984

Author: Vujaklija Milorad
Milorad Vujaklija

Approved by: John R. Neighbours
J. R. Neighbours, Thesis Advisor

Xavier K. Maruyama
X. K. Maruyama, Second Reader

G. E. Schacher
G. E. Schacher, Chairman,
Department of Physics

J. N. Dyer
J. N. Dyer,
Dean of Science and Engineering

ABSTRACT

The physical mechanism of Cerenkov radiation in air caused by the periodic electron bunches is presented here in a simplified and exact mathematical forms, as well, as some applications and evidence. The experiment is an effort to verify the theoretical prediction of the power increase and fall off with discrete harmonic frequency in the microwave region.

The radiation diagrams and absolute power measurements in the far field for the first four harmonics are provided by the improvements, such as: frequency selection by the YIG filter, power amplification by the TWT amplifiers, high sensitivity of the signal detection by the oscilloscope vertical differential amplifier along with the noise reduction and radiation shielding. Suggested experimental method may be expanded to the higher harmonics with appropriate equipment.

The experimental data reveal the unexpected spikes in the radiation diagrams. The absolute power results are reasonably close to the theoretical ones. The experimental method satisfies this Cerenkov experiment and may be improved. Further research may provide usable information for the electron beam monitoring or Cerenkov source at higher microwave frequencies, for which a certain interest exists.

TABLE OF CONTENTS

LIST OF TABLES

LIST OF FIGURES

ACKNOWLEDGEMENTS

I would like to express my gratitude and appreciation to Professor J. Neighbours and Professor X. Maruyama for guidance, advices and corrections throughout this research.

Also, I want to thank Professor J. Knorr and Professor M. Morgan for the equipment and suggestions concerning microwave measurements, as well as, Ms. D. Womble for computer program support, Mr. D. Snyder for the linac operation and many others who contributed before the last page of this paper was written.

At the end, many thanks to my wife Firdeza for her understanding and support during this research and complete study at the Naval Postgraduate School.

Vujaklija Milorad

I. INTRODUCTION TO CERENKOV RADIATION

The discovery, description and application of Cerenkov radiation are briefly introduced here. Physical explanations are simplified and referred to a single charged particle, which is extended for periodic electron bunches in the following chapter.

A. DISCOVERY

One of the very early observations of what was later-on called Cerenkov radiation, was made by Mme Curie in 1910 who observed bluish-white light[1] which appeared from transparent materials placed nearby a radioactive source. Although electromagnetic theory had been sufficiently developed at that time to describe this phenomenon, many years passed before it actually happened. Cerenkov radiation was very weak and usually masked by other effects, so that a more sensitive light detector than a photographic plate was required.

PAVEL ALEXEVICH CERENKOV carried out a series of experiments, between 1934 and 1938 related to the phenomenon. In 1937 ILYA FRANK and IGOR TAMM proposed a satisfactory theory of the radiation. The experimental results and theoretical predictions were in excellent agreement. For the contribution in Cerenkov radiation discovery and explanation, Frank and Tamm won NOBEL PRIZE in 1958. Complete description of Cerenkov Radiation, as well as exact mathematical treatment is done in [Ref. 1].

---

[1]In this text, 'light' is Cerenkov electromagnetic radiation, called simply, radiation.

The term $i\omega_j/c$ in equation 2.19 leads to the time derivative '$\dot{J}$'. According to radiation theory this has the meaning of radiation by an accelerated charge (in this case, by dipoles of the medium) ;

5. The expressions above for '$\vec{E}$' and '$\vec{B}$' give the ratio $|\vec{E}|/|\vec{B}|$ equal to the speed of radiation wave 'c' , which is another characteristic of a radiation field.

Thus, the fundamental assumptions of classical electromagnetic theory are satisfied for Cerenkov radiation. What is particularly interesting is to check if the Cerenkov relation is satisfied. The term '$\delta_{\omega_j, k_z v}$' in equation 2.15 requires $\omega_j = k_z v$ in order to have non-zero fields by equations 2.21 and 2.22 . Combining

$$k_z = k\cos\theta_c \quad , \quad \omega_j = kc \quad , \quad c_0 = cn \quad , \quad v = \beta c_0$$

it is easy to prove the Cerenkov relation (equation 1.1 in part B of preceding chapter)

$$\cos\theta_c = \frac{1}{\beta n}$$

B. RADIATED POWER

In order to calculate the radiated power, it is convenient to deal with the Fourier frequency components using equations 2.9 , 2.21 and 2.22 . This is provided by the Fourier series expansion for the electric and magnetic fields based on the periodicity of the linac electron bunches (time development was also done by Professor Buskirk, Naval Postgraduate School) . So, time average of the total radiated power per unit solid angle is

$$\frac{dP}{d\Omega} = r^2 \frac{1}{T}\int_0^T \vec{S}\cdot\hat{n}\, dt = \frac{2r^2}{\mu}\sum_{\omega_j=0}^{\infty} \frac{\omega_j^2}{c}\left|\hat{n}\times\vec{\tilde{A}}(\vec{r},\omega_j)\right|^2 .$$

Derived equations 2.18 to 2.22 for Cerenkov radiation should obey some general 'rules' for radiation phenomenon. They are checked by inspection as follows:

1. Vectors '$\vec{B}$', '$\vec{E}$' and '$\vec{k}$' are mutually perpendicular to each other which is obvious from equations 2.21 and 2.22 ;
2. Finite radiation power 'P_j' is as expected, since the radiation fields drop as 1/r each, yielding no r-dependency in

$$P_j = \oint \frac{1}{\mu} (\vec{E} \times \vec{B})\, r^2 \sin\theta \, d\theta \, d\varphi \quad ;$$

3. Using the inverse Fourier transform of equation 2.18 the retarded potential is

$$\Psi(\bar{r},t) = \sum_{\omega_j} e^{-i\omega_j t}\, \tilde{\Psi}(\bar{r},\omega_j) =$$

$$= \frac{1}{4\pi} \sum_{\omega_j} \int d^3 r' \, \frac{\tilde{f}(\bar{r}',\omega_j)}{|\bar{r}-\bar{r}'|}\, e^{-i\omega_j\left(t - \frac{|\bar{r}-\bar{r}'|}{c}\right)} =$$

$$\frac{1}{4\pi} \sum_{\omega_j} \int d^3 r' \, \frac{f(\bar{r}',t')}{|\bar{r}-\bar{r}'|} \quad ,$$

where $t' = t - |\vec{r}-\vec{r}'|/c$ is the retarded time. Physically, the retarded time is required for the wave, see Figure 2.1 , to travel from the bunch to the field point with the speed 'c' ;

4. Using the inverse Fourier transforms and equations 2.19 to 2.22 it is easy to show that

$$\vec{B}(\bar{r},t) = \sum_{\omega_j} e^{-i\omega_j t}\, \tilde{\vec{B}}(\bar{r},\omega_j) = \frac{\mu}{4\pi c r} \int d^3 r' \, \dot{\vec{J}}(\bar{r}',t') \times \hat{n} \quad ,$$

$$\vec{E}(\bar{r},t) = \sum_{\omega_j} e^{-i\omega_j t}\, \tilde{\vec{E}}(\bar{r},\omega_j) = \frac{\mu}{4\pi r} \int d^3 r' \, \hat{n} \times \left[\dot{\vec{J}}(\bar{r}',t') \times \hat{n}\right] .$$

The second step is to solve equation 2.17 using Green's function, yielding

$$\tilde{\Psi} = \frac{1}{4\pi}\int d^3r' \frac{\tilde{\mathcal{F}}(\vec{r}', \omega_j)}{|\vec{r} - \vec{r}'|} e^{i\frac{\omega_j}{c}|\vec{r} - \vec{r}'|} \quad . \tag{2.18}$$

Equation 2.18 is used for the derivation of the radiation fields and power. The complete derivation is reported in [Ref. 5]. Figure 2.1 shows the real situation. The radiation corresponding to the electrons of a particular bunch will produce the field at the field point. Also, we may consider $|\vec{r}| \gg |\vec{r}'|$ for the radiation (far) field which allows the following approximations in equation 2.18

$$\frac{1}{|\vec{r} - \vec{r}'|} = \frac{1}{r} \quad , \qquad e^{i\frac{\omega_j}{c}|\vec{r} - \vec{r}'|} \doteq e^{i\frac{\omega_j}{c}(\vec{r} - \hat{r}\cdot\vec{r}')} \quad .$$

Remembering that the generalized source function 'Ψ' contains 'M' or '$\mathcal{E}$' for '$\vec{J}$' and 'ρ' respectively, and using the approximations above the solutions for the potentials are

$$\tilde{\vec{A}}(\vec{r}, \omega_j) = \frac{\mu}{4\pi r} e^{i\frac{\omega_j}{c} r} \int d^3r' \tilde{\vec{J}}(\vec{r}', \omega_j) e^{-i\frac{\omega_j}{c}\hat{r}\cdot\vec{r}'} \quad , \tag{2.19}$$

$$\tilde{\Phi}(\vec{r}, \omega_j) = \frac{1}{4\pi\varepsilon r} e^{i\frac{\omega_j}{c} r} \int d^3r' \tilde{\rho}(\vec{r}', \omega_j) e^{-i\frac{\omega_j}{c}\hat{r}\cdot\vec{r}'} \quad . \tag{2.20}$$

Fourier components of the radiated fields are obtained from equations 2.19, 2.20 and 2.8 . Taking only the radiation terms (ones which drop as 1/r) this gives the fields

$$\tilde{\vec{B}}(\vec{r}, \omega_j) = i\frac{\omega_j}{c}\, \hat{r} \times \tilde{\vec{A}}(\vec{r}, \omega_j) \quad , \tag{2.21}$$

$$\tilde{\vec{E}}(\vec{r}, \omega_j) = -c\, \hat{r} \times \tilde{\vec{B}}(\vec{r}, \omega_j) \quad . \tag{2.22}$$

In the x and y-directions the source function is not periodic and a corresponding dependency may be expressed by Fourier integrals. Thus, the current density in the linac case becomes

$$\vec{J}(\vec{r}',t)=\frac{\vec{v}}{4\pi^2}\int_{-\infty}^{\infty}dk_x\int_{-\infty}^{\infty}dk_y\sum_{k_z=-\infty}^{\infty}e^{i(\vec{k}\cdot\vec{r}'-\omega_j t)}\,\delta_{\omega_j,k_z v}\,\tilde{\rho}_0(\vec{k}) \quad , \qquad (2.15)$$

with Fourier components

$$\tilde{\rho}_0(\vec{k})=\int_{-\infty}^{\infty}dx\int_{-\infty}^{\infty}dy\,\frac{1}{\lambda_0}\int_0^{\lambda_0}dz\,e^{-i\vec{k}\cdot\vec{r}'}\,\rho_0(\vec{r}') \quad . \qquad (2.16)$$

Now, it is obvious that potential function 'Ψ' and consequently fields '$\vec{E}$' and '$\vec{B}$' have the mathematical representation given by a Fourier series, see equations 2.7 and 2.8 . Because of that, the radiation will appear at harmonic frequencies $\omega_j = j2\pi\nu_0$ due to t-periodicity, and the radiation diagram will show diffraction effect due to finite emission length, which is shown in Figures 2.2 and 2.4 . This gives an idea as to how to solve wave equation 2.7 . Mathematically, it represents a partial differential equation with respect to time and space coordinates. The first step is to eliminate the time dependency which is provided by Fourier series expansion with respect to time 't' , working with Fourier components only. Up to this point the source function has a quite general form, which for every particular radiation problem must be investigated like it has been done here for the linac case (equation 2.15). Thus equation 2.7 transformed into the frequency domain is given by the Fourier series components

$$\left[\nabla^2+\omega_j^2\mu\varepsilon\right]\tilde{\Psi}(\vec{r}',\omega_j)=-\tilde{f}(\vec{r}',\omega_j) \quad . \qquad (2.17)$$

the electric dipoles in the medium, as described in the introduction part B, this derivation does not consider these dipoles directly. Instead, electron bunches are considered as sources since they create the dipoles.[4] The medium is air, the emission length 'L' is finite and the bunches are assumed to be undistorted pulses of finite size, which are periodic both in time 't' and direction of motion 'z' . Therefore the source function 'f' may be represented by a two-dimensional Fourier series with respect to variables 't', 'z' and corresponding variables 'k_z', 'ω_j' in the transformation domain, as follows

$$f(z,t) = \sum_{k_z} e^{ik_z z} \sum_{\omega_j} e^{-i\omega_j t} \tilde{f}(k_z, \omega_j) \quad , \tag{2.10}$$

with the Fourier components

$$\tilde{f}(k_z, \omega_j) = \frac{1}{\lambda_0} \int_0^{\lambda_0} dz\, e^{-ik_z z} \; \frac{1}{T} \int_0^{T} dt\, e^{+i\omega_j t} f(z,t) \quad , \tag{2.11}$$

where 'λ_0' and 'T' are the wavelength and period of the linac traveling wave. Using the assumption of undistorted pulses, a single bunch moving with the speed 'v' in the z-direction is given by source function 'f' in the following form

$$f(z,t) = f_0(z - vt) \quad . \tag{2.12}$$

Consequently, equation 2.11 may be reduced into a one-dimensional Fourier series having components

$$\tilde{f}(k_z, \omega_j) = \delta_{\omega_j, k_z v}\, \tilde{f}_0(k_z) \quad , \tag{2.13}$$

where

$$\tilde{f}(k_z) = \frac{1}{\lambda_0} \int_0^{\lambda_0} dz\, e^{-ik_z z} f_0(z) \quad . \tag{2.14}$$

---

[4]This simplifies derivation and experiment, because current of electron bunches is actually measured. However, this causes the misinterpretation that Cerenkov radiation is produced by electrons having constant speed, which disagrees with radiation theory. See Appendix B subsection Electron Beam.

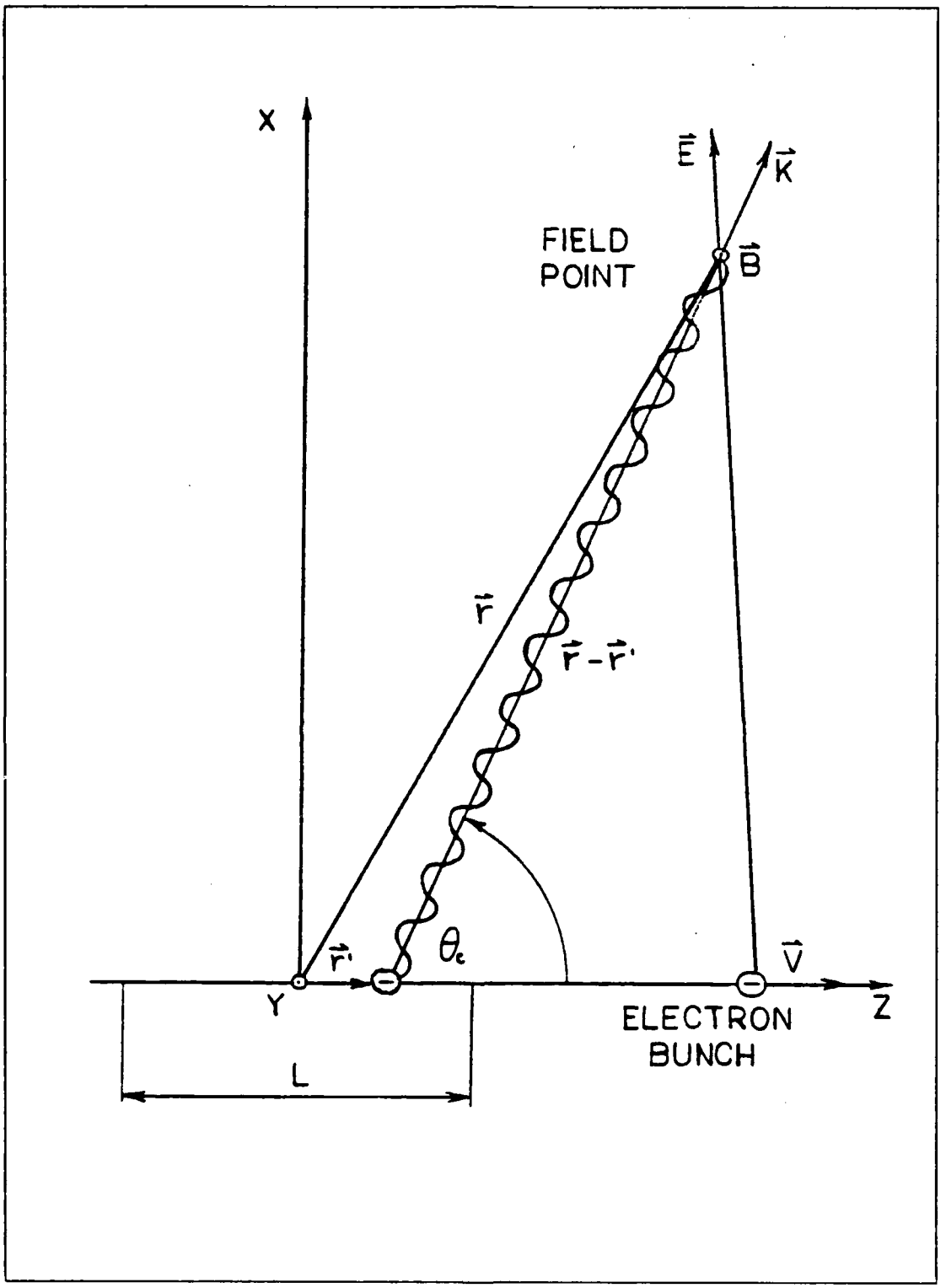

Figure 2.1 Cerenkov Radiation from Electron Bunches.

describe radiation phenomenon, Maxwell's equations are recast into inhomogeneous wave equations for magnetic vector potential '$\vec{A}$' and electric scalar potential 'ϕ'

$$\left[\nabla^2 - \mu\epsilon\frac{\partial^2}{\partial t^2} - \mu\sigma\frac{\partial}{\partial t}\right]\vec{A}(\vec{r},t) = -\mu\vec{J}(\vec{r}',t) \quad , \qquad (2.5)$$

$$\left[\nabla^2 - \mu\epsilon\frac{\partial^2}{\partial t^2} - \mu\sigma\frac{\partial}{\partial t}\right]\phi(\vec{r},t) = -\frac{1}{\epsilon}\rho(\vec{r}',t) \quad . \qquad (2.6)$$

Introducing general notation 'Ψ' for 'ϕ' and any component of '$\vec{A}$', as well as 'f' for 'ρ' and '$\vec{J}$' ('μ' or 'ϵ' are included in 'f'), and assuming a nonconducting medium (conductivity $\sigma = 0$), the equations above in general form are

$$\left[\nabla^2 - \mu\epsilon\frac{\partial^2}{\partial t^2}\right]\Psi(\vec{r},t) = -f(\vec{r}',t) \quad . \qquad (2.7)$$

The standard procedure in solving a radiation problem is to solve equation 2.7 and find the radiation fields '$\vec{E}$' and '$\vec{B}$' using the auxiliary relations

$$\vec{B} = \nabla \times \vec{A} \quad , \qquad \vec{E} = -\nabla\phi - \frac{\partial\vec{A}}{\partial t} \quad . \qquad (2.8)$$

Having the fields, the radiation power per unit area is calculated as the time average of the Poynting vector

$$\frac{1}{T}\int_0^T \vec{S}\cdot\hat{n}\,dt = \frac{1}{T}\int_0^T \left(\frac{1}{\mu}\vec{E}\times\vec{B}\right)\cdot\hat{n}\,dt \quad . \qquad (2.9)$$

But before that, it is of interest to study the source and potential functions 'f' and 'Ψ'.

As it has been mentioned, a linear accelerator (linac) is used to create electron bunches, for the radiation shown in Figure 2.1 . Although Cerenkov radiation is produced by

II. THEORY OF CERENKOV RADIATION

This chapter outlines the characteristics of Cerenkov radiation in the microwave region resulting from periodic electron bunches, which are produced by the linear accelerator at the Naval Postgraduate School. The main intention is to emphasize the most important points without all mathematical details, and to obtain a complete picture from Maxwell's equations to Cerenkov radiation. The sources for this chapter are [Ref. 2 , 5 , 6 , 7 , 8]. Proceding from Maxwell's equations, the expression and corresponding graphs for the radiation power are represented. This research was an effort to verify those results experimentally.

A. FROM MAXWELL'S EQUATIONS TO CERENKOV RADIATION

Fundamental results of classical electromagnetic theory are summarized in Maxwell's equations which are given in differential form

Gauss' law

$$\nabla \cdot \vec{D} = \rho \tag{2.1}$$

Gauss' law

$$\nabla \cdot \vec{B} = 0 \tag{2.2}$$

Faraday's law

$$\nabla \times \vec{E} = -\frac{\partial \vec{B}}{\partial t} \tag{2.3}$$

Ampere's law

$$\nabla \times \vec{H} = \vec{J} + \frac{\partial \vec{D}}{\partial t} \tag{2.4}$$

These are experimental laws, containing important informations about electric and magnetic fields. In order to

see Figure 1.3 . Using Cerenkov radiation, it could be possible to construct a monoenergetic X-ray source which would have applications in metallurgy and medicine, or as a damage mechanism for soft kill of a target.

Finally, a nice analogy to Cerenkov radiation, for people in Naval service is the bow wave produced by a ship which moves faster than the surface water wave.

C. APPLICATION

The first application of Cerenkov radiation was made in the optical region after the photomultiplier tube had been developed. That was a rather sensitive light detector, used by Curran and Baker in 1944 for the development of a scintillation counter. Later-on, in 1951 the first Cerenkov detector was developed by Marshall and Mather. Both devices were remarkable. The former found many applications in nuclear and cosmic ray research, the latter was used in the study of high energy particles and led to the discovery the of anti-proton.

One of the problems in present microwave technology is lower possible power as the frequency is raised. In fact, higher frequency implies smaller resonant cavity of microwave resonators, so that cavity break-down with arcing appears as a power limitation. Some of solutions are new devices like the gyrotron, the relativistic magnetron, etc. A successful approach in this is to achieve stimulated Cerenkov effect, when Cerenkov radiation is amplified along a hollow dielectric tube. Another application in the microwave region could be as a beam monitor for a free electron laser, which may find its application in directed energy weapons. Previous thesis work refers to stimulated Cerenkov radiation, as reported in [Ref. 3 , 4].

Recently, a group of Soviet scientists has produced Cerenkov radiation in the X-ray region and similar experiments are being conducted at the Naval Postgraduate School. This is significant, since in the X-region the refractive index $n<1$ except at very narrow regions near the resonance,

1. There exists a threshold speed $v_{TH}=c/n$ of charged particle above which Cerenkov radiation is possible;
2. The Cerenkov relation is frequency independent which implies a broad radiation spectrum;
3. The Cerenkov radiation requires n>1 . Figure 1.3 shows the index of refraction 'n' versus wavelength 'λ' and regions where Cerenkov radiation can be observed.

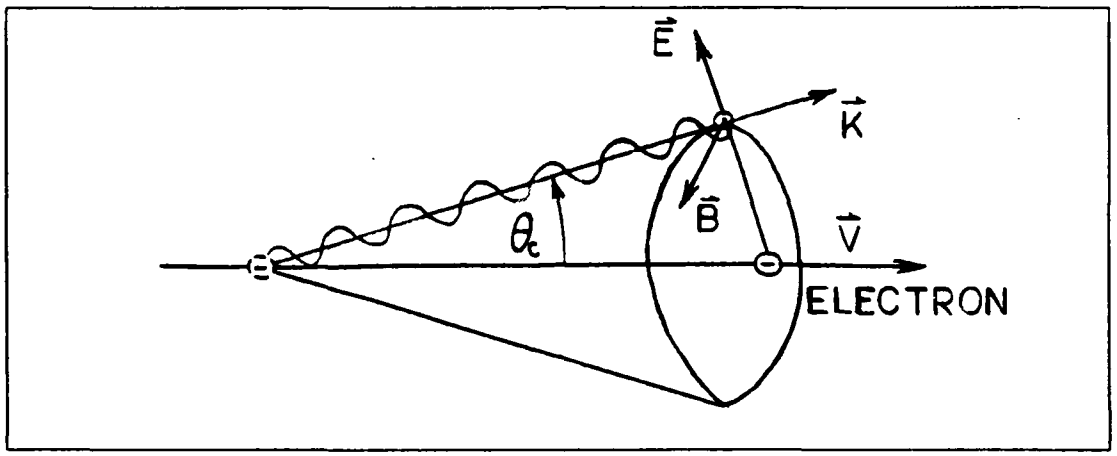

Figure 1.4 Polarization of Cerenkov Cone.

From the nature of the radiation, which has been described above, it may be concluded:

4. Radiation intensity approximates a Dirac δ-function centered about Cerenkov angle 'θ_c' ;
5. Polarization of the radiation corresponds to a plane wave which is shown in Figure 1.4 , propagating at the Cerenkov cone angle ;
6. Length FZ in Figure 1.2 must be much larger than the radiated wavelength in order to avoid diffraction effects. For a finite radiation length, the diffraction effect is significant, as shown in part B of the following chapter.

than phase speed of the radiation 'c' in the medium. In Figure 1.2 dipoles at F and E may be considered using Huygens principle, giving resultant plane wavefront ZA . In order to obtain constructive interference at the plane wavefront ZA the charged particle must pass distance FZ, and the radiation wave must pass distance FA, during the same time interval 'Δt' . A similar consideration is valid for all other dipoles behind Z . This means that the speed of the charged particle must be greater than the speed of the radiated wave: $v>c$ . . If the case were opposite it would not be possible to get the resultant plane wavefront ZA and have constructive interference .

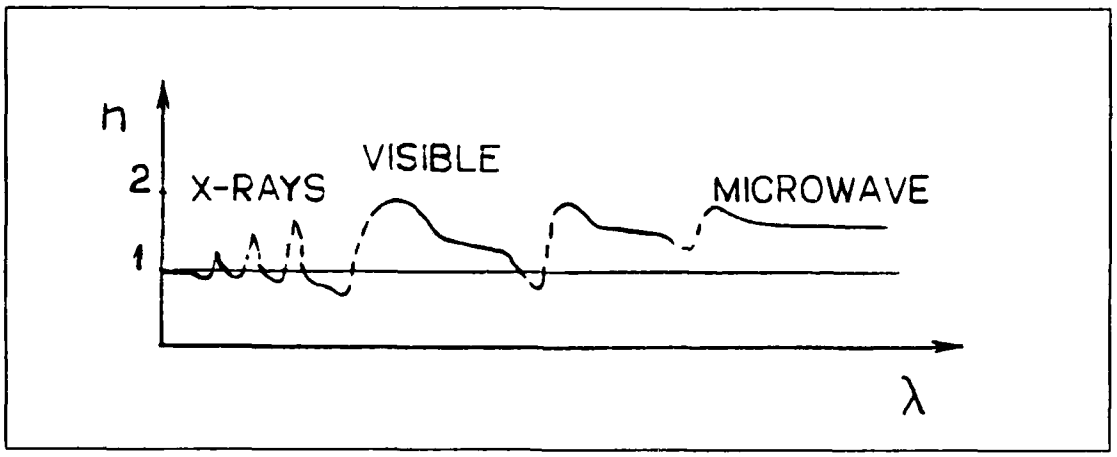

Figure 1.3 Dispersion Curve.

Using the quantities from Figure 1.2 , and $\beta=v/c_o$, $c_o=nc$ it is easy to show the Cerenkov relation[3]

$$\cos\theta_c = \frac{1}{\beta n} \quad , \tag{1.1}$$

which suggests the following conclusions :

[3]To avoid multiple variable definitions at different parts of this paper all variables are defined in Appendix A.

slowly the polarized atoms will be symmetrically distributed about the particle path. After the charged particle has passed, the polarized atoms will return into the unpolarized state. During this process there will be no net radiation, because of complete symmetry of the polarized atoms.

Now, let us suppose the charged particle moves very fast. This will cause an asymmetry of the polarized atoms along the path, Figure 1.1 b) , which is due to their inertia. In other words, a fast charged particle will cause a net electric dipole along its path, so that the polarized atoms will produce a net electromagnetic pulse upon returning into the unpolarized state. This is Cerenkov radiation. Also, the charged particle is decelerated by a small amount, since it loses energy when creating electric dipoles in medium. Thus, it produces bremsstrahlung radiation which is negligible in this case and its speed is assumed to to be constant (for dipole and Bremsstrahlung radiation, see [Ref. 2] or any other electrodynamics book) .

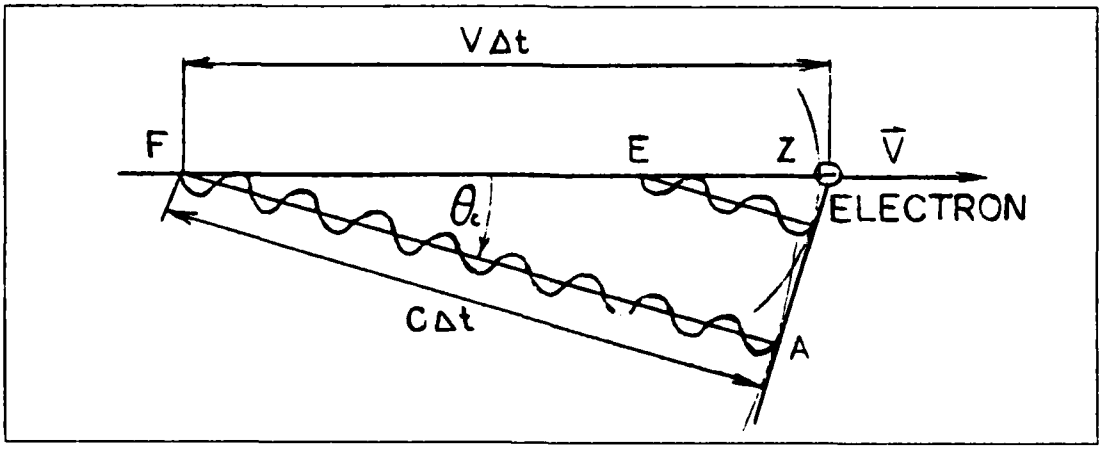

Figure 1.2 Cerenkov Radiation.

A particularly important characteristic of the radiation is that the speed of the charged particle 'v' is greater

B. DESCRIPTION

A simple description of Cerenkov radiation is that a fast, charged particle may cause electromagnetic radiation in a dielectric medium when it moves with a constant speed greater than the speed of the produced radiation.[2] It is interesting that the charged particle is not accelerated, but it moves with a constant speed. This does not mean that classical electromagnetic theory of radiation by accelerated charge fails in the case of Cerenkov radiation. On the contrary, Cerenkov radiation proves this theory. The radiation is produced by oscillating electric dipoles in the medium, which are created by the charged particle .

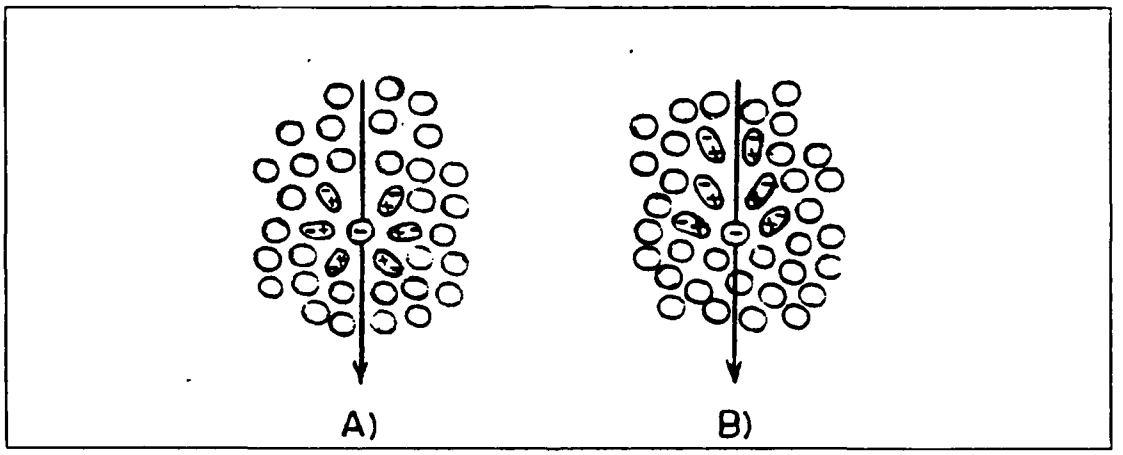

Figure 1.1 Polarized Atoms in a Dielectric.

In more details, Cerenkov radiation may be explained as follows. Let a negative charged particle move through a dielectric, see Figure 1.1 (a . The atoms of the medium surrounding the path of the particle will be polarized, due to the electric field of the particle. If the particle moves

[2]See Appendix B subsection 1 for the calculation and numerical values of these speeds.

Note that the time average is taken over the period of the linac traveling wave 'T' . Since, the linac pulse period is much longer than its pulse, Cerenkov effect is over after 1 μs of the pulse, but it repeats itself every pulse again. The cross-product term was calculated in detail in [Ref. 5], yielding the principal result of the calculation as given in [Ref. 7],

$$\frac{dP}{d\Omega} = \sum_{\nu_j=0}^{\infty} W(\nu_j,\theta) = \sum_{\nu_j=0}^{\infty} \frac{\mu c \nu_0^2 q}{8\pi^2} |F(\bar{k})|^2 \left[(kL)\sin\theta\, I(u)\right]^2 , \qquad (2.23)$$

where radiation parameters are

diffraction variable $$u = \frac{kL}{2}(\cos\theta_c - \cos\theta) , \qquad (2.24)$$

diffraction function $$I(u) = \frac{\sin u}{u} , \qquad (2.25)$$

and single pulse charge density

$$\tilde{\rho}_o'(\bar{k}) = \int_{-\infty}^{\infty} d^3x'\, e^{-i\bar{k}\cdot\bar{x}'} \rho_o'(\bar{x}') \equiv q\, F(\bar{k}) . \qquad (2.26)$$

This is the general expression for total radiated power from electron bunches through a finite emission length. Furthermore, for the linac electron bunches it is reasonable to assume a Gaussian charge distribution so that single pulse charge density

$$\tilde{\rho}_o'(\bar{k}) = q \exp\left[-\left(\frac{ak}{2}\sin\theta\right)^2 - \left(\frac{bk}{2}\cos\theta\right)^2\right] \equiv q F(\bar{k}) , \qquad (2.27)$$

where the radial size parameter of a single bunch 'a' may be neglected.[5] The radiated power per unit solid angle at harmonic frequency 'ν_j' is

$$W(\nu_j,\theta) = Q\, D_j(\theta) , \qquad (2.28)$$

---

[5] See Appendix B, Electron Beam.

with radiation function

$$D_j(\theta) = \frac{j^2}{4} \left(L \sin\theta \frac{\sin u}{u} \right)^2 \exp\left[-\left(\frac{bk}{2} \cos\theta \right)^2 \right] , \qquad (2.29)$$

and

$$Q = \frac{2\mu V_0^4 \alpha^2}{c} . \qquad (2.30)$$

The calculated expression for $W(w_j, \theta)$, equation 2.28, represents the central theoretical result which has been used in prior and the present experimental work concerning microwave Cerenkov radiation for finite emission length. Theoretical predictions and experimental evidence are summarized in the following chapter. It is of interest to discuss this expression in more detail.

Analyzing terms in equation 2.29 , it is easy to recognize the '$\sin\theta$' factor, as a usual term in the radiation power due to an electric dipole. In this way, the total radiation power given by equation 2.23 represents the interference (sum) of all dipole radiators along the emission length of the medium. This is in agreement with the physical interpretation given in part B of the preceding chapter.

The following term $(\sin u)/u$ is diffraction function assigned as $I(u)$. A similar expression may be obtained by analyzing the Fraunhofer single slit diffraction pattern. In that case $I(u)$ is the consequence of the diffraction effect of point sources along the single slit. Single slit point sources may be compared with the series of electric dipoles along the emission length having similar diffraction pattern. Physically, these two phenomena are different in their nature. At the first glance it is obvious that Cerenkov dipoles emit radiation at different times while Fraunhofer sources do that simultaneously. Of course, diffraction variables are different too. The first diffraction null 'θ_n' occurs at $u=\pi$ (see equation 2.24). Since $\cos\theta$ varies slowly, for a finite (small) emission length

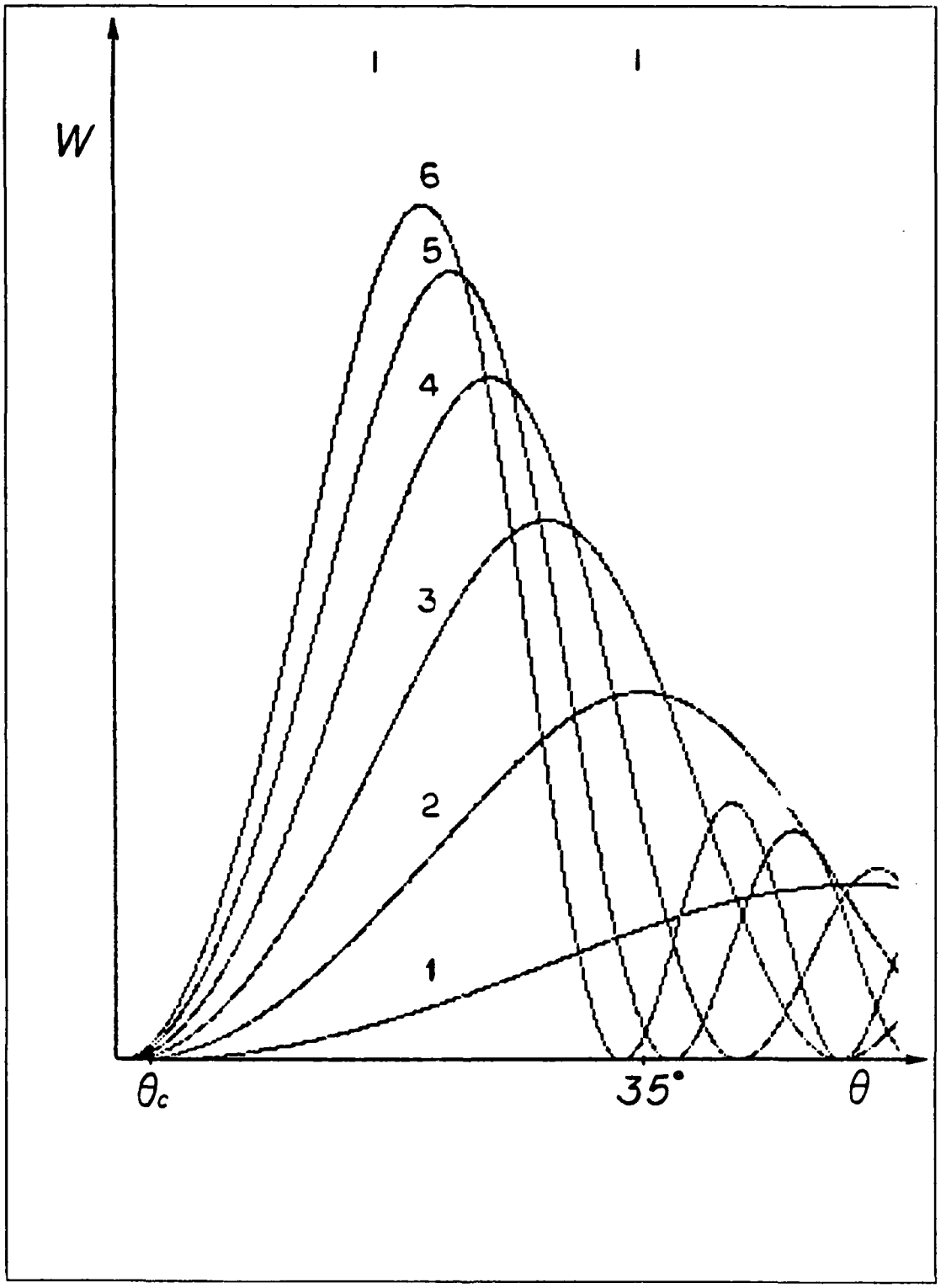

Figure 2.2 Diffraction Patterns for Harmonics j=1,2,3,4,5,6.

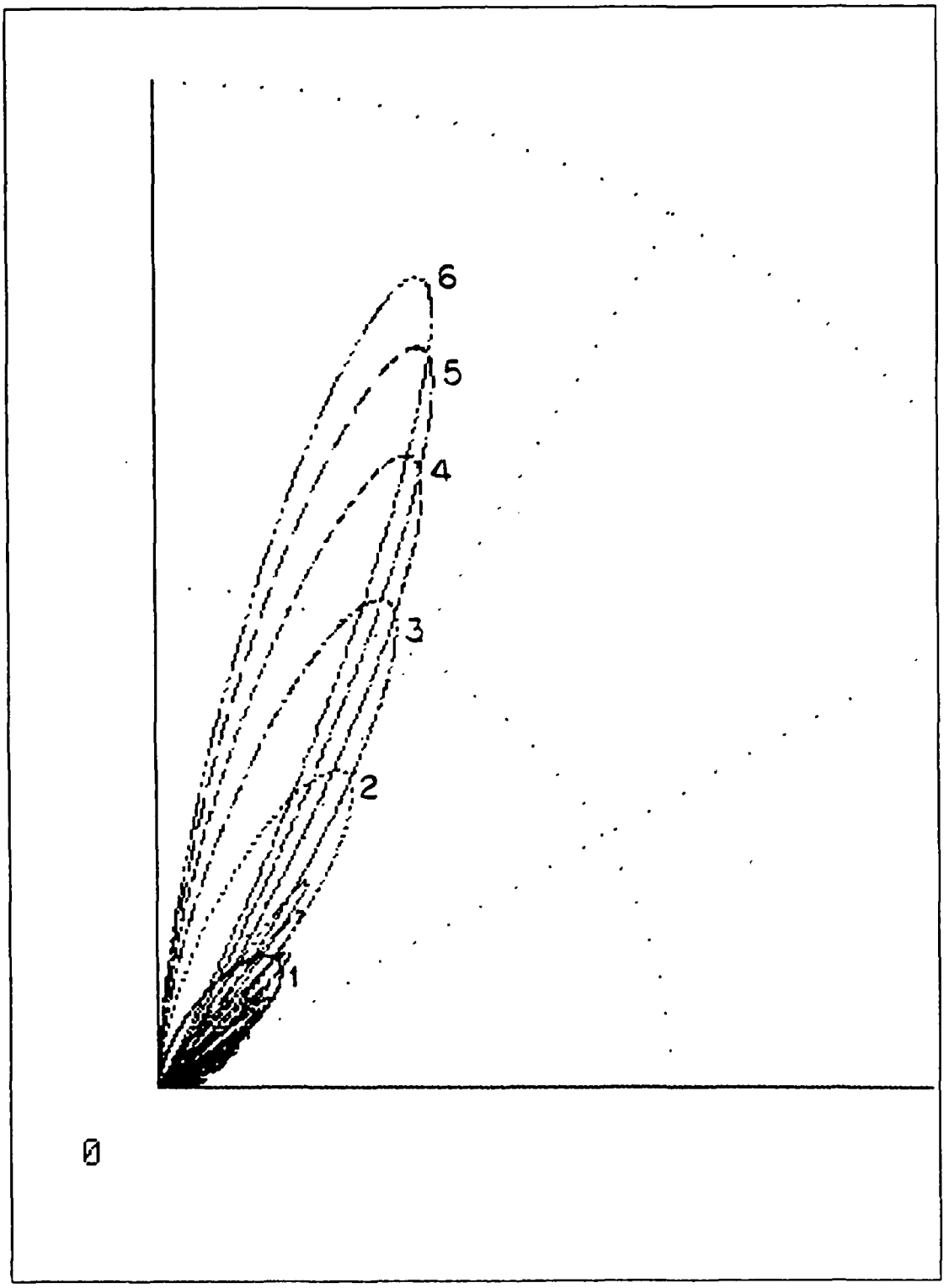

Figure 2.3 Harmonics j=1,2,3,4,5,6 (polar plot).

'L', 'θ_n' must be big and so, the radiation is smeared around 'θ_c'. Also, Huygens waves radiated from the front and rear of the emission length 'L' differ by 2π (see Appendix B). Diffraction patterns for the first six harmonics are shown in Figure 2.2 and polar plot is given in Figure 2.3 . They are investigated in the experiment. All plots are based on equation 2.28 and experimental parameters.[6]

A particularly interesting result appears for the maximum of radiation. Elementary considerations in the part B chapter 1, as well as as, u=0 in the diffraction function I(u), indicate that the maximum occurs at Cerenkov angle 'θ_c' This is really true for an infinite emission length 'L' . However, this calculation is done for a finite 'L', and Figure 2.2 indicates maximum at $\theta > \theta_c (=1.29^{\circ})$. Therefore, the radiated intensity is influenced by two other terms in equation 2.29, as well. The third exponential term in equation 2.29 exhibits very small changes with 'θ'. On the other hand, $\sin\theta$ term increases rapidly. Since, Cerenkov radiation is smeared around 'θ_c' it is greatly enhanced by the $\sin\theta$ term (coherent dipole radiation) and so, it is larger for $\theta > \theta_c$ than for $0 < \theta < \theta_c$. Consequently, the maxima in Figure 2.2 are shifted toward the greater angles and the total power is increased. The former is experimentally verified, as reported in [Ref. 7].

Smearing of the Cerenkov angle and power increase are the diffraction effects for a finite emission length so that, they are dependent on the frequency of the harmonic, as shown in Figure Figure 2.2 for different harmonics. A natural question which one may ask is what happens when all harmonics are summed together, as it is given by equation

---

[6]The experimental parameters vary in different measurements slightly, so that the values are not shown at the theoretical curves in this chapter, but they are considered with experimental results. All experimental parameters are summarized in Table VII, as a reference.

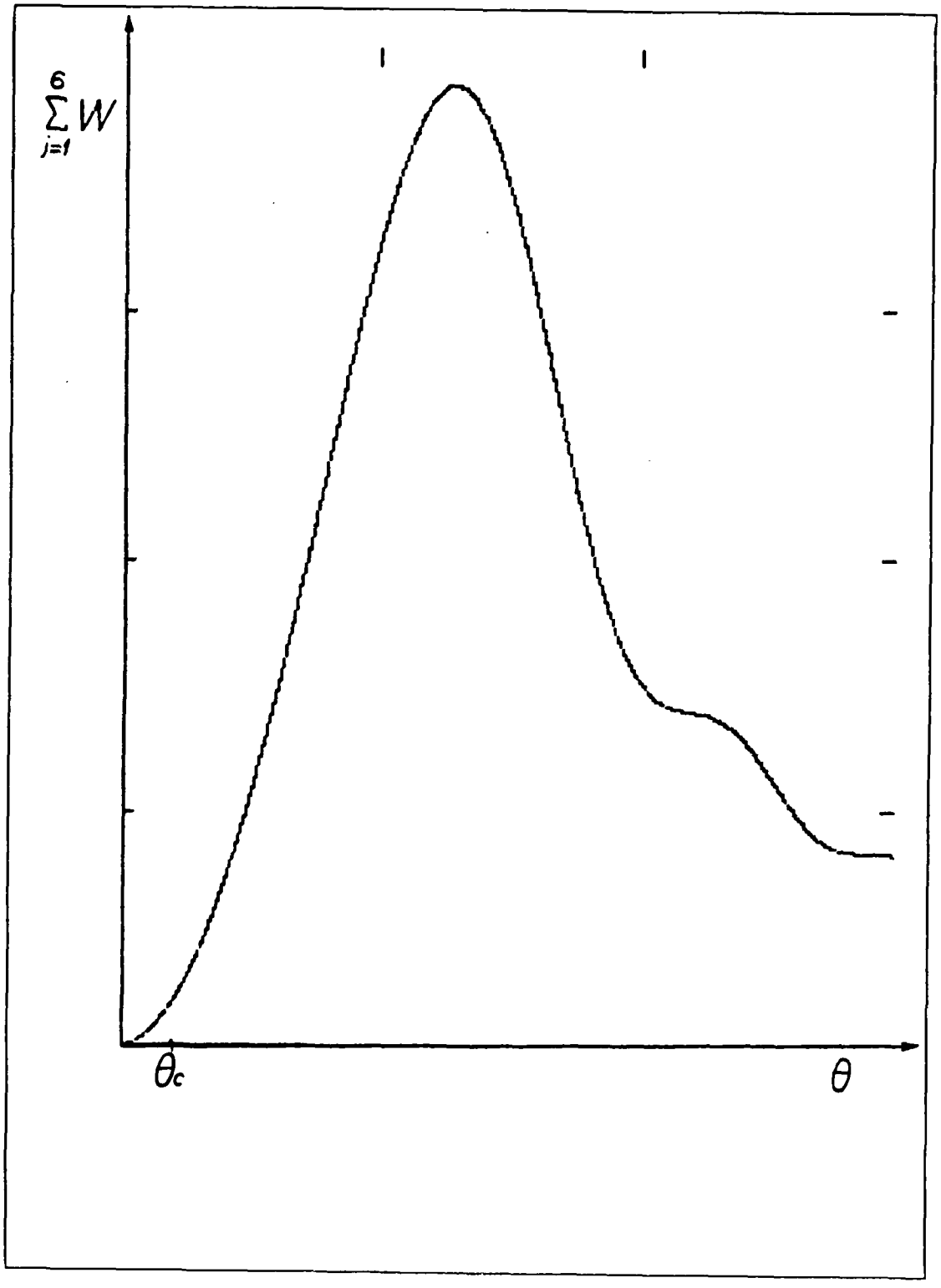

Figure 2.4 Sum of Harmonics j =1,2,3,4,5,6.

2.23. Figure 2.4 illustrates such a situation for the first six harmonics. The result is that the Cerenkov radiation cone is broadened, and smearing of the Cerenkov peak is asymmetric (assuming small 'θ_c'). Both effects are diffraction characteristic along a finite emission length, as discussed above. Another result is probably more surprising. The diffraction pattern moves to the smaller angles as the speed of electron decreases, which is obvious from equation 1.1 or from the more complicated equation 2.28. Due to the broadening at the Cerenkov cone , the radiation is expected even below threshold speed $v_{TH}=c_o/n$. This effect could be produced by reducing the electron energy and varying the other experimental parameters.

The final result of the calculations is given in Figure 2.5 . Two curves are obtained by numerical integration of diffraction patterns of Figure 2.2 : total radiated power 'P' and power radiated in the main lobe 'P_1'. The maxima of the radiation diagrams are 'Wm.' These curves are investigated in this paper for experimental verification. Since, the total power is proportional to the frequency, it is small in the microwave region. The linac provides rather energetic electrons and the radiation is enhanced. Power fall-off at the fourth harmonic is associated with the form factor '$F(\hat{k})$' (exp term in equation 2.29), as seen in Figure 2.5 , when radiation wavelength becomes comparable with bunch size. Then destructive interference takes place for the radiation produced along single bunches. This limits the power in the microwave region. Using the parameters from Table VII as a reference, the following summary of numerical data is given in Table I . The values for 'Wm' are used in the second experiment (see Table VI) .

As it has been emphasized, the power calculated is for finite emission length, which is of interest in the experiment. For the sake of the complete picture, the total power

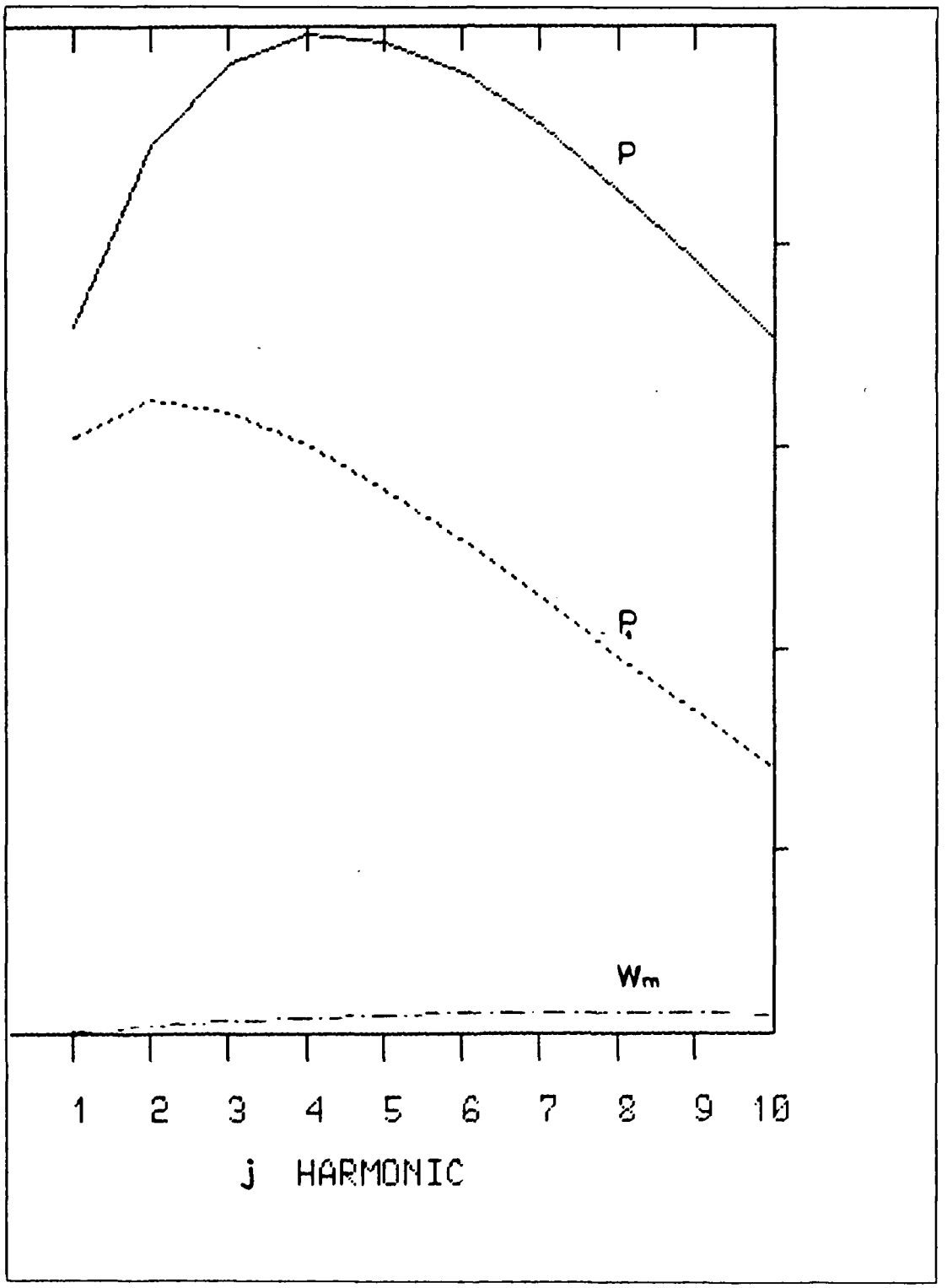

Figure 2.5 Radiated Power for Finite Emission Length.

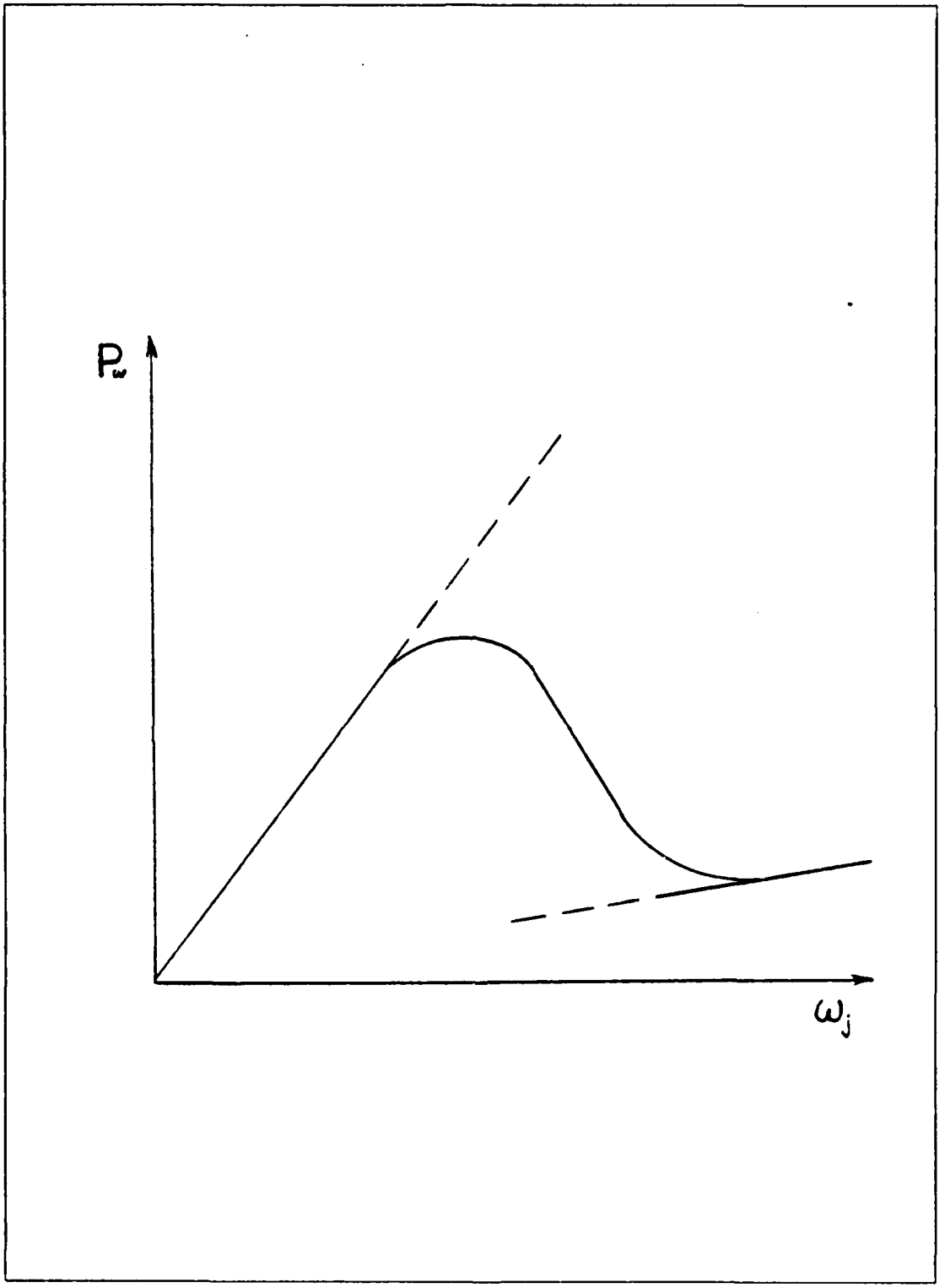

Figure 2.6 Radiated Power for Infinite Emission Length.

TABLE I

Theoretical Power Calculation

j	P (W)	P_4 (W)	Wm (mW/Sr)
1	0.179	0.154	1.089
2	0.227	0.164	2.287
3	0.248	0.162	3.361
4	0.256	0.154	4.247
5	0.255	0.142	4.908
6	0.247	0.128	5.320

TABLE II

Power for Infinite and Finite Regions

j	P	P_ω	P/P_ω
1	11.86	0.117	101.02
2	13.53	0.228	59.34
3	14.12	0.324	43.58
4	14.12	0.402	35.12
5	13.71	0.459	29.87
6	13.52	0.491	27.54

P_ω as calculated for infinite emission length in [Ref. 5], is depicted in Figure 2.6 . Essentially, P_ω shows the same behavior as P in Figure 2.5 . However, numerical values calculated in [Ref. 7], for different parameters than those used in this experiment show the surprising ratio P/P_ω, as given in Table II (units are arbitrary). Obviously, diffraction effect along a finite emission length is very significant.

III. COMPARISON OF THEORY AND EXPERIMENT

The object of this chapter is to state briefly the theoretical results and experimental evidence for the radiation in microwave region. Thus, it should provide comparison between theory and experiment and help the reader to follow further this paper.

A. THEORETICAL BACKGROUND

Characteristics of Cerenkov radiation from periodic electron bunches in microwave region for finite emission length are summarized as follows :

1. Enhanced Cerenkov radiation in the microwave region is accomplished by an intense relativistic electron beam produced by the linac ;
2. The radiation has a discrete frequency spectrum of harmonics of the bunch frequency $\nu_j = j\nu_0$;
3. Radiated power increases with frequency until power fall-off occurs ;
4. The Cerenkov angle is smeared depending on the harmonic frequency and Cerenkov cone is broadened ;
5. Power calculated for finite emission length is greater than the power for infinite emission length ;
6. There exists the possibility of Cerenkov radiation below the threshold velocity .

The theoretical assumptions which are used in the calculation are :

1. Electron bunches are periodic in time 't' and space 'z' ;
2. Charge distribution of a single bunch is Gaussian with negligible radial parameter 'a' ;

3. Single electron bunch is undistorted with finite longitudinal parameter 'b' ;
4. Beam current is constant ;
5. Emission length 'L' is finite ;
6. Distance to the radiation field $|\vec{r}| \gg |\vec{r}'|$ or r > L ;
7. Cerenkov effect repeats itself every linac pulse .

B. PRIOR EXPERIMENTS

Previously five series of experiments aimed to verify the theoretical results were conducted. The detection unit consisted of a horn antenna, and a crystal detector attached on the opposite ends of a short piece of waveguide. Usually, the signal was measured by oscilloscope. Alternatively, the pulse height analyzer was used.

The first series of experiments with the traveling detector unit provided observation of Cerenkov radiation in air for X-band with the maximum radiation angle greater than the Cerenkov angle. The second series of experiments with a fixed detector unit and spectrum analyzer confirmed the existance of linac harmonics in X-band. In the third series, the experimental setup consisted of a traveling detector unit and a fixed reflector so that the opposite sides of the Cerenkov cone were measured in the X and K-bands. The fourth series had a rather similar setup, except that the detector unit was fixed while reflector was rotated. Both of these later experiments confirmed that the observed radiation peak angle was in agreement with the calculation. Finally, the fifth series with traveling detector unit, fixed reflector and pulse height analyzer verified the shape of diffraction curves in the X-band.

Thus, theoretical predictions 1., 2., 4. from the preceding section are verified experimentally by prior experimental work. For more details see [Ref. 7 , 4 , 3 , 9 , 10].

C. PRESENT EXPERIMENT

This is a short introduction of what was currently done in linac experiments for microwave region and described as the main object of this work in the following chapters. Previous problems and results were studied carefully in parallel with the theory. It was decided to improve measurements and try to verify theoretical result 3. from section A. The measurements were done in the S,C,X and Ku-bands,[7] which covers the first six harmonics.

1. Radiation Diagram Measurements

In order to meet theoretical assumption r > L measurements should be done in the FAR field. However, the linac experimental area imposes space limitation so that it is not possible to measure far (radiation) field unless the emission length is drastically reduced . This generates another problem of a weak Cerenkov signal due to the far field and short emission length. Also, in the detection procedure the Cerenkov signal suffers attenuation and significant electromagnetic noise is always present. For these and other reasons, far field measurements are rather difficult and all previous experiments have been done in the NEAR field.

Obviously, additional experimental improvements are necessary. First of all, the weak Cerenkov signal should be amplified and selected properly in parallel with noise reduction and higher sensitivity. This was achieved in the present experiment, as discussed in the following chapter. According to the theoretical results, available equipment and experimental conditions radiation diagrams for the first four harmonics were measured in the far field.[8]

---

[7] In order to avoid ambiguity as for different notations of frequency bands, they are defined in Table X.

[8] 'Radiation diagram' , 'diffraction pattern' , 'one side of diffraction lobe' are synonyms.

2. Absolute Power Measurements

For proper measurements it is necessary to know the dynamic range of the equipment and fit the observed Cerenkov signal into the linear part. If not so, the worst case may occur that is, measurements in the saturation region. This procedure requires calibration curves, which show the detected voltage on an oscilloscope versus reference power from signal generator. Having calibration curves it is easy to calculate the Cerenkov power which is measured in the experiment. Precise power measurement for all harmonics requires some additional equipment, which was not employed in this experiment. Absolute power measurement for the first four harmonics was done by measuring the radiation diagrams.

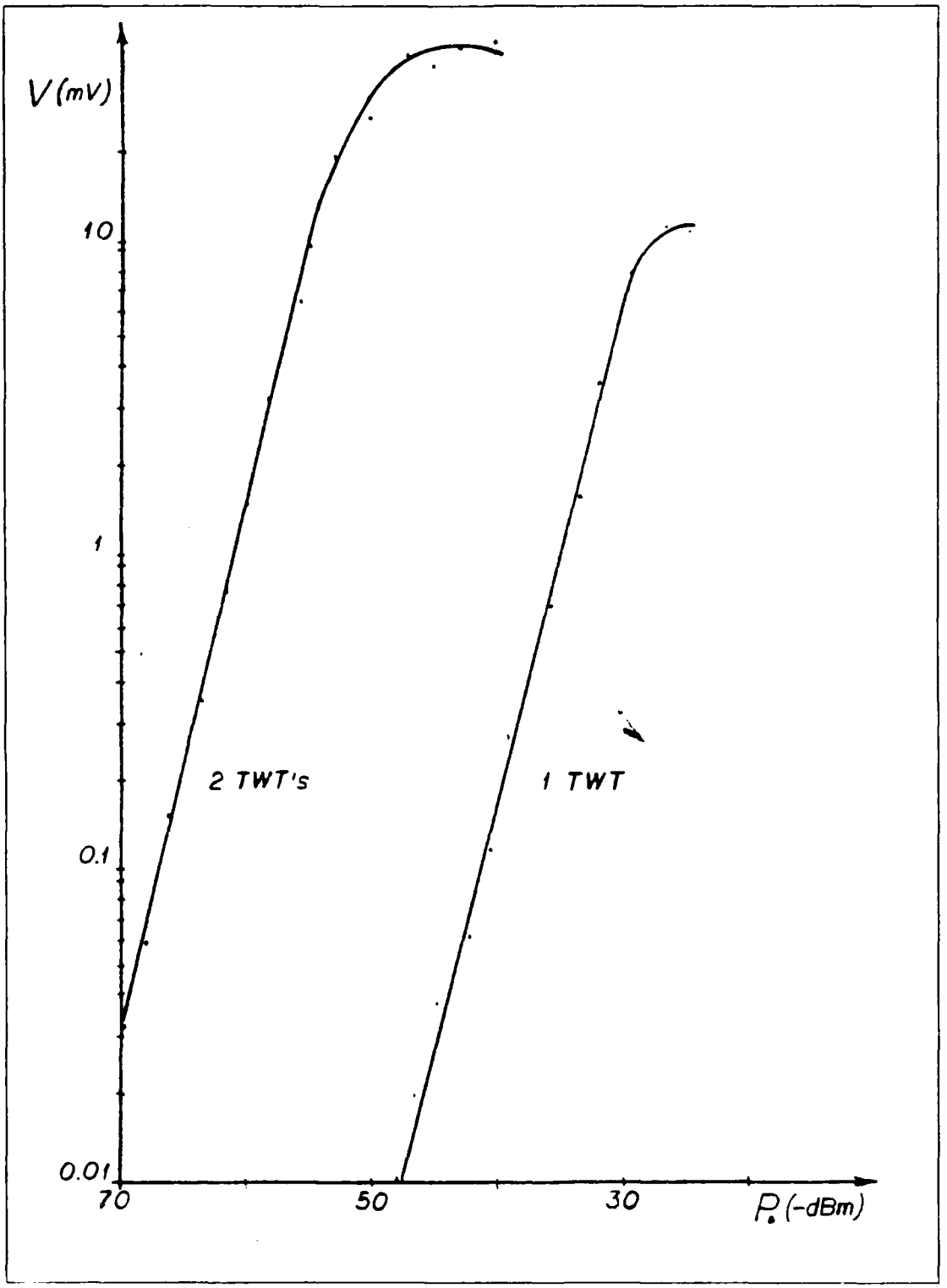

Figure 4.6 Calibration curves for the Second Harmonic.

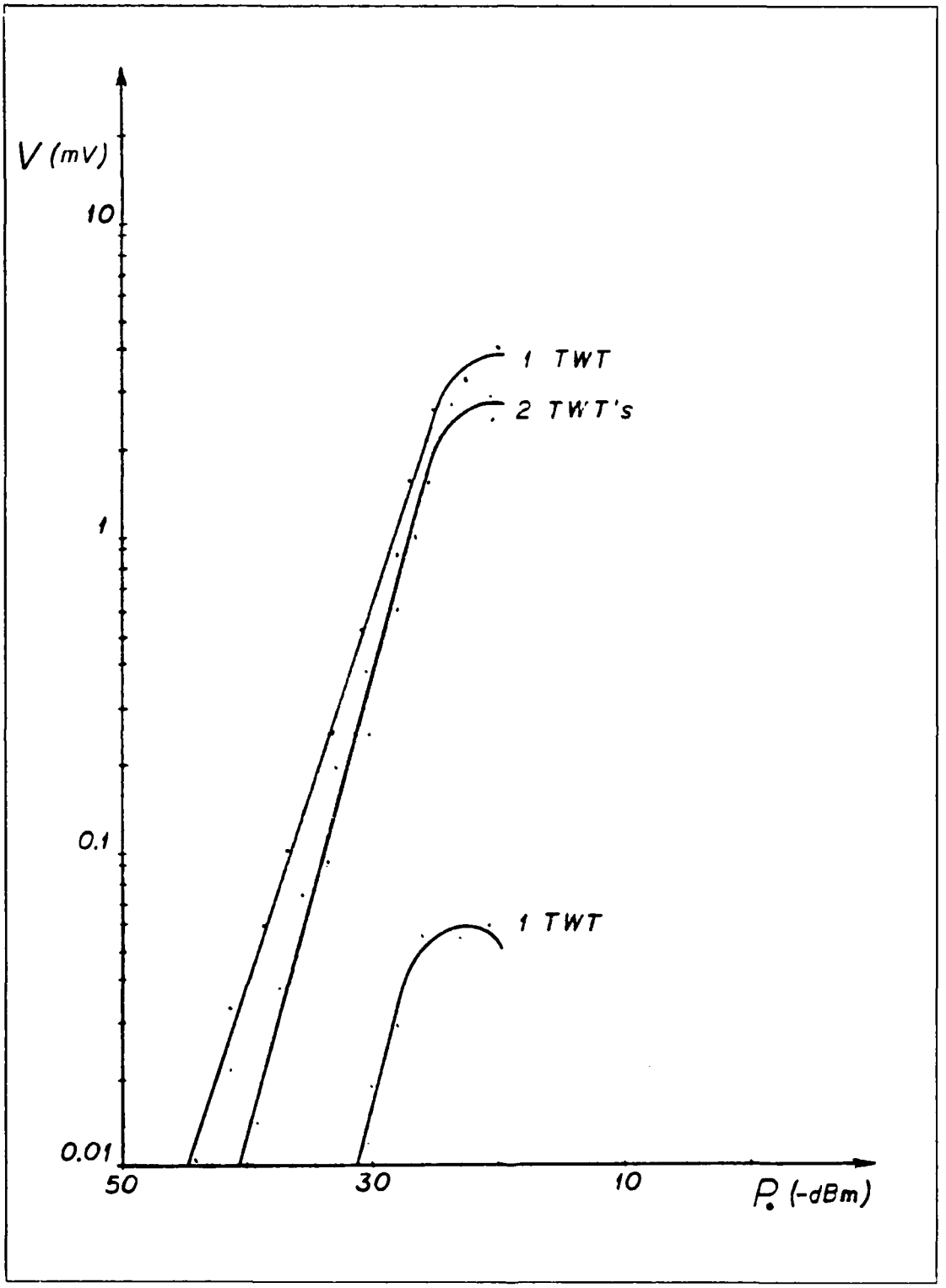

Figure 4.5 Calibration Curves for the First Harmonic.

and it covers rather wide frequency range for the first four harmonics.

The antenna mount with the bar and AC motor are critical mechanical parts of the arrangement. Sweeping over all angles the antenna must be pointed towards the center of rotation, keeping alignment with horizontally polarized Cerenkov radiation. This could be easily lost, so that it must be always checked in order to have reliable results.

4. Amplifier

For the measurements in the far field the Cerenkov signal is amplified by TWT amplifiers. A particularly good feature of these amplifiers is the low noise figure, since Cerenkov experiments always have noise problem. If the experimental setup consists of two TWT's with the filter between, the second TWT will not generate much noise. However, many measurements employ only one TWT in line before the filter, which cuts the noise and selects desired signal.

The average Cerenkov power at the antenna for the given experimental parameters is estimated to be in the dynamic range from -45 to -20 dBm for any of the first six harmonics. Saturated power output for TWT's is about -5 dBm so, it is not advisable to use two TWT's . However, two TWT's have greater dynamic range and for some harmonics this helps to fit the signal into the range of linear amplification. Use of calibration curves and fitting by appropriate attenuators is the general procedure. Calibration curves were measured for the equivalent signal from signal generator, as shown in Figure 4.1 . All curves are given in Figures 4.5 , 4.6 , 4.7 , 4.8 . 'V' is the oscilloscope voltage and 'P_o' is the reference peak power from signal generator. To avoid misleading, Cerenkov power 'P' is averaged over T=350 ps, within linac pulse period Tp=1 μs . 'P_o'

time direct measurement may be done in the area of higher noise. The signal cannot be measured for small angles. Antenna bar cannot be mounted, so that antenna slides along the track. However, such antenna is not pointed towards the center 'C' and receives the signal at different points of its own radiation diagram when slides along the track. This reduces experimental accuracy drastically and direct measurement is just qualitative. Another consequence of direct measurement is much longer beam path in air which results in strong Cerenkov signal. The experimental emission length is only 0.14 m and the rest of Cerenkov radiation is undesired. It turns out that it is not so easy to get rid off 'Cerenkov excess'. The aluminum wall and absorber represent a compromise for the beam (Cerenkov radiation) confinement. The radiation still may bounce among the walls. If the beam were confined by a long pipe the electrons could bounce in it and create radioactivity problem. A wider pipe may help but it blocks biger 'θ' angle, see Figure 4.4 .

To conclude, for these experimental conditions, indirect measurement with the mirror is the most appropriate one. Direct measurement as a comparative method may be useful in resolving some particular problems of indirect measurement.

3. Antenna

There are three antennas used in the experiment, according to the frequencies of the desired harmonics. Two horn antennas represent good choice as for the experimental requirements. They have high gain, relatively narrow beam width and small aperture area, which provide good detection and angular resolution less than 0.5°. The pyramidal antenna does not represent such a good choice, since its wide beam width allowes interference from other directions than the desired one. But it is the only available antenna

flange. This is undesired Cerenkov ray # 3 , as shown in Figure 4.3 . Such problem may be solved using a narrow strip instead of the mirror, which reflects only the desired side of the Cerenkov cone. Undesired rays # 1 and # 3 are discarded and desired ray # 2 is measured. The strip is aligned using the mirror as reference and centered up to the point 'M' . A fluorescent screen on the mirror may be used to indicate when electrons hit point 'M' . The width of the strip is arbitrary since the electric field determines polarization and reflection planes, see Figure 1.4 . In other words, the incident and reflected rays are in radial planes around the beam line and the antenna will receive only those which are reflected in the horizontal plane. This determines the antenna polarization.

In addition to the mirror geometry, which permits measurement of the reflected radiation, a comparative method could be direct measurements. This geometry is depicted in Figure 4.4 . The antenna is driven along the track 'OP' by AC motor. The corresponding dimensions are : WM=0.14 m, CO=CP=2 m, OP=1.1 m and angle between 'MP' and electron beam is 18.5° . The antenna position 'ϕ' is measured from the point 'P'. The corresponding 'θ' angles of the antenna with point 'C' and electron beam are given in Table IV . Analyzing all practical problems of the linac limited space and electron beam confinement, direct measurement is almost the opposite case of indirect measurement, that is there are many disadvantages and one big advantage of direct experiment. The big advantage of direct measurement is a much simpler geometry and experimental alignment. Consequently, it provides precise angular measurements, and does not make any problem with the flange etc.

Among the many disadvantages of direct measurements limited linac space and beam confinement are the most serious, and are very complex. For example, at the present

appears as though all reflected rays came from the point 'P'. This is the center of the antenna rotation. All rays measured at different angles are of the same length, which is equal to the length of the antenna bar 'R'. The radius of antenna rotation 'R' , (raylength, length of the bar) can be calculated exactly for the given mirror offset angle 'α' . However, experimental precision and actual alignment are not so exact and the approximate values for L=0.14 m are $\alpha = 20^{\circ}$, R=2.10 m . Mirror alignment and zero adjustment of 'θ' angle using a laser beam should be done before every measurement of Cerenkov radiation. Note that 'R' fits harmonics when compared with 'r_n' in Table III . So, this mirror geometry allows measurements of the radiation diagrams of all six harmonics in the limited area.

TABLE IV

Conversion from Antenna Position to Angle

d (m)	θ (°)	d (m)	θ (°)	d (m)	θ (°)
12.5	22.5	42.5	30.8	72.5	39.7
15.0	22.8	45.0	31.6	75.0	40.5
17.5	23.5	47.5	32.3	77.5	41.2
20.0	24.2	50.0	33.1	80.0	41.9
22.5	24.9	52.5	33.8	82.5	42.7
25.0	25.7	55.0	34.5	85.0	43.4
27.5	26.4	57.5	35.3	87.5	44.1
30.0	27.1	60.0	36.0	90.0	44.9
32.5	27.9	62.5	36.8	92.5	45.6
35.0	28.6	65.0	37.5	95.0	46.3
37.5	29.4	67.5	38.3	97.5	47.0
40.0	30.1	70.0	39.0	100.0	47.7

But, it is necessary to mention the main mirror disadvantage. Since the exit window has an end flange 0.09 m in diameter, due to the short emission length L=0.14 m multiple reflections are possible between the mirror and

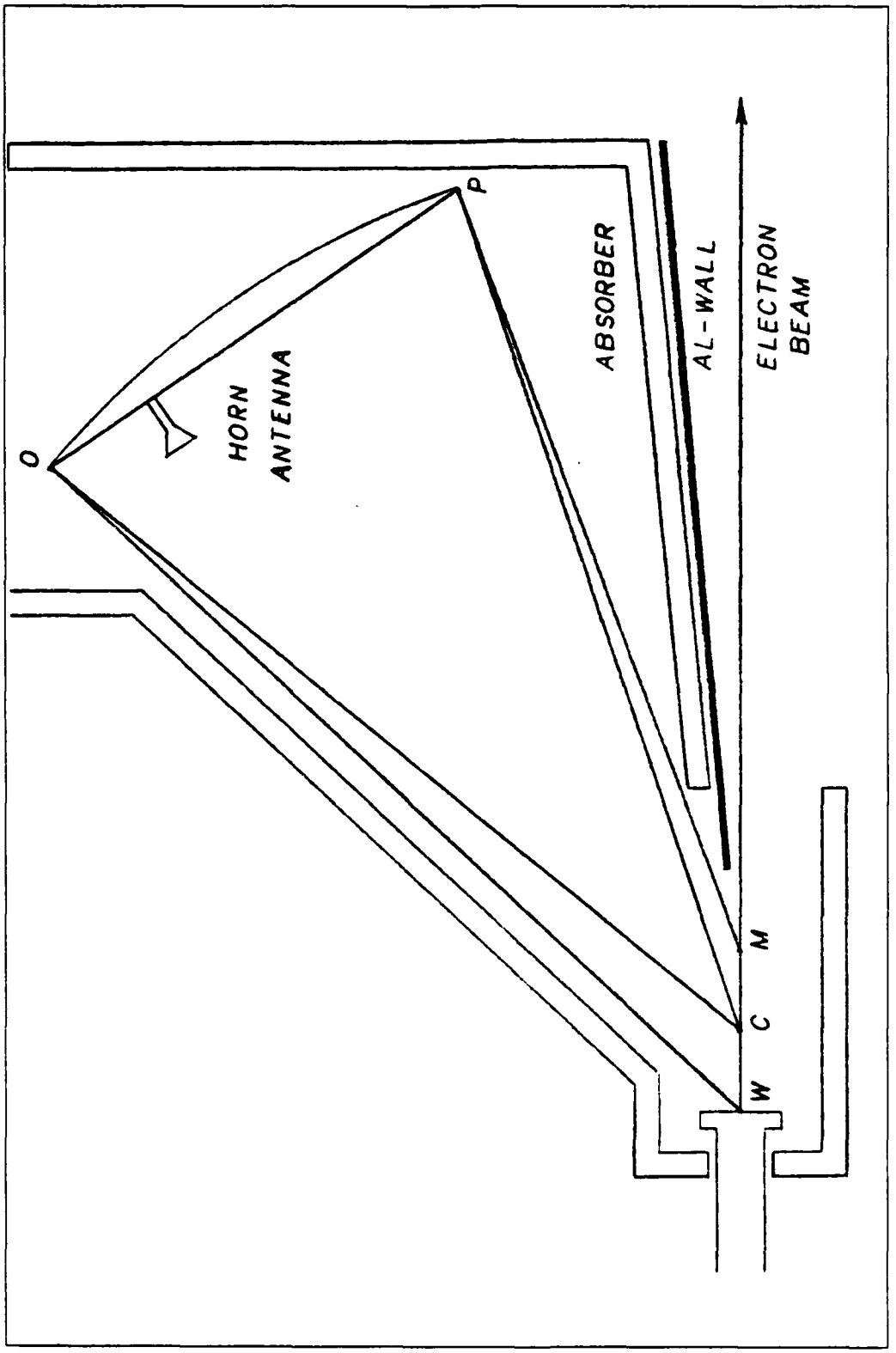

Figure 4.4 Direct Measurement.

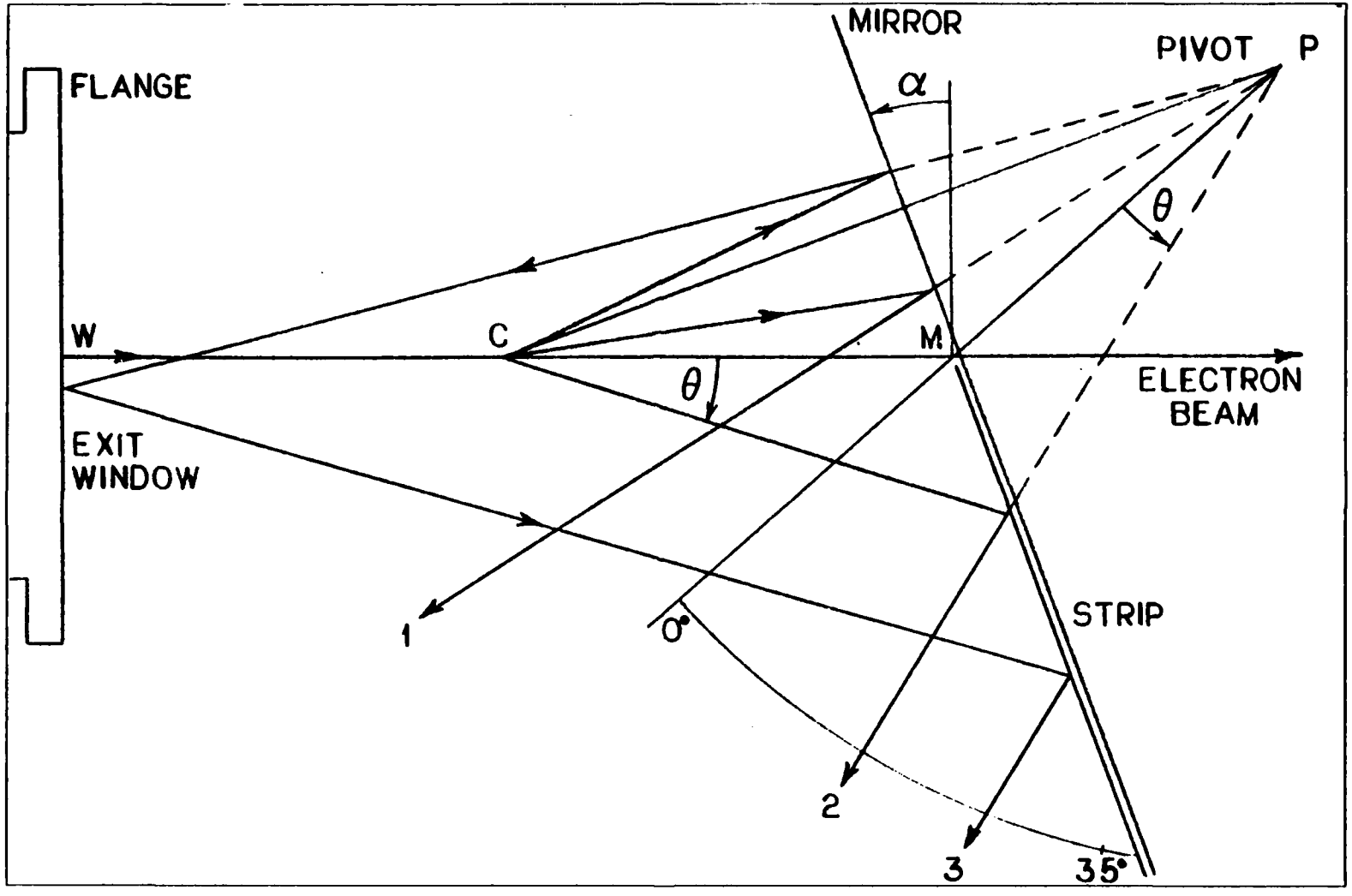

Figure 4.3 Indirect Measurement.

into a specially designed, cylindrical metalic wave guide. Coupled klystrons produce a traveling electromagnetic wave along the waveguide in TM mode. The electron speed and the wave speed are about the same, so that longitudinal electric field of the wave will accelerate electrons. Thus, the electrons gain energy at the expense of the wave. The wave speed is increased and electrons sitting on the crests of the wave are accelerated continuously. Magnets 'M' bend the electrons at different angles depending on their energy. The desired energy is selected by the slit 'S'. In this way, relativistic periodic electron bunches are produced. The electrons gain in energy and in mass getting parameter $\beta = 0.999987$. This is known as 'stiffening' of the beam. Magnetic quadrupoles 'MQ' focus the electrons at the exit window, which on their way through air cause Cerenkov radiation. Continuing their path, the electrons proceed through the mirror and secondary emission monitor (current meter) to the beam dump in the wall (last two are not shown in Figure 4.1). Due to many reasons, the beam current may vary. During the measurements it must be constantly adjusted to the prescribed value.

2. Mirror

There are many advantages and one big disadvantage of having the mirror in the experiment. Essentially, the mirror is a polished aluminum plate which reflects Cerenkov radiation and allows the electron beam to pass through. The experiment with the mirror is called indirect. The mirror geometry is shown in Figure 4.3. The actual emission region, length WM=L is a distributed line source, which is approximated by a point source at the middle point 'C' . For the short emission length and far field such an approximation is reasonable. This provides a diffraction angle 'θ' to be measured, as constructed in Figure 4.3 . The equivalent point source at 'C' has its mirror image at 'P' and thus it

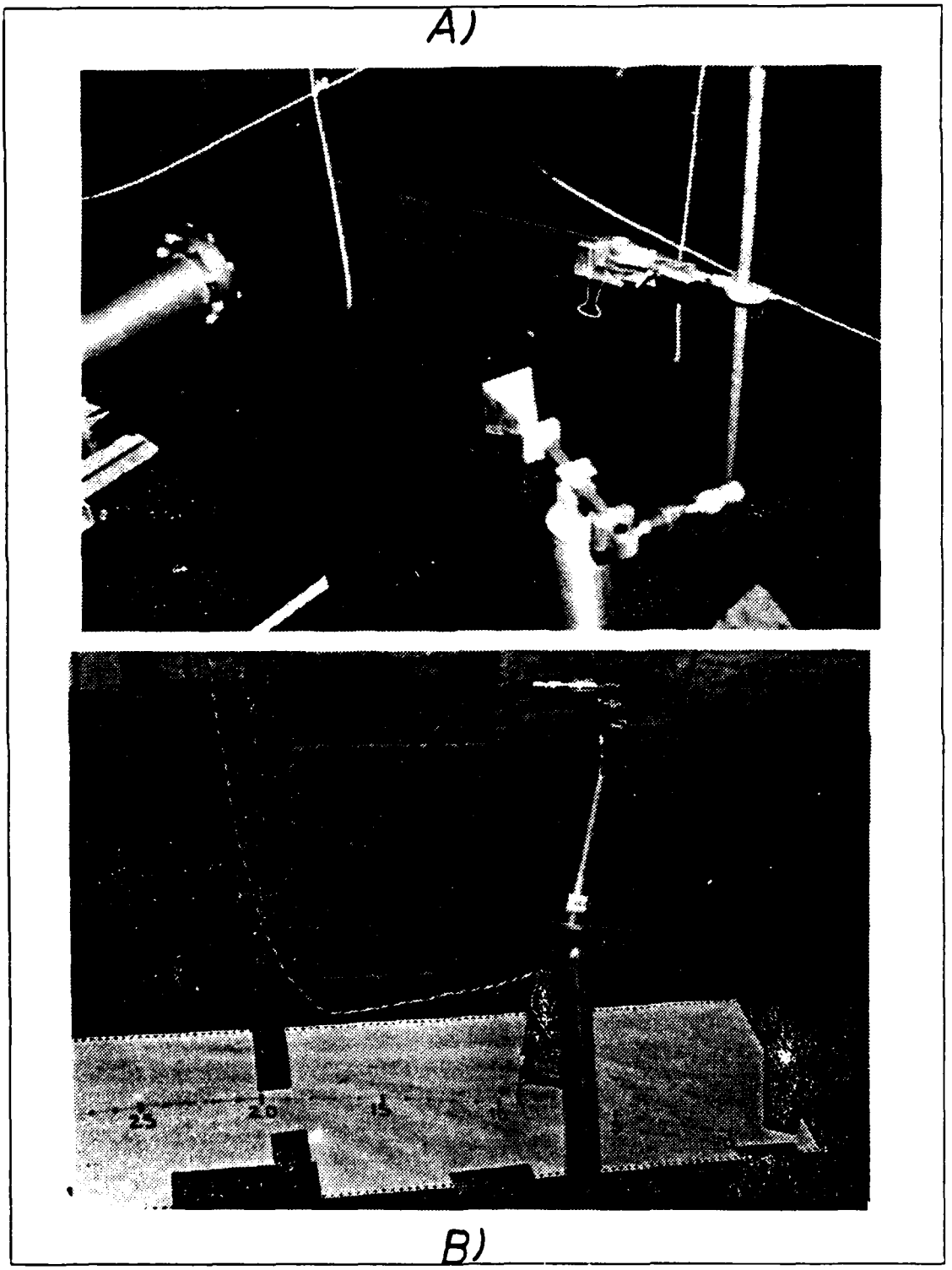

Figure 4.2 Mirror and Antenna in a) Near field, b) Far Field.

trigger to show the real time Cerenkov signal. When the signal generator simulates the Cerenkov signal it also triggers the oscilloscope. The radiation diagrams are measured by sweeping the antenna over the desired angles. The antenna is mounted on a bar with the center of rotation below the mirror and driven by an AC motor operated from the control room. The angle readings and whatever else happens in the experimental area, are observed on two monitors. Particular components of the experimental arrangement are described in the following section. Figure 4.2 shows two important details from Figure 4.1 : a) emission length from the exit window to the mirror and antenna in near field and b) antenna in far field with angular scale.

B. EQUIPMENT PERFORMANCES

Technical characteristics of the equipment are summarized in Appendix C. Since many different components of the equipment play an important role in the experiment, their performances are discussed here in the order of the signal generation/propagation.

1. Linac

The linear accelerator (linac) at the Naval Postgraduate School is used to produce high-energy electron bunches. As for general characteristics, the linac is similar to the Stanford linear accelerator Mark 3, which is 67 m long with 1000 MeV kinetic electron energy, while corresponding values of the NPS linac are 9,14 m and 100 MeV.[9] See [Ref. 12] for more informations. Principles of linac operation will be explained using Figure 4.1 . Electrons having parameter β=0.5 are injected by the gun

[9]Linac parameters are given in Table IX ; Electron beam parameters are given in Appendix B .

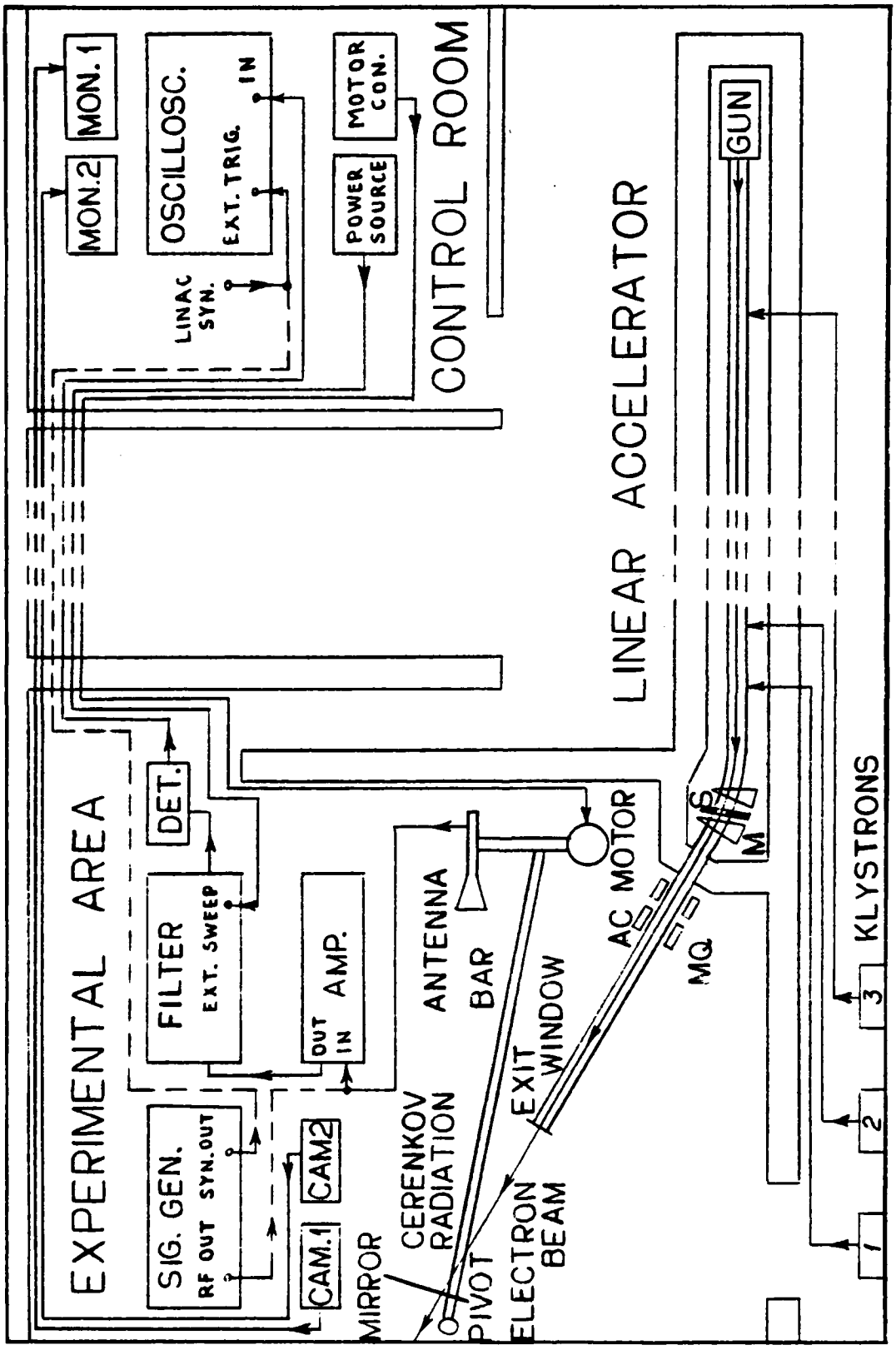

Figure 4.1 Experimental Arrangement.

TABLE III

Far Field for Emission Length 0.14 m

j	ν_j (GHz)	λ_j (m)	r_n (m)	θ_n (deg)
1	2.8557	0.1050	0.373	75.5
2	5.7114	0.0525	0.746	51.3
3	8.5671	0.0350	1.120	41.4
4	11.423	0.0263	1.490	35.7
5	14.278	0.0210	1.866	31.8
6	17.134	0.0175	2.240	28.9

cable and movable absorbers. The desired harmonics are selected by a tunable YIG filter which has narrow bandwidth. The important theoretical assumption of finite emission length is achieved placing an aluminum plate (mirror) across the electron beam line at L=0.14 m and measuring the reflected radiation. This is the concept in short.

The experimental setup is shown in Figure 4.1 . The linear accelerator produces an electron beam, which causes Cerenkov radiation in air. During the linac experiment the experimental area is dangerous, because of γ, X and neutron radiations. Therefore, the majority of the instruments is in the experimental area under remote control from the control room (AC motor, filter) or with appropriate initial settings (filter, cameras, amplifiers). A signal generator is used only for calibration and equipment check, when it simulates the Cerenkov signal. During the actual experiment the Cerenkov signal from air is captured by the antenna and amplified by the amplifier. The desired harmonic is selected by the filter, which is adjusted by the power source from control room. After detection at the detector the signal travels via double shielded coaxial cable to control room. The oscilloscope is synchronized by the linac

IV. EXPERIMENTAL APPARATUS

This experiment represents continuation of the previous work, which is summarized in [Ref. 7]. The method is modified due to new aims. Many more microwave components of equipment had to be employed and therefore, the equipment characteristics are emphasized to show experimental possibilities and problems .

A. EXPERIMENTAL CONCEPT

Experimental design is based on the theoretical results and assumptions, which are described in the preceding chapters. In order to measure radiation diagrams and absolute power of Cerenkov radiation, the measurements should be done in the far field. From the physical picture of the radiation, see Figure 2.1 , the emission length 'L' may be treated as a distributed line source. The corresponding formula for the distance to the far field is, [Ref. 11],

$$r_0 \doteq \frac{2L^2}{\lambda_i} \qquad (4.1)$$

Performing the necessary computations, optimum values which fit the linac experimental area for the desired measurements are found for L=0.14 m and given in Table III . Values 'θ_n' are the main lobe spreadings, or the first nulls in the diffraction patterns like in Figure 2.2 . Calculation of all experimental parameters is given in Appendix B .

A weak Cerenkov signal and electromagnetic noise are problems in the far field. Solutions of these problems, are provided by TWT amplifiers and a very sensitive oscilloscope. Noise reduction is done by double shielded coaxial

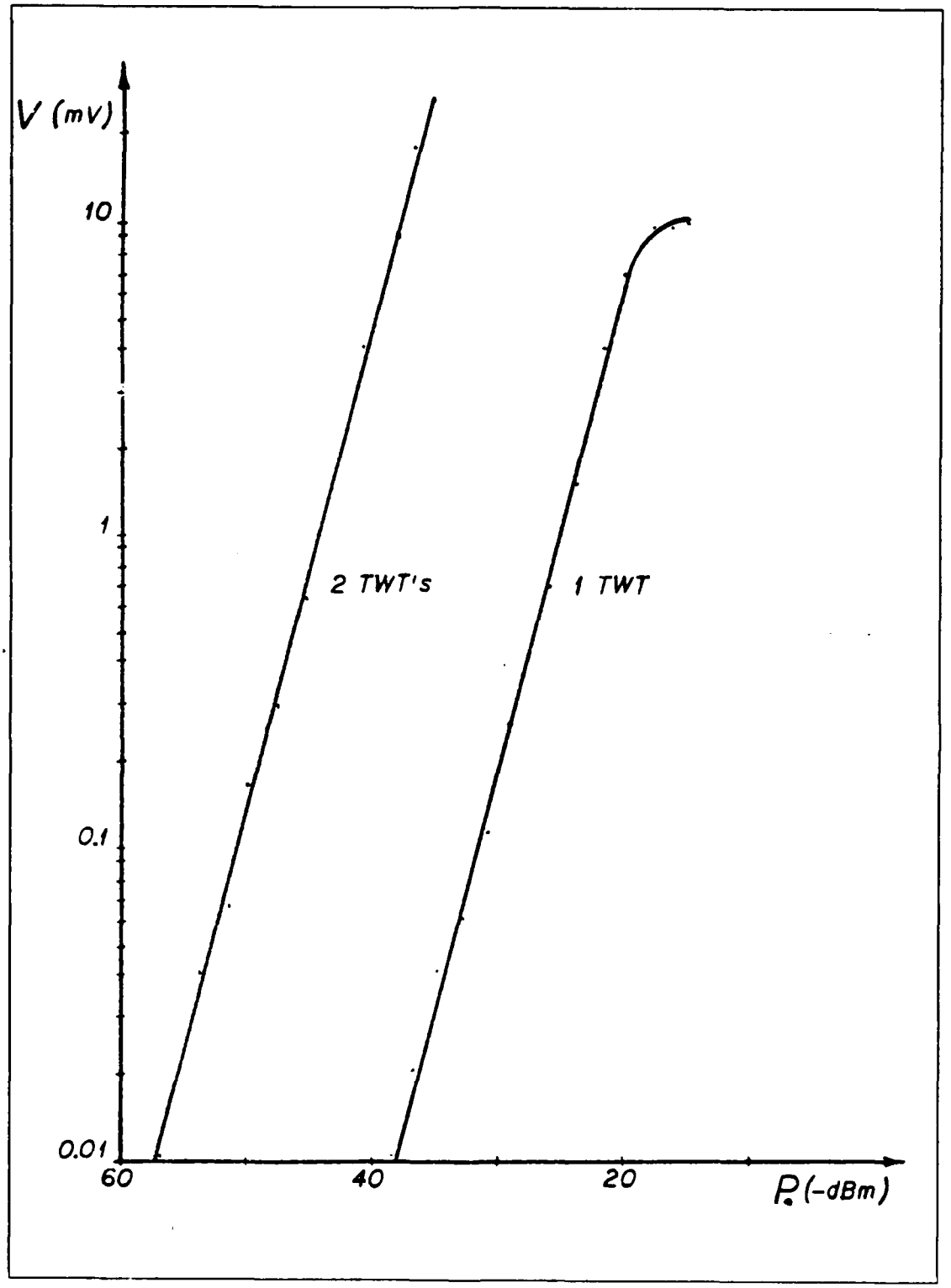

Figure 4.7 Calibration Curves for the Third Harmonic.

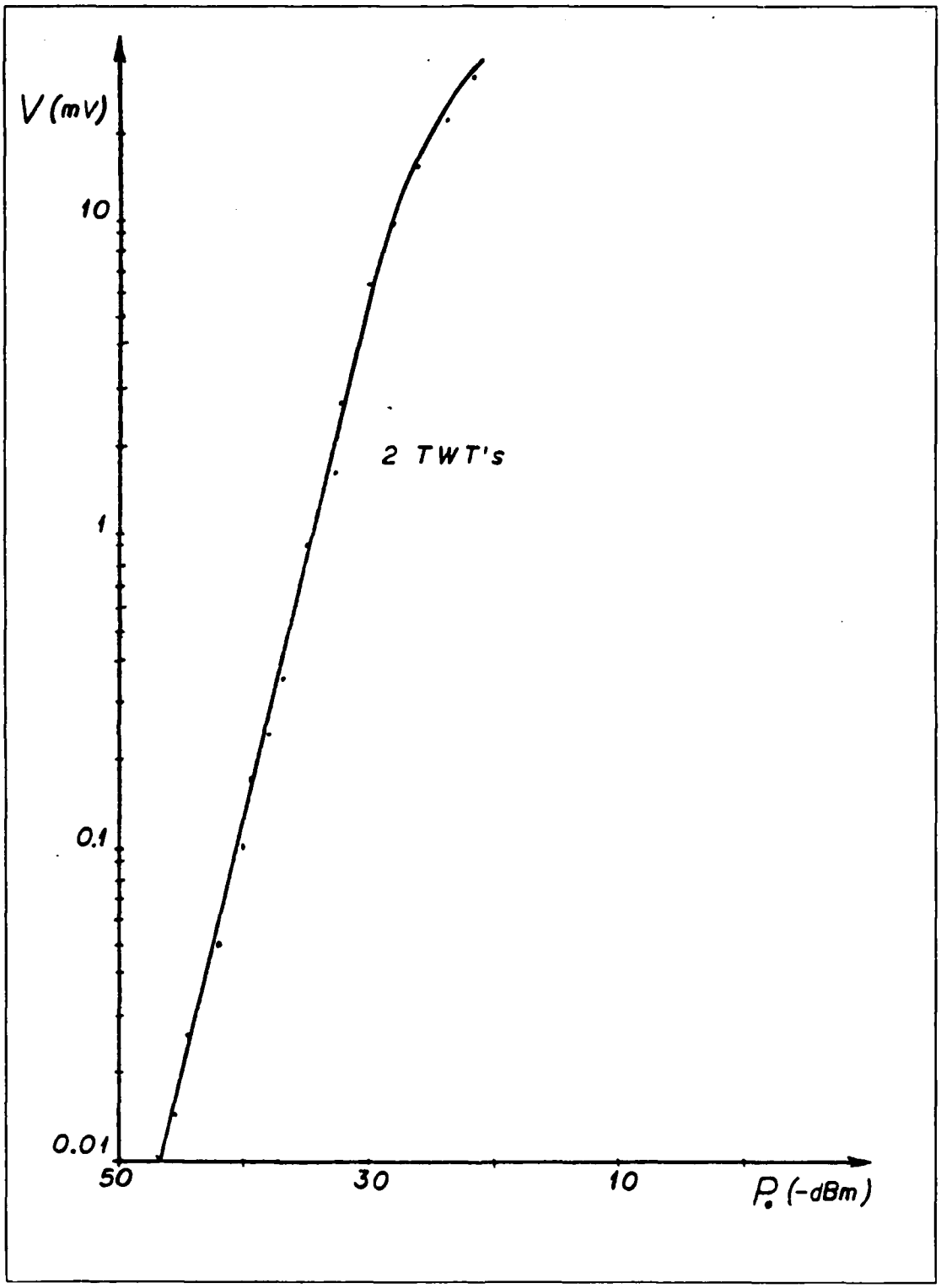

Figure 4.8 Calibration Curve for the Fourth Harmonic.

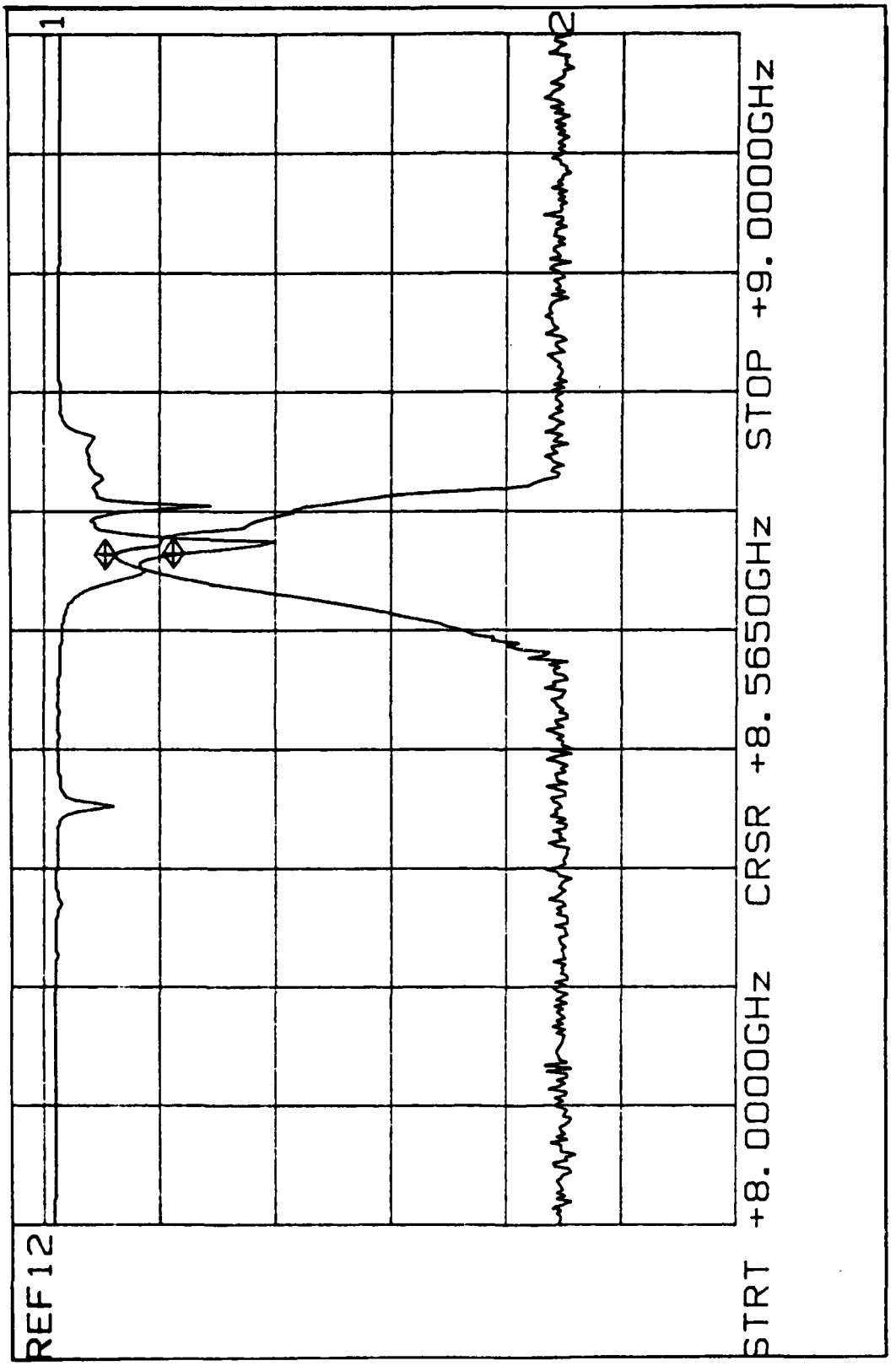

Figure 4.9 YIG Frequency Characteristics.

is the peak power in 1 μs, and as a matter of fact, these two powers coincide. To conclude, the TWT's provide important amplification, but they must be used with appropriate calibration curves to avoid undesired nonlinearity and saturation.[10] A certain precaution is required for a very low signal of the order of 10 μV . Some of the calibration curves are nonlinear at this range, which is not shown in the figures because it limits the lowest measurable signal in this experiment. Also, the curves may differ slightly for different TWT's and signal generators in the same arrangement and for the same frequency.

5. Filter

Without doubt, the YIG filter is great improvement for harmonic measurements in microwave Cerenkov experiment. Technical characteristics of the filter listed in Appendix C are fascinating. It is tunable over the first six harmonics, very narrow bandwidth and high selectivity. This is exactly what is needed to select desired harmonic and improve its signal to noise ratio. The insertion loss <8 dBm can be easily compensated by TWT amplification. Frequency characteristics of the YIG filter is shown in Figure 4.9 .

There are two curves shown, numbers 1 and 2 at the right side. Curve # 1 is signal reflection and curve # 2 is signal transmission by YIG. Horizontal scale is from 8 to 9 GHz with the cursor marking 8.565 GHz point on both curves. Vertical scale is 10 dBm/div. with zero reference level, as shown at the left side. The cursor at the top of the curve #2 shows the YIG insertion loss -6.07 dBm. Down by 3 dBm , frequency bandwidth is about 22 MHz .

---

[10]All calibration curves are done with 50 Ω matching impedance at oscilloscope, except the upper curve for 1 TWT in Figure 4.5 which is done with 5.6 kΩ. In the case of a very weak signal this provides much biger detected signal at the oscilloscope but it is much wider (mismatching).

However, the case is not quite ideal. Frequency accuracy of the filter control unit and linac frequency instability may likely run out of the narrow bandwidth and the signal is lost if the filter operates in CW mode (fixed frequency setting). On the other hand, SWEEP mode, when YIG bandwidth sweeps over desired frequency range, is not convenient for the measurement by oscilloscope (the signal appears and disappears in short time intervals). The third choice is EXT. mode, when YIG is tuned by an externally applied voltage from 1 to 10 V . This still generates a problem for manual adjustment at the peak of the bandwidth, along with beam current adjustment during the measurement, but it was accepted as the best filter operating mode for this experiment.

6. Detector

The main concern for the detectors is their maximum input power and sensitivity. Fortunately, they are available at all frequencies with good sensitivity to detect Cerenkov signal of the order of μW . Thus, if the sensitivity is 0.15 $mV/\mu W$, this will produce a detector output about 1 mV and less, which is attenuated for example by 10 dB along double shielded cable and easy measurable by the oscilloscope. Of course, 10 μV/div. sensitivity of the oscilloscope is an important parameter for detection too.

According to the maximum Cerenkov signal and TWT amplification, there is no chance that the detector will be burnt out. Maximum signal at the oscilloscope for calibration curves (greater than any Cerenkov signal) does not exceed 150 mV . Considering the 10 dB attenuation by the double shielded cable and a detector sensitivity of the 0.15 $mV/\mu W$, the input detector power is 3.16 mW , much less than the allowed 100 mW . So, the detectors satisfy the experiment completely.

7. Cables

Generally, cables make more problems than benefits in delicate experiments due to attenuation, poor connectors etc. This is the case in Cerenkov experiment, too . The only exception is double shielded cable which eliminates outer electromagnetic noise.[11] Special precaution must be taken with respect to connectors. They must be checked and tightened properly, otherwise the signal may be drastically changed and even lost.

8. Oscilloscope

For the signal observation and measurement it is advisable to use an oscilloscope, which shows effects on the signal in time. Particularly, the maximum signal at a fixed angle indicates beam current and the YIG adjustment and its shape may reveal undesired saturation, integration etc. A vertical differential amplifier is used as a very sensitive device with 10 μV/div. Even the displayed noise of 16 μV/div cannot make this feature worse. Cerenkov pulse width is 1 μs, so that it is observed nicely with 1 MHz bandwidth. Just as the TWT's improve the amplification and the YIG improves the frequency selection, the oscilloscope vertical differential amplifier improves the signal sensitivity.

9. Power Supply

It has been mentioned that the accepted YIG operating mode is EXT. with external frequency adjusting. Any power supply providing 0 to 10 V DC may be used. Figure 4.9 shows a very narrow bandwidth, which produces a problem for precise manual adjustment at the top of the curve # 2 . The

---

[11]The cable attenuation is measured by using the experimental setup in Figure 4.1 and the signal from the signal generator modulated by 1 μs and 60 Hz . See Appendix C for the values.

solution is an additional potentiometer of 50Ω and ten turns for fine tune, which is connected in series with the 50KΩ potentiometer of the power supply. Coarse adjustment should be done decreasing the voltage by the 50KΩ potentiometer until the signal is found. Further voltage decreasing and fine adjustment of the signal maximum is possible by the 50Ω potentiometer. This provides rather stable and precise YIG adjustment for stable signal. The opposite method, that is increasing the voltage does not work effectively.

10. Absorber

At the time of the experiment there was not much information about black spongy absorbers, except that they may be used both as acoustic and electromagnetic absorbers. In order to determine their efficiency for electromagnetic absorption, a simple experiment was arranged modifying the original experimental setup Figure 4.1 . Cerenkov radiation was replaced by the equivalent signal produced by signal generator and transmitting antenna (not shown) . The testing absorber was placed between the transmitting and receiving antennas and absorption effect was observed with an oscilloscope.

At the frequency of the third harmonic ν_3=8.568 GHz absorber 0.075 m thick lowers the signal on the oscilloscope from 10 V to 30 μV . However, at the frequency 7 GHz the same signal is lowered to 75 μV. At higher frequency 11 GHz the signal is attenuated below our sensitivity.[12] This says that as long as signal levels are below 10 mV , the absorber is sufficient for harmonics 3, 4, 5 and 6 . For the first two harmonics absorber thickness must be increased. However, 0.02 m thick absorbers are not effective even if doubled, so

[12] For the values of the absorber measurements see Table VIII .

it is better to use the 0.075 m thick absorber. This testing may be used as a reference for particular measurement with absorber shielding.

A good experimental procedure would be first to have the antenna sweep over all angles and absorber in front of the mirror, when no signal is detected. This should confirm that no other signal than Cerenkov will be measured. In this experiment absorbers are used mainly to shield out the klystron electromagnetic noise in the experimental area.

11. Signal Generator

The purpose of the different signal generators is to replace Cerenkov signal whenever is possible. This saves complicated and expensive linac operation and simplifies the experiment. Reference signal from signal generator corresponds to Cerenkov signal at particular harmonic frequency, pulse repetition frequency 60 Hz and pulse width 1 μs . Adjustable peak output power covers the Cerenkov dynamic range. Thus, equivalent signal from signal generators is used for calibration curve measurements, cable attenuation measurements, absorber testing and equipment check whenever something goes wrong with Cerenkov signal.

Perhaps power accuracy $\pm$2 dBm and frequency accuracy $\pm$1% are not the best choice of a reference signal in the case of absolute power measurements, but uncertainty due to other factors is greater. So, these signal generators are both very helpful and satisfy the experiment .

V. EXPERIMENTAL RESULTS

In order to measure radiation diagrams and absolute power of Cerenkov radiation for different harmonics, there were conducted three experiments at different periods during the year. They were based on the experimental concept as described in subsection A chapter IV including some additional measures aimed to explain unexpected result : spikes in the radiation diagrams.

A. FIRST EXPERIMENT

The very first measurements were a short repetition of what was done in [Ref. 9 , 10]. Later, new equipment was introduced one at a time according to the experimental arrangement depicted in Figure 4.1 . The purpose of the measurements was to become familiar with Cerenkov radiation and equipment. This experiment had to confirm applied experimental method and reveal some problems.

1. Initial Measurement

The Cerenkov signal was measured for emission length WM=L=0.89 m , see Figure 4.3 . X-band antenna was swept along the track perpendicular to the line 'MP' and at a distance of 0.99 m from the mirror. Cerenkov signal was detected and led to the oscilloscope in the control room. Both sides of the Cerenkov cone were observed. The signal was changing gradually, as predicted by theoretical curve Figure 2.4 for one side of the cone. The maximum detected signal is shown Figure 5.1 a). After that, the TWT amplifier was introduced between the antenna and detector, which increased the signal about eight times.

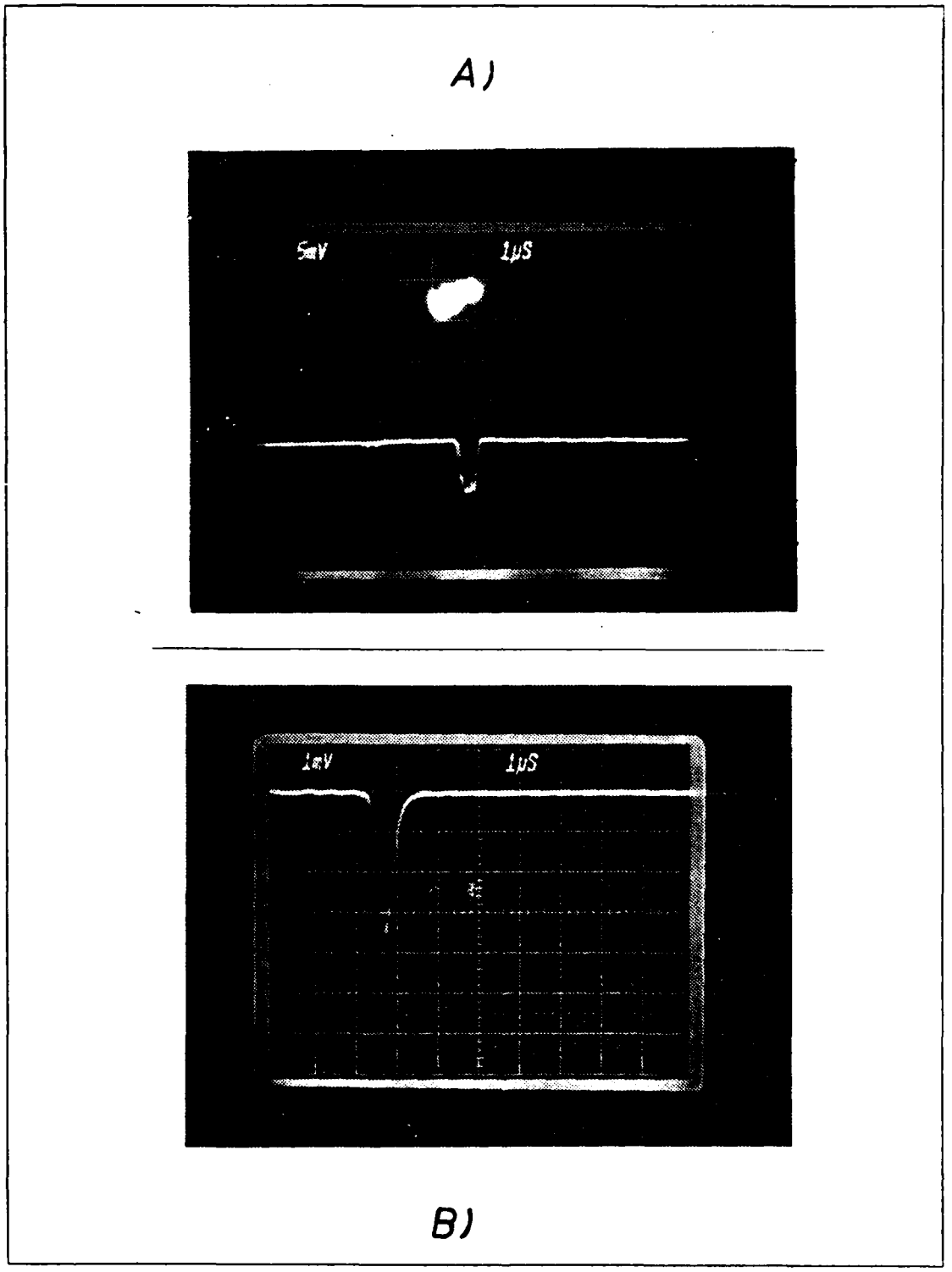

Figure 5.1 Cerenkov Signal in a) Near Field, b) Far Field.

The following measurement was done for the arrangement in Figure 4.1 . Note that emission length was L=0.14 m and the bar length R=2.1 m . Power amplification by the TWT was just enough to observe the signal in X-band. However, the signal could be hardly measured due to its weakness. This problem was successfully solved by introducing the oscilloscope vertical amplifier, having the sensitivity 10 μV/div. The final goal was to select one of the harmonics, so the YIG filter was introduced. This was the critical point when the signal was lost. The insertion loss of the YIG was high and its narrow bandwidth had to be adjusted for maximum transmission (two changes at a time !).

The case became quite interesting when two TWT's provided good amplification and the YIG was adjusted to transmit the third harmonic. An additional signal grew up from the noise together with Cerenkov signal. Also, when the antenna was sweeping over the angles from 0° to 45° , the signal was not changing gradually, as predicted by Figure 2.2 for j=3 , but showed many minima and maxima following the theoretical curve.[13] This was the unexpected result !

At this point Cerenkov experiment stopped and all efforts were directed to eliminate or explain the additional signal and the minima and maxima (spikes) .

2. Noise Reduction

It was obvious that the additional signal came through the antenna. A simple test verified this, since for a blocked antenna aperture the signal was not detected. What could be observed on the oscilloscope is shown in Figure 5.2 a) . Cerenkov signal width is 1 μs , so that it could be recognized as right hand signal (lower peak) . The additional signal is on the left hand side (higher peak)

---

[13]Later-on these minima and maxima became quite famous, so that they were named 'spikes' .

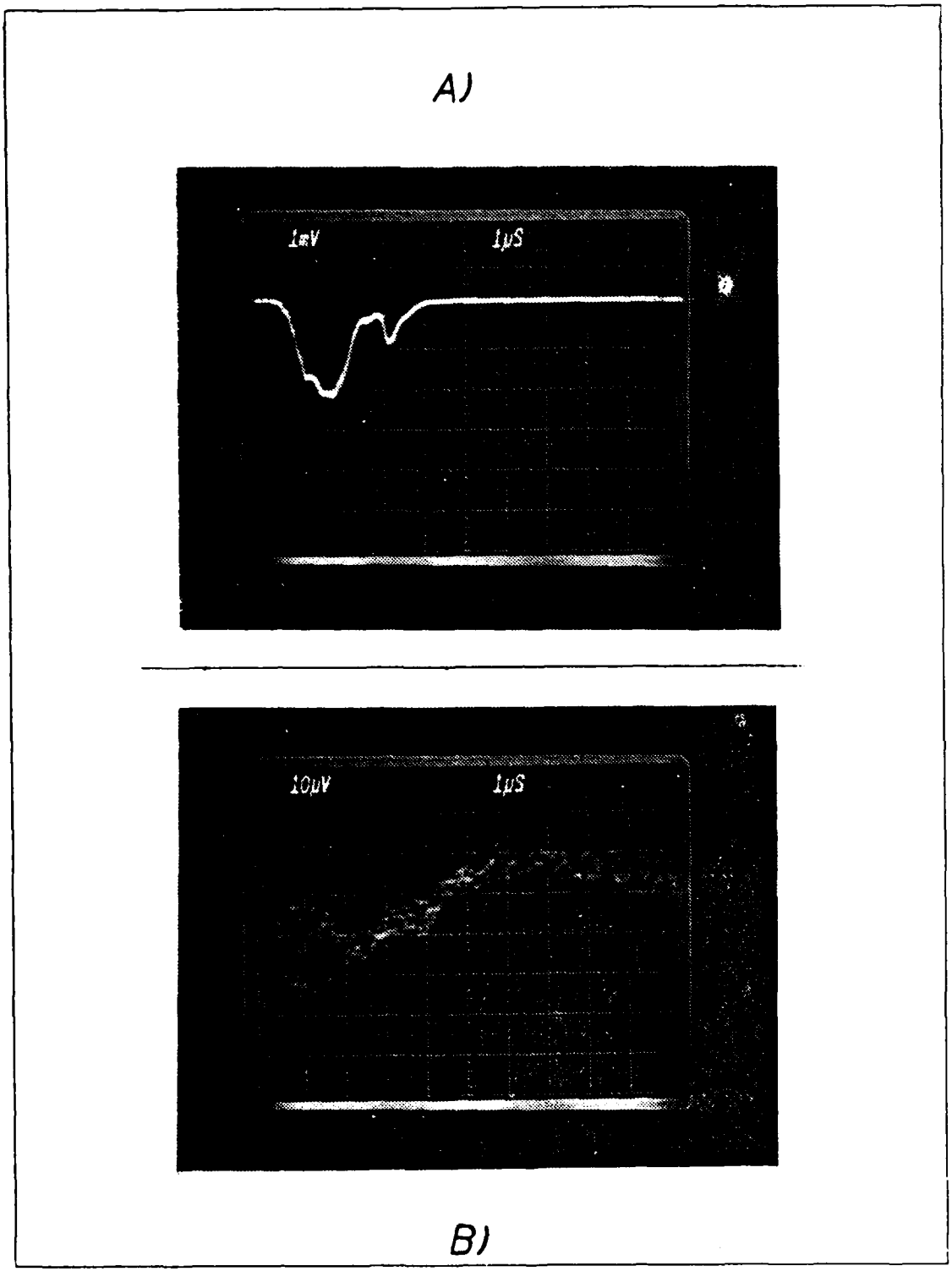

Figure 5.2 Experimental Room : a) Cerenkov Signal and Klystron noise, b) Reduced Klystron Noise.

having width 3 μs. This was a very useful information which helped to identify the signal as the linac klystron signal (noise). From Figure 4.1 it was obvious that the klystron noise could come into the antenna through the door in front of the klystron #1 , since complete experimental area and linear accelerator are shielded by thick wall and lead bricks. When the klystron door was closed by aluminum plates the oscilloscope showed the signal in Figure 5.2 b) . This figure does not show Cerenkov signal but reduced klystron noise only. Klystron noise may be observed separately if the electron beam is not produced. Also, Cerenkov signal may be observed separately when the klystron door is closed. These two cases are shown in Figure 5.3 a) and b) to confirm previous discussion.

Klystron noise has been a continuing problem, which has been partially alleviated by using double shielded coaxial cable between the experimental area and the control room. Klystron noise present in the control room having an ordinary coaxial cable is shown in Figure 5.4 a) . Double shielded coaxial cable reduces this noise as shown in Figure 5.4 b) . The rest of the noise is oscilloscope display noise.

3. Radiation Shielding

The other problem, that of spikes in the radiation diagram is much more involved than the klystron noise. The first guess was that the spikes were interference of the desired Cerenkov radiation with some undesired reflections. In Figure 4.3 ray #3 illustrates the possibility of the reflected opposite side of Cerenkov cone. This was experimentally verified inserting the absorber between the flange and mirror, which considerably reduced the detected signal. The absorber efficiency was also tested as summarized in Table VIII .

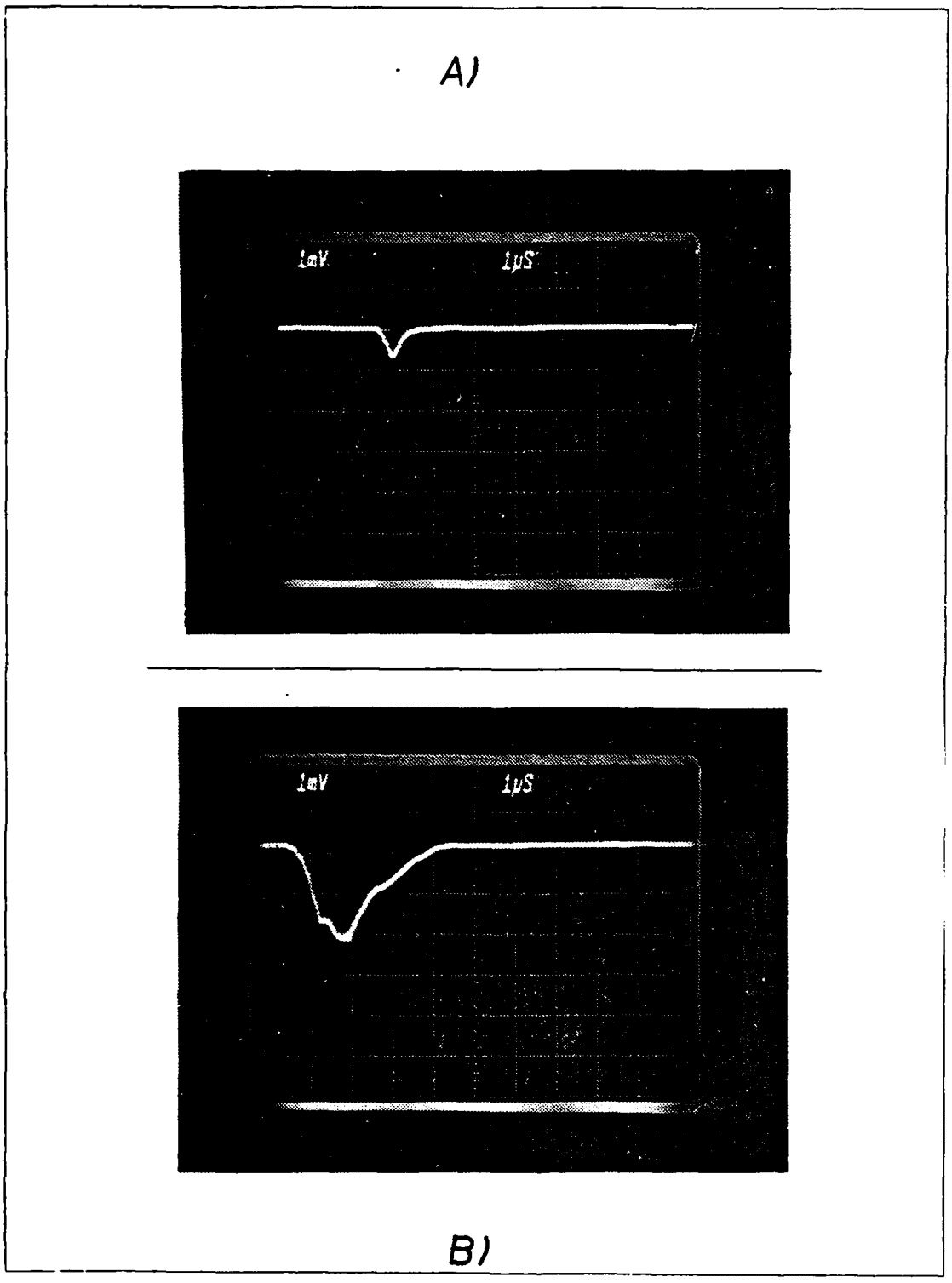

Figure 5.3 Experimental Room : a) Cerenkov Signal, b) KLystron Noise.

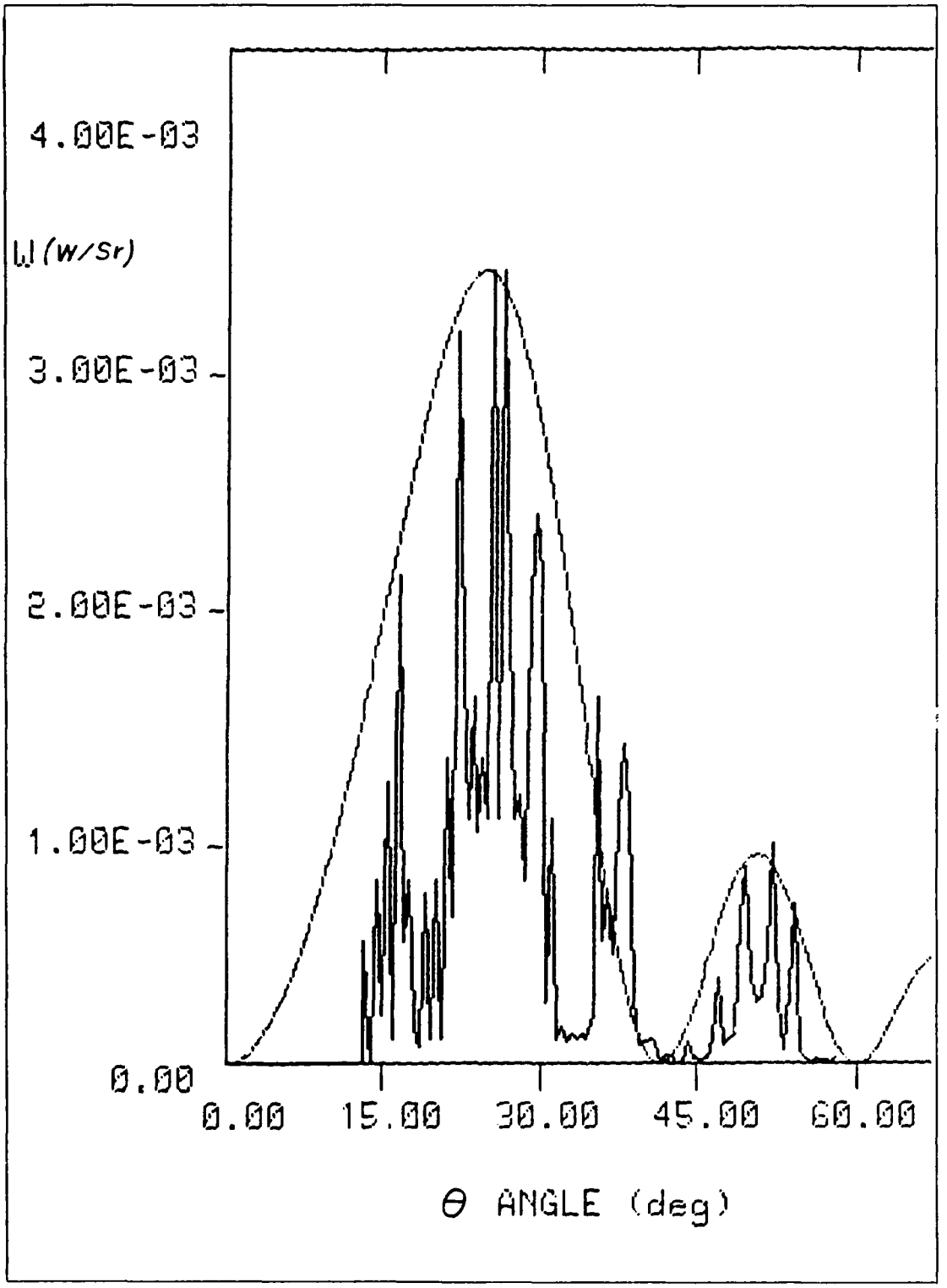

Figure 5.9 Second Experiment : Data for the Third Harmonic.

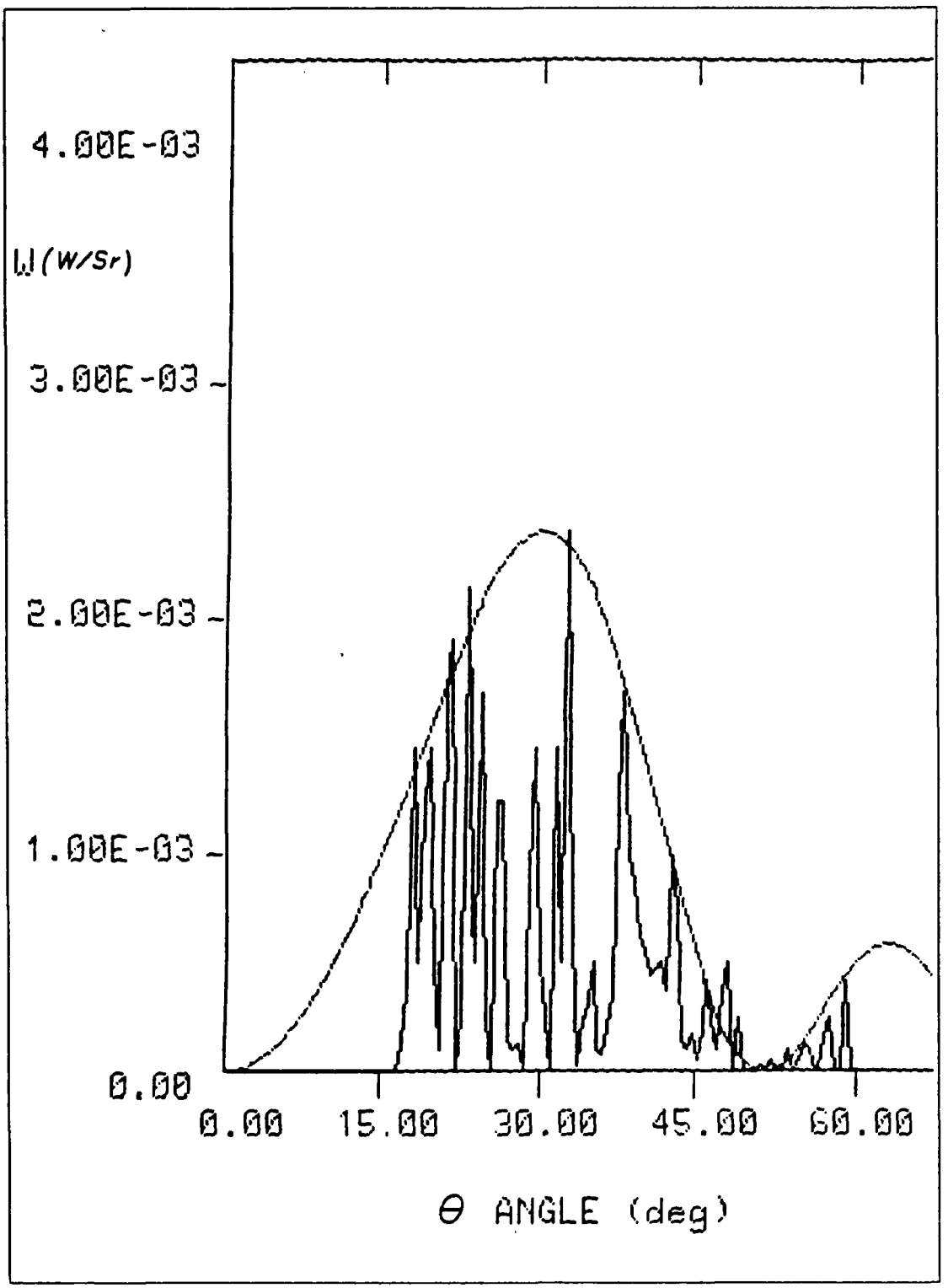

Figure 5.8 Second Experiment: Data for the Second Harmonic.

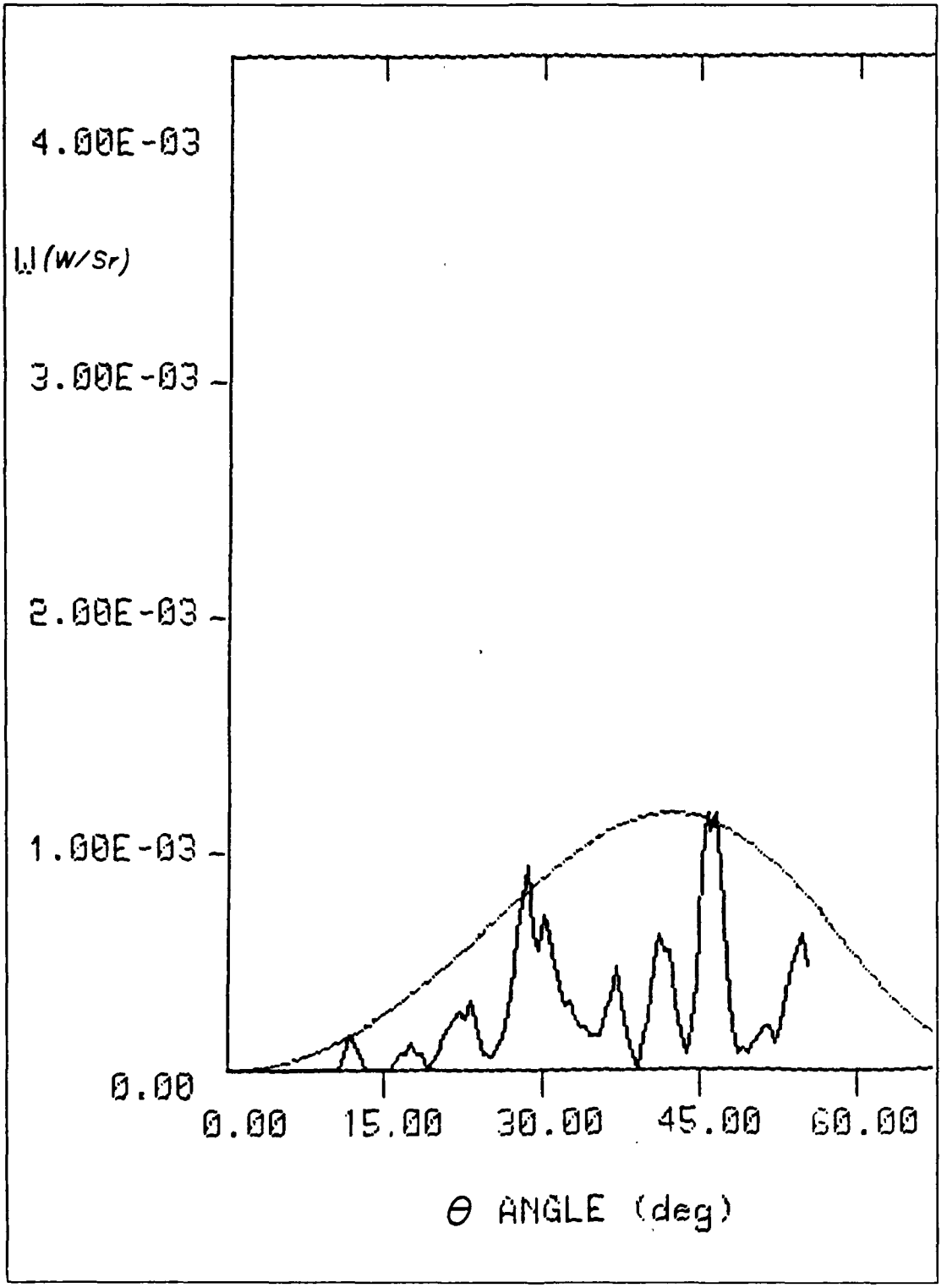

Figure 5.7 Second Experiment : Data for the First Harmonic.

linac slit opening 'S_e' . It was observed that S_e =50 provides a stronger detected signal than S_e=300 for the beam current Iav=20 $\times 10^{-8}$ A in the far field, by almost a factor of two. Complete measurements were done for the fourth harmonic, and these two slits having fixed values of the other experimental parameters, but the spikes still appeared at the same angles.

For the same experimental parameters as listed in Table VII , the 'spiked' experimental data for the first, second, third and fourth harmonics are given along with the smooth theoretical curves in Figures 5.7 , 5.8 , 5.9 , 5.10 respectively. Corresponding angular shifts are given in Table V . The beam current was Iav=20.0 $\times 10^{-8}$ A and slit opening S_e=225 . The data were taken in steps by 0.5 degrees. The calibration curves which are used for this data set are given in Figures 4.5 , 4.6 , 4.7 , 4.8 .

Corresponding measurements with the available equipment and standard experimental parameters in Table VII, for the fifth and sixth harmonics were not successful. Namely, having Ku-band antenna and detector only in the near field, a small Cerenkov signal was detected. When the YIG filter was inserted for a harmonic selection, due to its insertion loss, the signal was lost. Note that TWT amplifiers were not available for Ku-band.

Maximum radiation intensity for the first and second harmonics was calculated by equation 5.1 and for the third and fourth harmonics by equation 5.2 . The procedure was as described in subsection A4 above. Corresponding data are summarized in Table VI .

2. Discussion

In spite of all additional measures for the precise measurements, the spikes are still present in the radiation diagrams. A simple comparison for the second and third

B. SECOND EXPERIMENT

This experiment was a continuation of the first experiment and the effort to resolve the spikes in the radiation diagrams. According to the analysis in the subsection A5 above, the following refinements were done in the original experimental setup , Figure 4.1 . The mirror was replaced by the strip with an additional absorber shielding as shown in Figure 4.2 a) . A special precaution was taken to maintain the same beam shape and constant beam current for each data reading. Also, a series of different tests was done to check validity of the experimental data.

Another aim of this experiment was to expand the measurements to all other achieveable harmonics, from one to six, which was possible with the available equipment. In this way, the additional informations could help better understanding of the radiation diagrams and power.

1. Second Data Set

There had been performed several short tests before the final data were taken. Although the calibration curves provide information about the occurrence of saturation effect, it was tested again by a single linac pulse for the maximum detected signal. In all checks, a single pulse produced exactly the same detected signal as the pulse train. In an exit window test, a four times thicker exit window did not change the spikes at a certain angular range. However, the antenna located in the near field, see Figure 4.2 a) provided a smooth radiation diagram, as expected. Of course, the signal in the near field was much stronger and the attenuator was inserted to avoid saturation.

Reproduciblity of data for a particular measurement with the same Cerenkov pulse shape and constant beam current was obtained. However, an additional variable appeared as

7. The Cerenkov pulse shape was changeable for different linac adjustment having different amplitude. This is a very important parameter and rather unknown ;
8. Linac exit window may be a possible source of Cerenkov radiation, which could interfere with weak Cerenkov radiation along the emission length ;
9. A certain bending of linac traveling wave ;
10. Backward Cerenkov radiation for large angles.

In short, since the generated Cerenkov signal is weak, any other small signal or small change of the standard experimental conditions and theoretical assumptions is capable of changing the measured signal. This extra sensitivity of Cerenkov experiment is the price for the far field measurement in the small experimental area. The listed possible reasons for the spikes were not considered properly in this experiment. Probably, there are some more relevant factors. A particularly interesting question is if the spikes reproduce themselves in successive measurements. The second experiment took account of some of them.

Absolute power measurement requires complete solution for the spikes. Some equipment components of better quality should be employed too, such as better TWT amplifiers, signal generators etc. At this point they all satisfy because uncertainty in power due to the linac and the other factors causing the spikes is much higher. In spite of that, the method introduced here offers rather close results having in mind all uncertainties of the spikes. This does provide a good confidence that Cerenkov measurement had to be done in the far field as it was. Unfortunately, (or fortunately) the far field revealed many new questions, which ought to be answered.

To conclude, the applied method for the radiation diagrams and power measurement of Cerenkov radiation satisfies and offers new theoretical and experimental interest.

angular resolution less than 0.5° . If the spreading were less, the antenna could not tell a minimum between two neighboring maxima. The experiment would show a smooth curve which follows the theoretical one to some extent. This may explain that the second harmonic with larger angular spreading shows more space between the spikes. So, the far field measurement combined with a short emission length provided the conditions for the observed spikes.

A possible reason for the spikes could be :

1. Some reflections caused by Cerenkov radiation from the emission length, if it could survive multiple reflections from the walls and come to the antenna ;
2. It is possible that the absorber did not perform properly in blocking the opposite side of Cerenkov cone. Its exact alignment along the beam was really problem. It is fairly certain that secondary Cerenkov radiation did not interfere, since it was experimentally tested (see subsection A4) ;
3. A very good reason for the spikes is instability of the linac current during the measurements, which varies the detected signal drastically, although it was considered during the measurements ;
4. The medium, air is rather unpredictable. Let us recall that the air molecules produce the radiation getting polarized by the electrons. The only way how the air comes in the theory is with constant index of refraction ($n>1$) . However, the temperature, the density and the humidity of air were very changeable during the experiments ;
5. The assumed single bunch charge density or form factor $F(k)$ to bee Gaussian, must be reconsidered ;
6. The theory assumes undistorted electron bunches of negligible radial extent, but the beam dispersion was observable even at the short emission length of 0.14 m ;

spikes in the radiation diagrams need appropriate theoretical explanation and further experimental research to be accepted or rejected. In more detail, this experiment may be explained as follows.

The crucial change in the experiment is measurement in the far radiation field. Note that the initial measurement with emission length L = 0.89 m for the third hármonic (X-band) gives far field, equation 4.1

$$r_0 = \frac{2L^2}{\lambda_3} = \frac{(2)(0.89^2)}{(0.035)} = 45.26 \quad m \quad ,$$

which means that the initial measurement at 1 m was done in the near field. However, far field measurement in the linac limited space implies short emission length of 0.14 m and weak Cerenkov signal with large angular spreading in the radiation diagrams. This was the beginning of the problems.

The weak Cerenkov signal is quite comparable with the klystron noise, see Figure 5.3 . It is also much weaker than the secondary Cerenkov signal, which causes undesired reflections. Noise reduction and radiation shielding decreased this influence to the lowest achieveable level, as shown in Figure 5.4 b) . The Cerenkov signal was amplified and selected properly so that it could be measured on a very sensitive oscilloscope. Also, appropriate calibration curves were used to fit this signal into the linear amplification. No doubts, these measures provided far field measurements. The method and approach look correct.

However, experimental spikes in the radiation diagrams disagree with the smooth theoretical curves, see Figures 5.5 , 5.6 . They are wider than the theoretical curves, which may mean that the mirror was slightly convex. A certain angular shift may be associated with the misalignment of the zero of 'θ' angle. The measurements at R=2.1 m with a large angular spreading (short 'L') provided

TABLE V

Angular Shift of Experimental Data

(unit: degree)

j	1	2	3	4
1st exp.	-	7	2	-
2nd exp.	10	16	13	10
3rd exp.	0	0	0	0

λ_2=0.0525 m and the bar length R=2.1 m. Thus, maximum radiation intensity for the second harmonic by equation 5.1

$$W_m = \frac{(2.5\times10^{-6})(4\pi)(2.1^2)}{(6.31)(0.0525^2)} \doteq 7.9 \quad mW/Sr \quad .$$

Compared with theoretical value from Figure 5.5 Wm=6.3 mW/Sr, this gives a relative error of 25 % .

The maximum detected voltage for the third harmonic Vm=13 mV reads P_o=-37 dBm in Figure 4.7 for 2 TWT's . Including the 4 dB attenuator this gives Pm=0.5 μW . Thus, the maximum radiation intensity for the third harmonics by equation 5.2

$$W_m = \frac{(0.5\times10^{-6})(2.1^2)}{(0.7)(0.03\times0.04)} \doteq 2.6 \quad mW/Sr \quad .$$

Compared with theoretical value from Figure 5.6 Wm=3.3 mW/Sr, this gives a relative of error 21 % .

5. Discussion

Generally, this experiment showed many practical problems in the efforts to make a precise measurement of the radiation diagrams and power in the far radiation field. It is obvious that practical problems and theoretical results are closely related. Unexpected experimental results, the

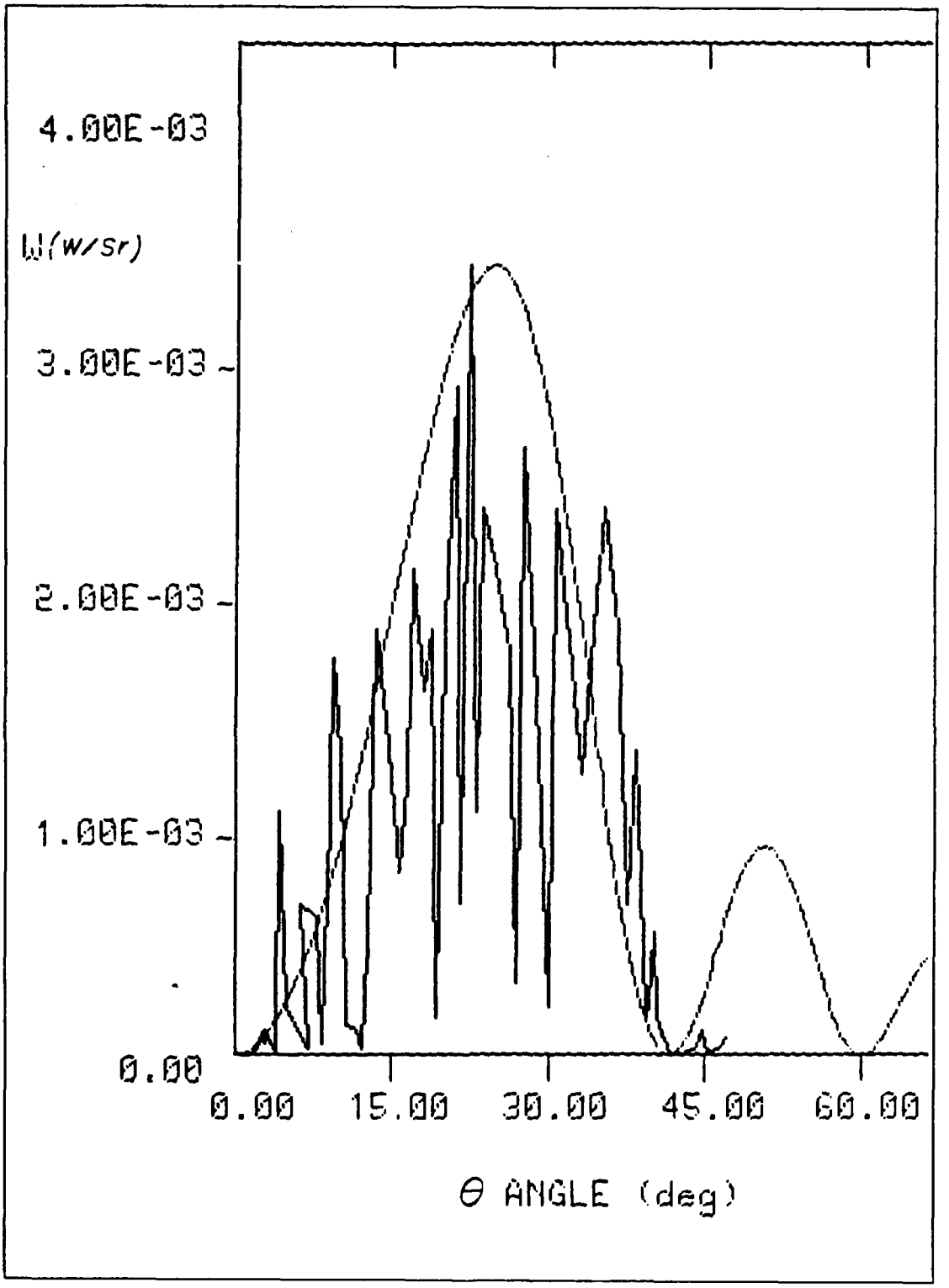

Figure 5.6 First Experiment : Data for the Third Harmonic.

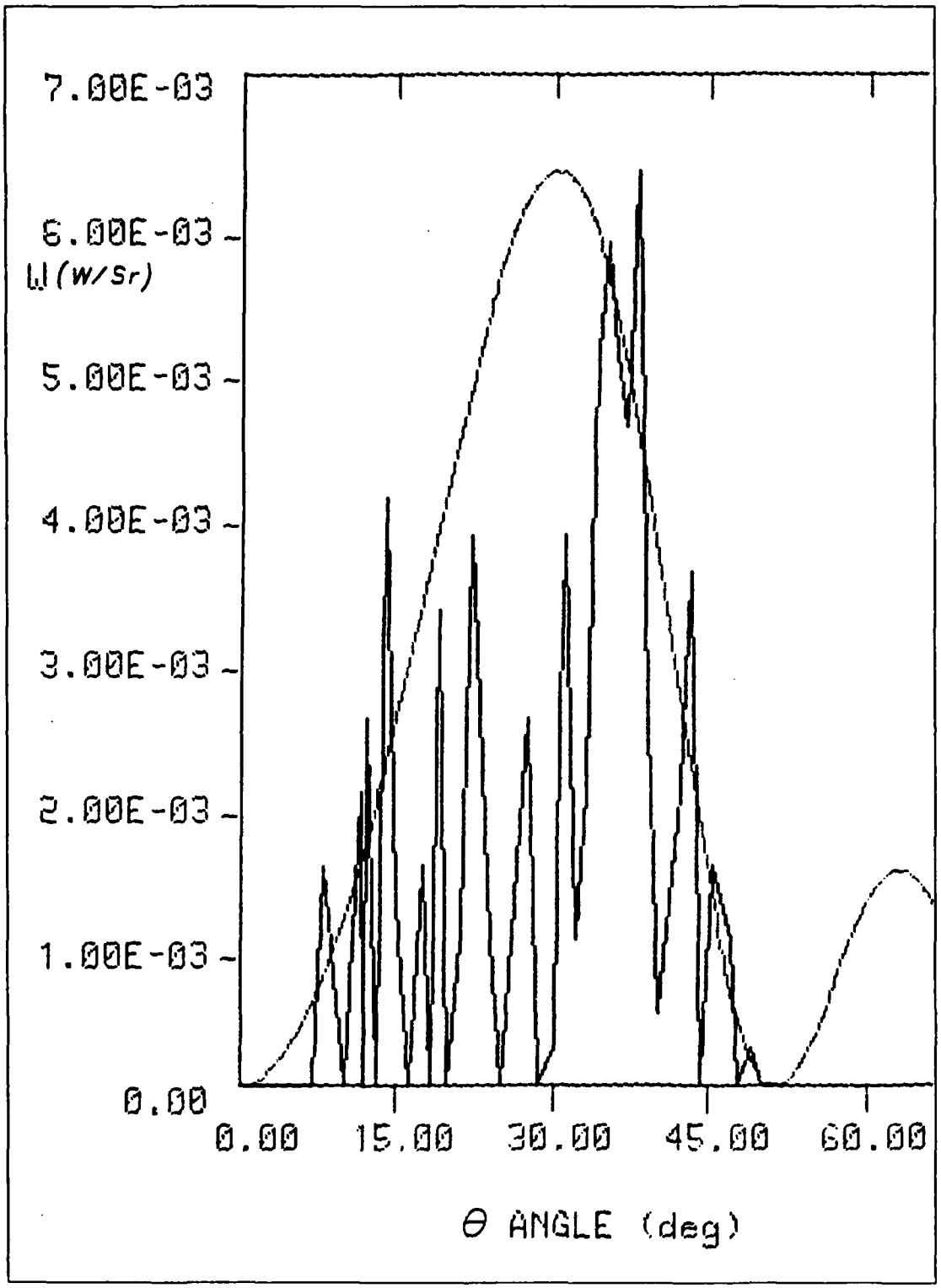

Figure 5.5 First Experiment : Data for the Second Harmonic.

The 'spiked' experimental data for the second harmonic are shown along with smooth theoretical curve in Figure 5.5 . The beam current was $Iav=33.33 \times 10^{-8}$ A .

The 'spiked' experimental data for the third harmonic are shown with the smooth theoretical curve in Figure 5.6 . The beam current was $Iav=20.0 \times 10^{-8}$ A .

Both sets of experimental data were normalized by equating the maximum experimental value with the theoretical maximum, and centered to fit the theoretical curve and match the first diffraction null. Corresponding angular shifts for all experimental curves are given in Table V . All data were taken for the angles at which maximum or minimum signal occured.

Power calculation for the maxima of the radiation diagrams was done as follows. The received maximum radiation power at the antenna is

$$P_m = W_m \Omega$$

where

$$\Omega = \frac{A_e}{R^2} \quad , \quad A_e = \frac{G\lambda_j^2}{4\pi} \quad , \quad A_e \doteq 0.7\,A \quad ,$$

(see [Ref. 11], for these relations). The maximum radiation intensity measured by the pyramidal antenna is

$$W_m = \frac{P_m 4\pi R^2}{G\lambda_j^2} \quad , \tag{5.1}$$

and by the horn antenna (0.7 is chosen arbitrarily)

$$W_m = \frac{P_m R^2}{0.7\,A} \tag{5.2}$$

The maximum detected voltage for the second harmonic Vm=250 μV reads P_o =-38 dBm in Figure 4.6 for 1 TWT. Adding 12 dB attenuator,[15] Pm=2.5 μW. The gain of pyramidal antenna is G=8 dB or G=6.31, the wavelength for j=2 is

---

[15]The unit conversion for power is given by definition Pm(dBm)=10log(Pm(W)/1mW), where Pm=P_o + attenuator dBm.

The other possibility of reflections was also confirmed. From Figure 4.1 it is obvious that the electron beam passing through the mirror will generate secondary Cerenkov radiation behind the mirror. Since this air path is much longer than the emission length, this Cerenkov signal is much stronger. It reflects from the walls and comes to the antenna. Having closed emission length by absorbers, secondary Cerenkov signal was measured perfectly well. For some angles it was greatly enhanced reflecting directly from the secondary emission monitor which was placed on the beam path behind the mirror.

A natural solution for the reflections was radiation shielding by the absorbers, which block the opposite side of Cerenkov cone and secondary Cerenkov radiation. Klystron door was closed by aluminum plates with the absorbers towards the experimental area, so that the klystron noise was shielded out too. With such preventions and closed emission length by absorbers, no signal was measured for antenna sweep through all angles.

4. First Data Set

Having done the noise reduction and radiation shielding as described above, the Cerenkov experiment was continued. A 'refined' Cerenkov pulse is shown in Figure 5.1 b) . The measurements were done for the experimental arrangement from Figure 4.1 . The experimental parameters[14] were those given in Table VII . The calibration curves from Figures 4.6 , and 4.7 were used to fit the Cerenkov signal into the linear amplification region.

[14]Due to some particular experimental interests, the values of the experimental parameters are modified. Important parameter values are specified with the data set.

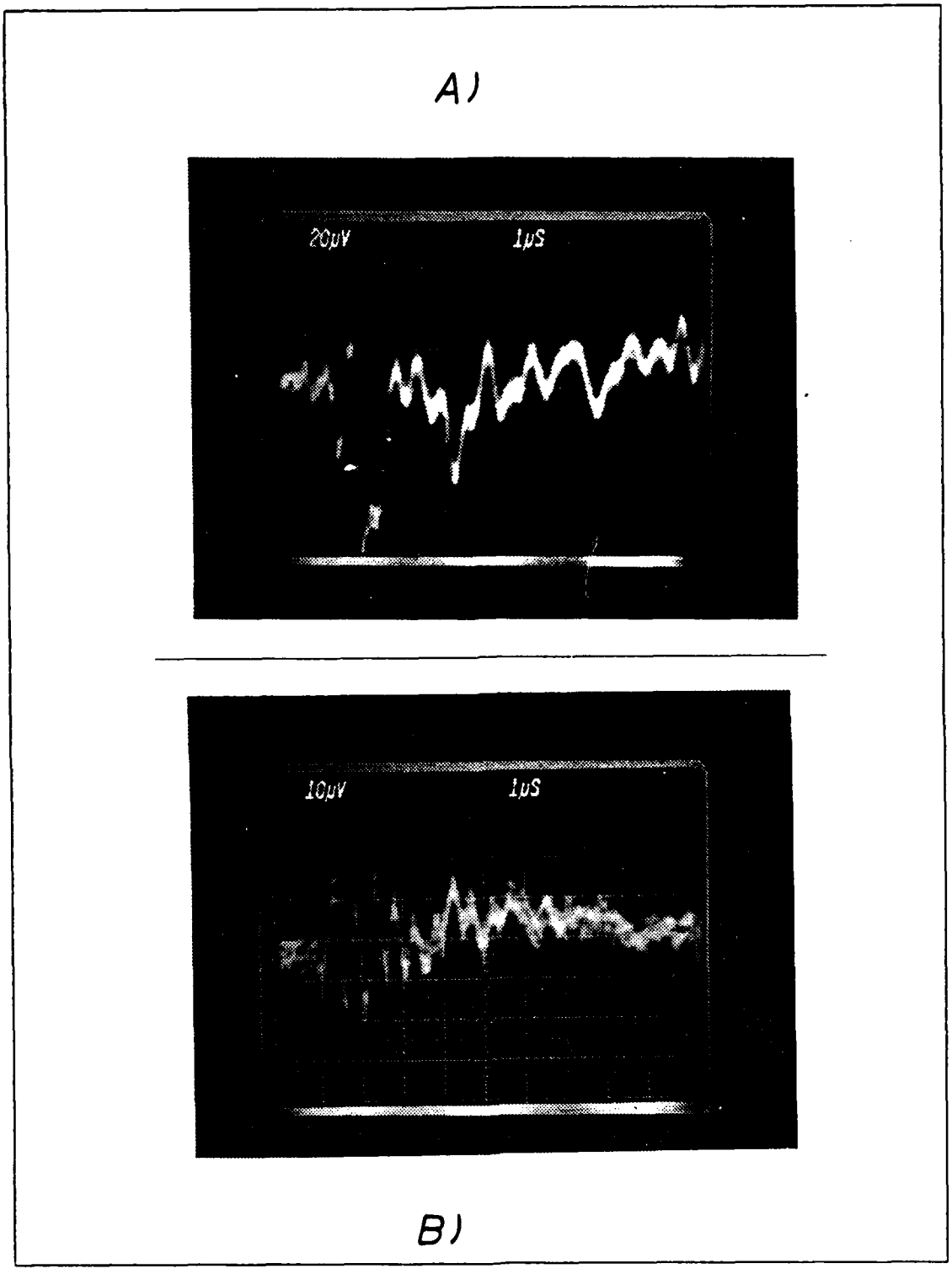

Figure 5.4 Control Room : a) Klystron Noise, b) Reduced Klystron Noise and Display Noise.

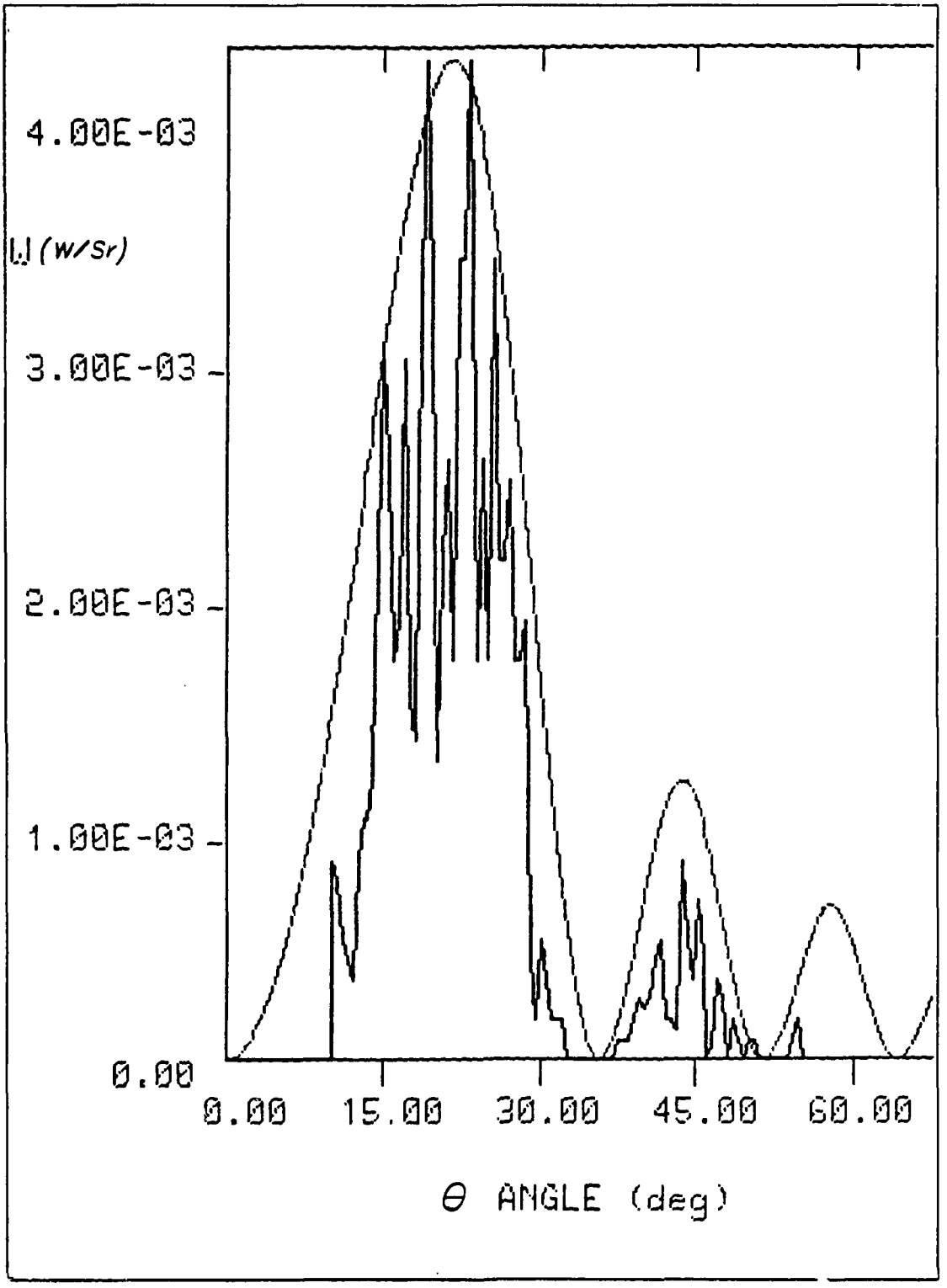

Figure 5.10 Second Experiment: Data for the Fourth Harmonic.

TABLE VI

Experimental Power Calculation

j	1	2	3	4
Vm (mV)	0.2	1.0	6.5	0.5
# of TWTs	2	1	2	2
P_o (-dBm)	32	36	39.5	37.5
Att. (dB)	0	4	8	8
Pm (-dBm)	32	32	31.5	29.5
Pm (μW)	0.6	0.6	0.7	1.1
Wm(mW/Sr) (exper.)	0.5	2.0	3.6	5.7
Wm(mW/Sr) (theory)	1.1	2.3	3.3	4.2
error (%)	54	13	9	36

harmonics with results from the first experiment show that the spikes differ although the harmonics are the same. This confirms the conclusion from the discussion in subsection A5 that this Cerenkov experiment is rather sensitive to slightly different experimental conditions. Recall that the second experiment had certain refinements in order to get more precise results. The beam current and slit opening differ, as well as general linac operating parameters. The medium, air also differed, since the second experiment was done during the cold autumn weather. However, reproduciblity test confirmed the same data in several successive measurements under the same circumstances.

Comparing the spikes in all four diagrams of the second experiment, it is again obvious that for higher harmonics (meaning smaller angular spreading) the spikes are less distanced, due to the fixed angular resolution. This effect forbids zero points in the main lobe of the fourth harmonic and allows zero's and wide spike spacing in the radiation diagram of the first harmonics. It is very

hard to deduce any general rule for the spikes which would lead to their accurate explanation. Generally, when the experimental data are centered below the theoretical curves and the first diffraction null is matched, the spikes follow the theoretical curves. If a sampling procedure was taken an average theoretical curve would follow the smooth theoretical curve. However, this requires more precise data. Also, a theoretical game with the form factor was done by the computer program, for different 'ρ_o''s, equation 2.26, such as

$$\rho_o'(z) = \begin{cases} A & -b \le z \le b \\ 0 & -b > z > b \end{cases}$$

and

$$\rho_o'(z) = \begin{cases} A + B\cos kz & -b \le z \le b \\ 0 & -b > z > b \end{cases}$$

where A and B were an arbitrary constants. This did not produce any spikes similar to the experimental ones.

The experimental diagrams reveal some undesired effects of the strip which reduce experimental accuracy. The little strip is not ideally flat, but slightly concave (recall the mirror may have been convex). Thus, the spikes are compressed below the theoretical curve, which is very obvious from Figure 5.10 . The second and third harmonics, Figures 5.8 , 5.9 reveal an unusual gap at about 35° which may be associated with a surface imperfectness (ridge) of the strip. All diagrams show rather big shift from the zero angle even much bigger than for in the first experiment for the mirror. There could be found many theoretical and practical reasons for the shift, but the most dominant one is uncertainty in zero setting by the strip. It is hard to achieve good alignment with the little strip. Having the experience with the mirror and the strip, and knowing Cerenkov polarization, see Figure 1.4 , the experimental

requirements would be perfectly satisfied with half rigid mirror. It reflects only one side of Cerenkov cone and surface imperfectness should be eliminated. Due to Cerenkov polarization, the detected slice of Cerenkov cone is determined by the antenna vertical dimension, not much by the narrow strip. On the other hand, a wide half mirror may be easily aligned for the zero of 'θ' angle.

Finally, power calculation for all harmonics as summarized in Table VI , shows improvement in the experimental precision, since relative errors for the second and third harmonics are less than in the first experiment. The experiment was successfully expanded to the first and fourth harmonics, but not to the fifth and sixth harmonics. Additional TWT amplifiers are required. In this way the experiment may be expanded to the much higher harmonics for which a certain interest exists. Expanded to the four harmonics, the power calculation and radiation diagram measurements confirmed again that the experimental method fits Cerenkov experiment. Additionally, the experiment rejected the strip as imprecise component of the equipment and suggested a half rigid mirror. Also, the role of the linac slit and Cerenkov signal shape were emphasized as two new topics available in this experiment. They may be related to the spikes for their better explanation.

C. THIRD EXPERIMENT

Direct experiment was another trial to explain the spikes which were found in the first experiment. This time the original geometry from Figure 4.3 was replaced by the geometry from Figure 4.4 . The signal from the antenna was processed as usually, see Figure 4.1 .

1. Third Data Set

The experimental setup for the direct measurement was realized with many practical problems. Electron beam confinement by a copper pipe confirmed the electron bouncing inside the pipe and the radiation of 100 mr appeared in a short time during the experiment. Aluminum wall and absorber were set properly in many trials, so that the antenna could not sense any signal for closed emission length. The problem was very long electron beam in air, which produced very strong Cerenkov radiation. This signal bounced among the walls and ceiling, so that the radiation shielding was hardly achieved. The secondary emission monitor was located far from the emission length with an angle of inclination to avoid reflection towards the flange, but the beam current could not be measured precisely.

The experimental data for the first four harmonics are given along with the theoretical curves in Figures 5.11 , 5.12 , 5.13 , 5.14 respectively. The experimental parameters are similar to those in Table VII . The data were taken at angles from Table IV in different ranges.

Power calculation is not done since the antenna was not pointed towards the center of the emission length and the electron beam current was not measured precisely.

2. Discussion

This experiment supplements the second experiment in the efforts to accept or reject the spikes. It eliminates the mirror (strip) and flange as a possible reason for reflections (spikes) . Comparing corresponding harmonics from the first and third experiments it looks as though the spikes are reduced, since the minima are not very low ! However, the data are imprecise at the ends of the measured range and precise only in the middle when the antenna points

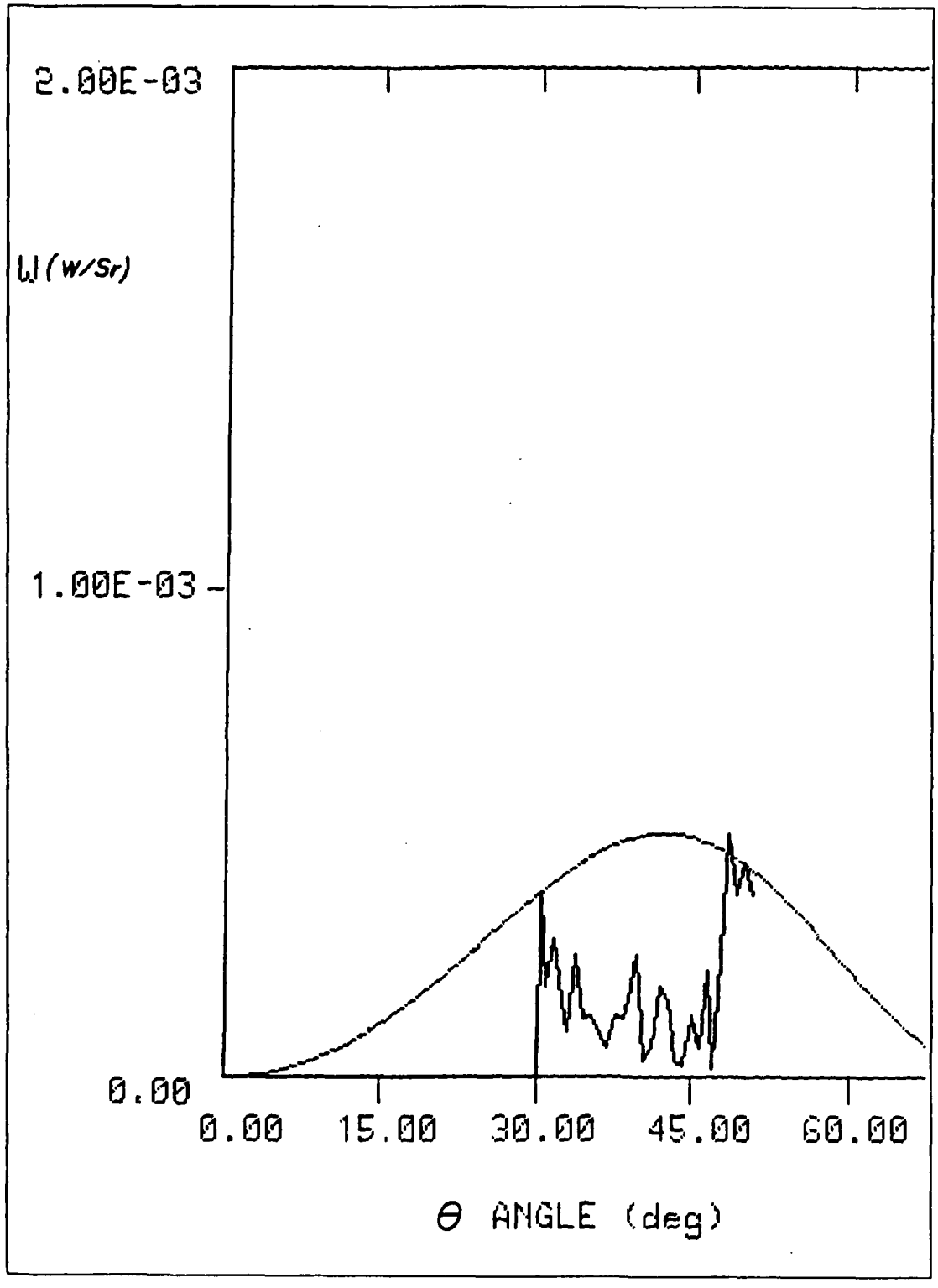

Figure 5.11 Third Experiment : Data for the First Harmonic.

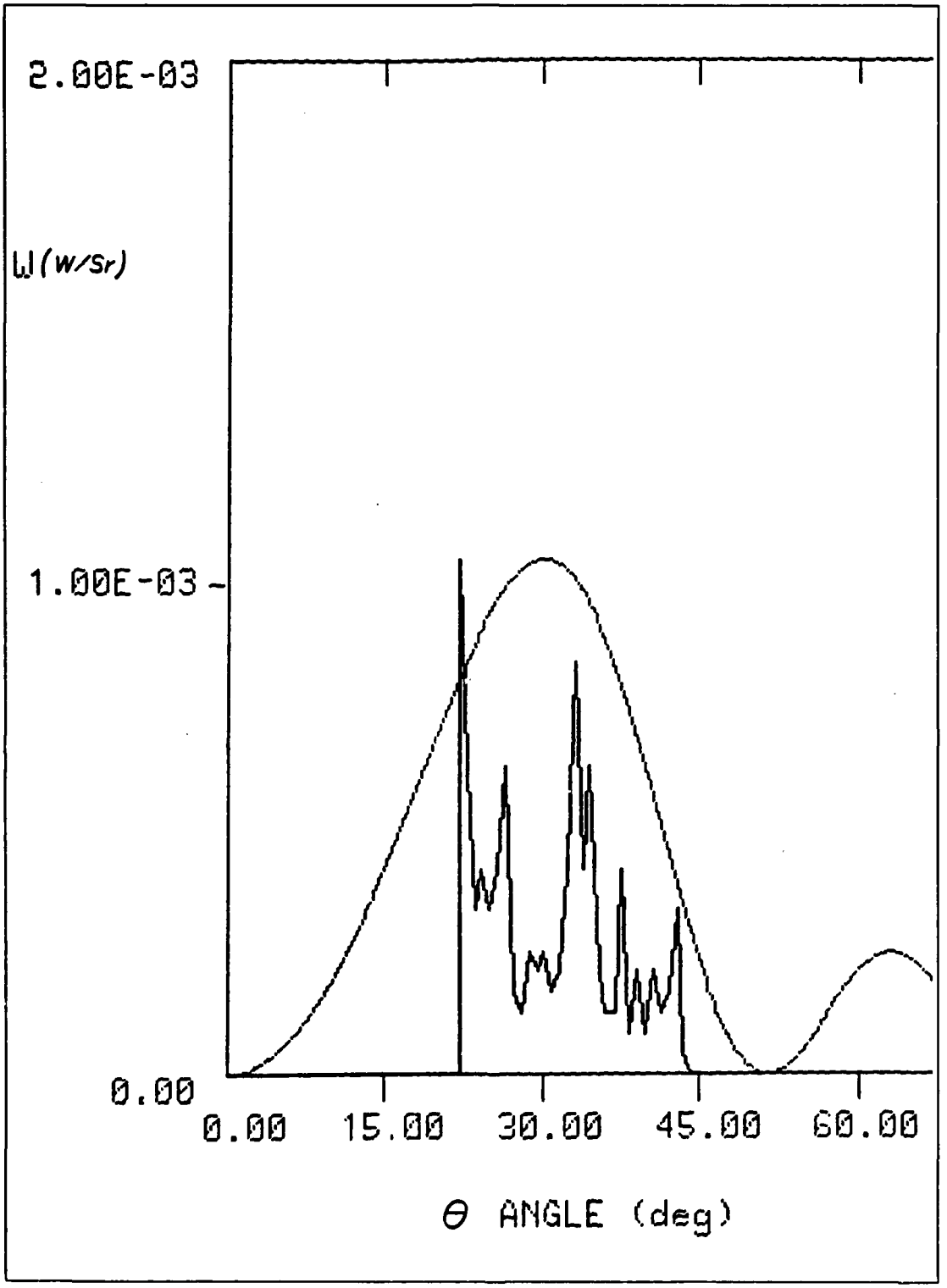

Figure 5.12 Third Experiment : Data for the Second Harmonic.

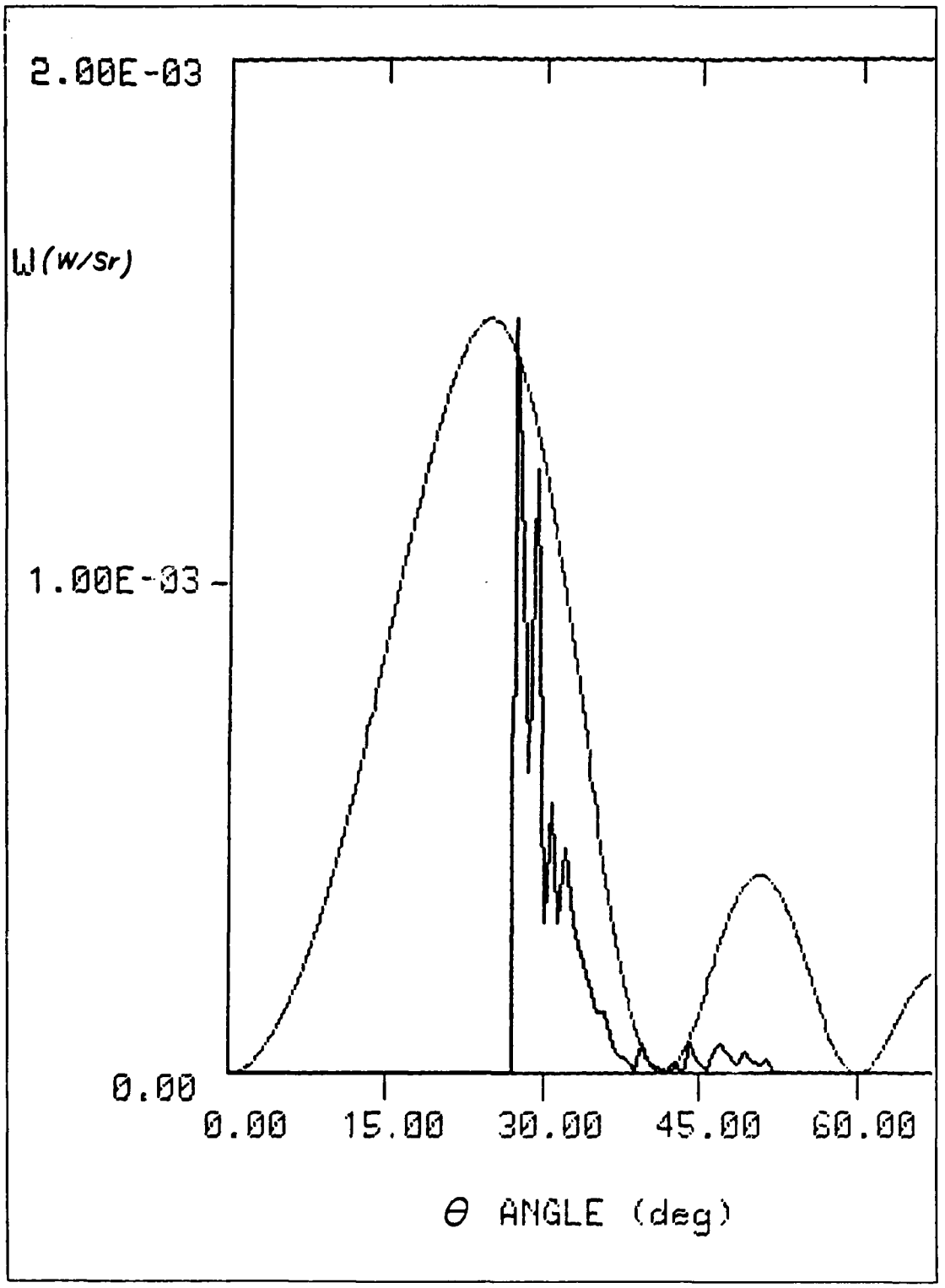

Figure 5.13 Third Experiment : Data for the Third Harmonic.

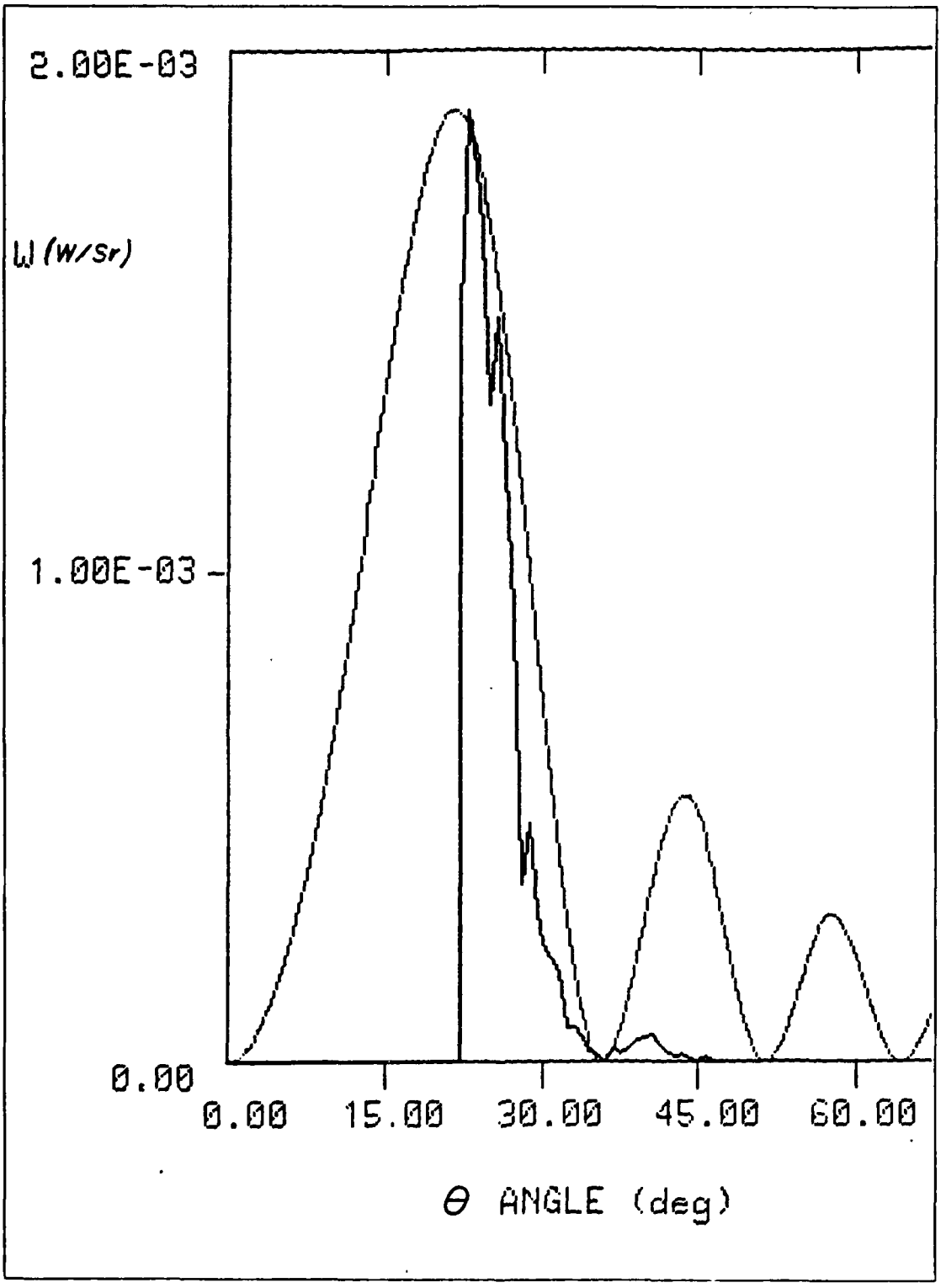

Figure 5.14 Third Experiment: Data for the Fourth Harmonic.

to the center of the emission length. Thus, the spikes are probably cut down by an amount, which is hard to estimate. Since the computer program does normalization with respect to the largest experimental value, and this is the value for the smaller angle which is cut down, the minima may grow up. This does not prove the spikes are real, but also does not disprove. Certainly this eliminates the mirror and the flange as a reason for the spikes. The mirror may only change configuration or shape of the spikes. It is obvious that any further measurement has to be done with a half rigid mirror as suggested in subsection B2.

Regardless of all that, the spikes still exist. For this experimental parameters the direct measurement eliminates possibility of a backwards Cerenkov radiation, which could interfere with reflected Cerenkov radiation from the mirror and cause the spikes. An interesting observation is that the third and fourth harmonics drop down faster than the first and second harmonics for larger angles. This is so, because the antenna used for the first two harmonics has much wider radiation diagram and the signal was cut down slower.

As usual, some additional effect appeared. The direct measurement provides very precise angular measurement. No angular shift was required to fit experimental data with the theoretical curves and match the first diffraction null, see Table V . This is a useful information for indirect measurements with mirror.

VI. CONCLUSIONS

The starting points in this research were the theoretical study of Cerenkov radiation produced in air by periodic electron bunches and comparison of theory with experiment. Previous experimental results and problems were discussed, as well as suggestions for improvements. It was decided to improve the experimental method for measurement of radiation diagrams and absolute power in the far radiation field. The latter were to verify predicted power increase and fall-off with discrete harmonic frequency in the microwave region, see Figure 2.5.

Far field measurements in the limited space available at the end of linac imply the very short emission length of 0.14 m and a correspondingly weak Cerenkov signal of the order of microwatts. The proper detection of the first four harmonics was rather delicate, but successfully achieved employing the YIG filter for frequency selection, the TWT amplifiers for power amplification and the oscilloscope vertical differential amplifier to achieve high sensitivity. These measures along with the noise reduction and radiation shielding proved adequate to detect the weak signals produced by the rather short emission length. The other consequence of the far field measurements with the short emission length is wide angular spreading of the radiation diagrams, such that the main diffraction lobes occured at more than 35°, see Figure 2.2. Having an angular resolution less than 0.5°, the measurements revealed unexpected spikes in the radiation diagrams, with the spike envelope following the smooth theoretical curves, see the figures with the experimental data in chapter V . A general characteristic of this Cerenkov experiment is extra sensitivity to any

change of the standard experimental parameters and theoretical assumptions, which had direct influence in the results.

Among many theoretical and practical reasons for the spikes, which were discussed and tested in chapter V , two of them were not tested properly. They both explain the spikes as an interference of the measured Cerenkov signal and some undesired reflections. If the klystron noise in the experimental area was not reduced sufficiently it could interfere with a weak Cerenkov signal, since both signals have the same time structure. Then, the interference would be the largest at the first harmonic and less and less as the harmonic number increases. This effect was observed in the second experiment and explained as a consequence of the high angular resolution. The appropriate test is the measurement in a 'deaf' chamber.[16] Similarly, if the measured Cerenkov signal reflects and interferes with itself, again the appropriate test is the 'deaf' chamber. However, summarizing all experiments it looks as though the spikes are rather realistic. They could be explained by the extra sensitivity of the experiment, particularly with respect to the beam current, Cerenkov pulse shape and general air conditions. It turns out that this influence could hardly enter the theory and exact mathematical description of the radiation. Special significance of the spikes is that their better understanding may provide the electron beam monitoring. They are also related to any application of Cerenkov radiation as a microwave source.

The absolute power measurements were controlled by the calibration curves, Figures 4.5 to 4.8. The experimental results in Table VI are of the same order as the theoretical ones. This confirms the approach of the far field measurements and the theoretical predictions from Figure 2.5 to

[16]The 'deaf' chamber is a housing of absorbers around the experimental area.

some extent, which is the aim. In a more precise measurement the results could be improved, for example in the 'deaf' chamber, and employing better TWT amplifiers and signal generators. Having the method for the power measurements (calculation) , the total power may be calculated summing (or integrating) the intensity curves. However, this does require more knowledge about the spikes. An accurate information of Cerenkov power is very useful for a possible Cerenkov microwave source, particularly at higher frequencies.

The experimental method used to determine the radiation diagrams and measure absolute power fits this microwave Cerenkov experiment with the linac and it may be expanded to higher harmonics with the appropriate equipment. For a further experiment it is recommended to build up a 'deaf' chamber and use a half rigid mirror. An investigation of the relationship of the linac slit, air conditions and the Cerenkov pulse shape to the spikes would be particularly interesting. In this experiment the oscilloscope offers very good information about the signal. A spectrum analyzer may be used, as well, but it requires corresponding waveguides some parts of which must be flexible, to lead the signal from the experimental area to the control room. In addition, digital data processing could be used to plot the experimental curves precisely. Such improvements would replace tedious and error prone point by point measurements, but this is expensive. The experimental data may be plotted by a plotter, which requires additional conversion of the detected voltage and synchronization with the antenna motor.

To conclude, this Cerenkov experiment is like an adventure, where people gain in experience and knowledge, achieving some useful goals.

APPENDIX A
VARIABLE DEFINITIONS

'$\vec{A}$' magnetic vector potential ;

'A' physical area of antenna ;

'Ae' effective area of antenna ;

'α' mirror offset angle ;

'a' radial size parameter of electron bunch ;

'b' longitudinal size parameter of electron bunch ;

'$\vec{B}$' magnetic induction vector ;

'β' relativity constant ($\beta = v/c_o$) ;

'c' phase speed of electromagnetic wave in a medium ;

'c_o' absolute speed of electromagnetic wave in vacuum ;

'd' antenna position along track ;

'$D_i(\theta)$' radiation function ;

'$\vec{D}$' electric displacement vector ;

'δ' Dirac δ-function ;

'$\vec{E}$' electric field vector ;

'ε' electric permittivity ;

'E_o' electron rest energy ;

'φ' spherical coordinate (azimuthal angle) ;

'$F(\vec{k})$' form factor of a single electron bunch in $\vec{k}$-domain ;

'Ψ' generalized potential function ;

AD-A156 156 CERENKOV RADIATION FROM PERIODIC ELECTRON BUNCHES FOR FINITE EMISSION LENGTH IN AIR(U) NAVAL POSTGRADUATE SCHOOL MONTEREY CA M VUJAKLIJA DEC 84 2/2

UNCLASSIFIED F/G 2/0.30 NL

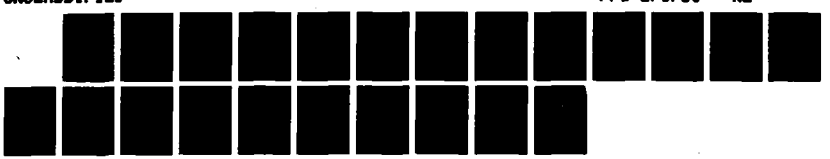

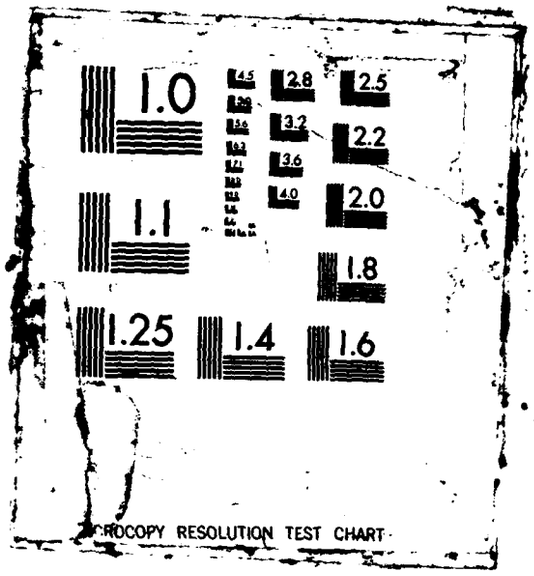
1.0
1.1
1.25
1.4
1.6
1.8
2.0
2.2
2.5
2.8
3.2
3.6
4.0
4.5
ROCOPY RESOLUTION TEST CHART

'$\vec{J}$' generalized source function ;

'Φ' electric scalar potential ;

'γ' relativity constant ($\gamma^2 = (1 - \beta^2)^{-1}$) ;

'G' antenna gain ;

'$\vec{H}$' magnetic field vector ;

'I(u)' diffraction function ;

'Iav' average beam current ;

'Ip' peak beam current ;

'j' harmonic number (j = 1, 2, 3 ...) ;

'$\vec{J}$' current density vector ;

'$\vec{k}$' propagation vector ;

'K' electron kinetic energy ;

'k_z' component of '$\vec{k}$' in z-direction ;

'L' emission length ;

'λ_0' wavelength of linac traveling wave; bunch spacing ;

'λ_j' wavelength of j-th harmonic ($\lambda_j = \lambda_0/j$) ;

'μ' magnetic permeability ;

'm_e' electron rest mass ;

'$\hat{n}$' unit vector in '$\vec{k}$'-direction ;

'n' refractive index ;

'Ne' number of electrons per bunch ;

'Nb' number of electron bunches per linac pulse ;

'ν_j' radiation frequency of j-th harmonic ($\nu_j = j\nu_0$) ;

'ν_o' linac operating frequency ;

'ω_j' angular radiation frequency of j-th harmonic ($\omega_j = j2\pi\nu_o$);

'Ω' solid angle substanded by antenna ;

'P' total radiated power for finite emission length ;

'P_ω' total radiation power for infinite emission length ;

'P_j' power radiated into main diffraction lobe ;

'P_o' reference power from signal generator ;

'Pm' maximum radiation power ;

'q' total charge of a single electron bunch ;

'R' radius of antenna rotation; raylength; bar length ;

'ρ' charge density ;

'$\vec{r}$' position vector of field point ;

'$\vec{r}$'' position vector of source point (retarded position) ;

'r_o' distance to the far field ($r_o = 2L^2/\lambda_j$) ;

'ρ_o' charge density of electron bunch train ;

'ρ_o'' charge density of a single bunch ;

'σ' electric conductivity ;

'$\vec{S}$' poynting vector (power density) ;

'S_o' slit opening ;

's' cross-section area of the electron beam ;

'θ' diffraction angle ;
spherical coordinate (elevation angle);

'θ_n' angular spreading of the main lobe in diffraction pattern (first null) ;

'T' period of linac traveling wave ;
period of electron bunches ;

'Tl' period of linac pulses ;

'Tp' width of linac pulse ;
width of Cerenkov pulse ;

'Tb' width of bunch pulse ;

't' time ;

't'' retarded time ;

'u' diffraction variable ;

'v' speed of a charged particle; electron bunch speed ;

'V' voltage of a detected signal measured by oscilloscope ;

'Vm' maximum detected signal by oscilloscope ;

'$W(\psi_i,n)$' time average of radiated power per unit solid angle at 'ψ_i' (radiation intensity) ;

'Wm' maximum radiation intensity ;

'z' direction of motion of electron bunches ;

APPENDIX B
EXPERIMENTAL PARAMETERS

1. Cerenkov Parameters

Having parameters :

linac frequency $\nu_0 = 2.8557$ GHz ,
electron kinetic energy $K = 100$ MeV ,
electron rest mass $m_0 = 9.11 \times 10^{-31}$ kg ,
refractive index of air $n = 1.000268$,
absolute speed of light $c_0 = 2.997925 \times 10^8$ m/s ,
emission length $L = 0.14$ m
it follows :

speed of Cerenkov wave in air

$$c = \frac{c_0}{n} = \frac{2.997925 \times 10^8}{1.000268} \doteq 2.997122 \times 10^8 \ \text{m/s} ,$$

electron rest energy

$$E_0 = m_0 c_0^2 = (9.11 \times 10^{-31})(2.997925 \times 10^8)^2 \doteq$$
$$\doteq 81.88 \times 10^{-15} \ \text{J} \doteq 0.511729 \ \text{MeV} ,$$

electron relativity constants

$$E = E_0 + K = \gamma E_0 \quad \Rightarrow \quad \gamma = \frac{E_0 + K}{E_0}$$

$$\gamma = \frac{(0.511729 \times 10^6 + 100 \times 10^6)}{0.511729 \times 10^6} = 196.415933 ,$$

$$\gamma^2 = (1 - \beta^2)^{-1} \quad \Rightarrow \quad \beta = (1 - \gamma^{-2})^{1/2}$$

$$\beta = \left[1 - (196.415933)^{-2} \right]^{1/2} = 0.999987 ,$$

electron speed

$$v = \beta c_o = (0.999987)(2.997925 \times 10^8) \doteq$$
$$\doteq 2.997886 \times 10^8 \quad m/s \ ,$$

Cerenkov angle (see equation 1.1)

$$\theta_c = \cos^{-1}\left[\frac{1}{\beta n}\right]$$

$$\theta_c = \cos^{-1}\left[\frac{1}{(0.999987)(1.000268)}\right] \doteq 1.29^\circ \ ,$$

harmonic wavelength, for the first harmonic (j = 1)

$$\lambda_j = \frac{c}{j\nu_o} = \frac{(2.997122 \times 10^8)}{(1)(2.8557 \times 10^9)} \doteq \frac{0.105}{1} = 0.105 \quad m \ ,$$

harmonic frequency, for the fifth harmonic (j = 5)

$$\nu_j = j\nu_o = (5)(2.8557 \times 10^9) = 14.2785 \quad GHz \ ,$$

far field 'r_o' for the sixth harmonic (j = 6)

$$r_o \doteq \frac{2L^2}{\lambda_j} = \frac{(2)(0.14^2)}{\left(\frac{0.105}{6}\right)} \doteq (0.3733)(6) = 2.24 \quad m \ ,$$

the first null 'θ_n' in diffraction pattern,
f. e. for $\lambda_3 = 0.035$ m requires u=π
(see equation 2.24 and Figure 2.2)

$$\frac{kL}{3}(\cos\theta_c - \cos\theta_n) = \pi \quad , \quad k = \frac{2\pi}{\lambda_3}$$

$$\Rightarrow \quad \theta_n = \cos^{-1}\left[\cos\theta_c - \frac{\lambda_3}{L}\right]$$

$$\theta_n = \cos^{-1}\left[\cos(1.29^\circ) - \frac{0.035}{0.14}\right] \doteq 41.4^\circ \ ;$$

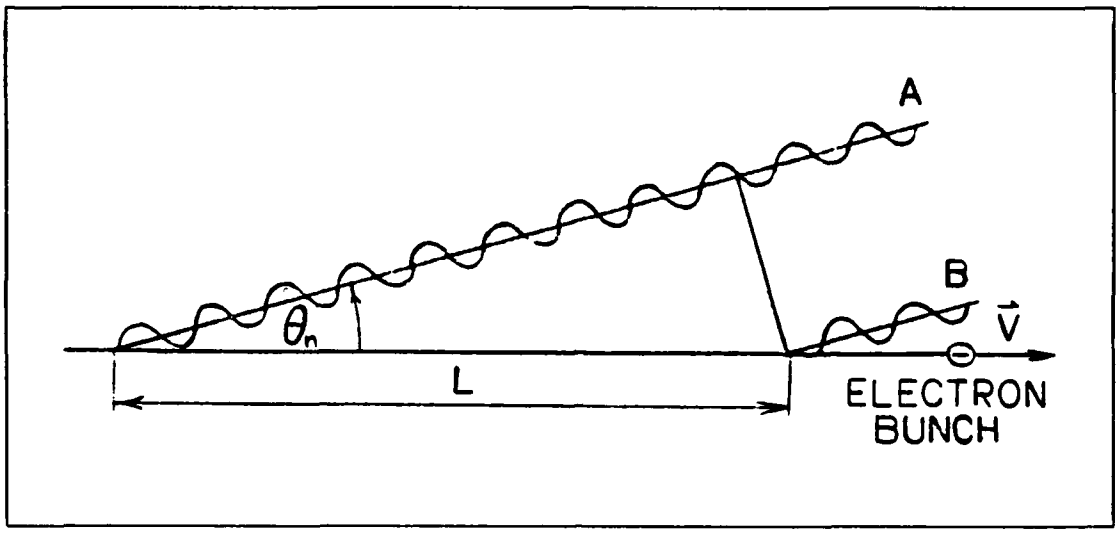

Figure B.1 The First Diffraction Null.

An interesting consideration for the first diffraction null may be done by using Figure B.1 . If A-wave is emitted at t = 0 , at the moment when B-wave is emitted, its phase is $\omega_j(L\cos\theta)/c$. However, B-wave is emitted at t = L/v with the phase $\omega_j L/v$. The phase difference between these waves is

$$\omega_j \frac{L}{v} - \omega_j \frac{L\cos\theta}{c} = \omega_j \frac{L}{c}\left(\frac{c}{v} - \cos\theta\right) .$$

Equating the difference to 2π and using $\omega_j = kc$, $\varepsilon = \frac{c_0}{n}$, $\beta = \frac{v}{c_0}$ with equations 1.1 and 2.24

$$\omega_j \frac{L}{c}\left(\frac{c}{v} - \cos\theta\right) = 2\pi$$

$$\frac{kL}{2}\left(\cos\theta_c - \cos\theta\right) = \pi$$

$$u = \pi \quad ; \quad \theta = \theta_n$$

This is the requirements used above for the first diffraction null ! Thus, Huygens waves radiated from the front and rear of the emission length 'L' differ by 2π , for the first null in the diffraction pattern.

2. Electron Beam

Principles of linac operation are explained in subsection B1 chapter 4 . Electron bunches correspond to the crests of linac traveling wave, propagating through the wave guide with a low pressure. Knowing linac operating frequency ν_0=2.8557 GHz

bunch spacing or wavelength of linac traveling wave is

$$\lambda_0 = \frac{c_0}{\nu_0} = \frac{2.997925 \times 10^8}{2.8557 \times 10^9} \doteq 0.105 \quad m \ .$$

In [Ref. 4], it was estimated that an electron bunch covers 4.5 % of linac cycle, so

bunch length

$$2b = \lambda_0 (4.5\%) = (0.105)(0.045) \doteq 4.7 \quad mm \ .$$

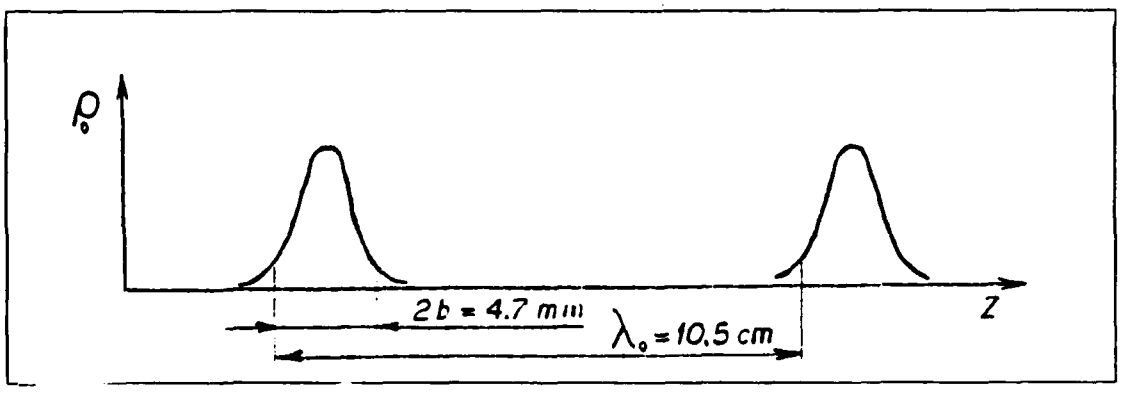

Figure B.2 Gaussian Charge Distribution of the Bunches.

Using these numbers and theoretical assumption that a single bunch charge density is Gaussian (see equation 2.27), charge density of electron bunch train is depicted in Figure B.2 for a fixed time. Within Tp=1μs of linac pulse such

electron bunches fly through air causing Cerenkov radiation. They repeat themselves in T1 = 16.6 ms , which is the period of linac repetition frequency. Flying electrons represent current (by definition, charge per time). This current is

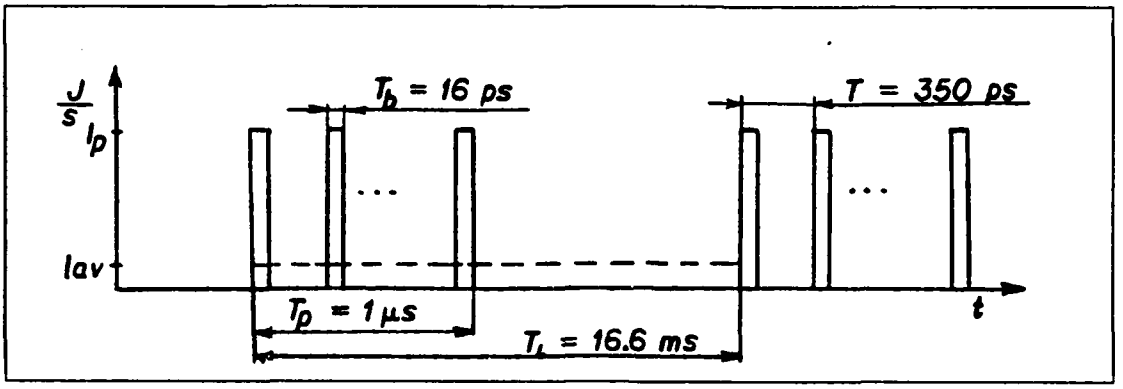

Figure B.3 Electron Beam Current.

shown in Figure B.3 for a fixed point on electron beam line. Values Tb = 16 ps and T = 350 ps are 'flying times' obtained dividing '2b' and 'λ_0' by 'c' respectively . In order to make connection with equation 2.15 the current is expressed by the current density 'J' and constant 's' , the beam cross-section. Figures B.2 and B.3 illustrate z-periodicity and t-periodicity, which are discussed in the section A chapter 2 . The current density as function of discrete harmonic frequencies is shown in B.4 . All together is expressed in the more complicated mathematical description of the beam, equation 2.15.

. The electron beam current is assumed to be constant for the calculation in chapter 2 with negligible radial parameter 'a' (or cross-section 's') , which is reasonable for a short emission length. In reality, 's' is not constant, because the beam disperses after focusing at linac exit window and linac electron production varies in time.

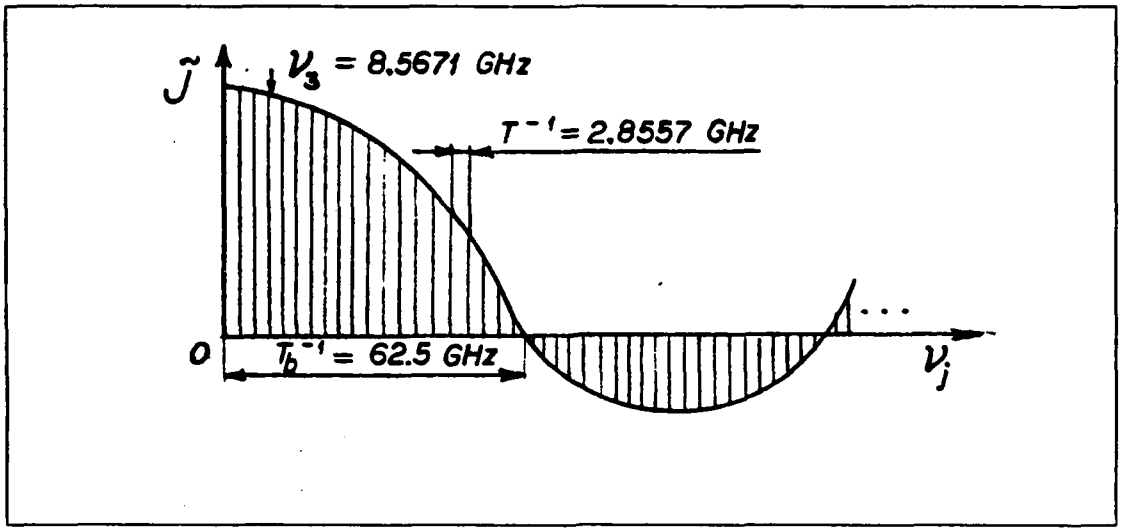

Figure B.4 Frequency Components of the Current Density.

From the Figure B.3 it is obvious that Cerenkov effect is significant within Tp = 1μs of linac pulse, when beam current is present. Thus, an actual measurement shows detected Cerenkov pulse on oscilloscope, which is 1 μs wide (see Figure 5.1 b)). This is the reason that the power is averaged over T = 350 ps in section B chapter 2 . Further calculation, using Figure B.3 implies

number of bunches per linac pulse

$$N_b = \frac{T_p}{T} = \frac{1 \times 10^{-6}}{350 \times 10^{-12}} \approx 2857 \ ,$$

if measured average beam current 1.2×10^{-8} A with the efficiency 6% of the secondary emission monitor,

average beam current

$$I_{av} = \frac{1.2 \times 10^{-8}}{0.06} = 20 \times 10^{-8} \ A \ ,$$

peak beam current

$$I_{av}\, T_l = I_p\, T_b\, N_b$$

$$I_p = \frac{(20 \times 10^{-8})(16.6 \times 10^{-3})}{(2857)(16 \times 10^{-12})} = 72.6 \text{ mA} .$$

total charge per bunch

$$q = I_p T_b = (72.6 \times 10^{-3})(16 \times 10^{-12}) = 1.16 \times 10^{-12} \text{ C} ,$$

number of electrons per bunch

$$N_e = \frac{q}{e} = \frac{1.16 \times 10^{-12}}{1.6 \times 10^{-19}} \doteq 10^7 .$$

TABLE VII

Experimental Parameters

electron kinetic energy	$K = 100$ MeV
electron rest mass	$m_e = 9.11 \times 10^{-31}$ kg
electron rest energy	$E_e = 0.511729$ MeV
linac operating frequency	$\nu_o = 2.8557$ GHz
electron bunch length	$2b = 4.7$ mm
electron bunch spacing and period of linac traveling wave	$\lambda_o \doteq 0.105$ m
harmonic frequency	$\nu_j = j(2.8557)$ GHz
harmonic wavelength	$\lambda_j \doteq 0.105/j$ m
period of electron bunches and linac traveling wave	$T = 350$ ps
period of linac pulses	$T1 = 16.6$ ms
width of bunch pulse	$Tb = 16$ ps
width of linac pulse	$Tp = 1 \mu s$
number of electrons per bunch	$Ne \doteq 10^7$
number of bunches per linac pulse	$Nb = 2857$
total charge per bunch	$q = 1.16 \times 10^{-12}$ C
electron charge	$e = 1.6 \times 10^{-19}$ C
average beam current	$Iav = 20.0 \times 10^{-8}$ A
peak beam current	$Ip = 72.6$ mA
refractive index of air	$n = 1.000268$
magnetic permeability of air	$\mu_o = 1.256643 \times 10^{-6}$ H/m
absolute speed of light in vacuum	$c_o = 2.997925 \times 10^8$ m/s
speed of electromagnetic wave in air	$c \doteq 2.997122 \times 10^8$ m/s

TABLE VII

Experimental Parameters (cont'd.)

electron speed	$v \doteq 2.997886 \times 10^8$ m/s
slit opening	$S_o = 225$
relativity parameters:	$\gamma = 196.415933$
	$\beta = 0.999987$
Cerenkov angle	$\theta_c \doteq 1.29°$
emission length	$L = 0.14$ m
far field distance	$r_o = j(0.3733')$ m
mirror offset angle	$\alpha = 20°$
radius of antenna rotation	$R = 2.1$ m

APPENDIX C
EQUIPMENT CHARACTERISTICS

The equipment was checked out from the EE department and partially from the linac lab at NPS.

1. CABLES :

RF CABLES

JEFFERSON, RG-9B/U 07883

length	1.7 m
measured attenuation	3.5 dB at 5.7 GHz
impedance	50 Ω
coaxial N connector	

DEARBORN, RG-8A/U 6008A

length	0.35 m
measured attenuation	0.5 dB at 5.7 GHz
impedance	50 Ω
coaxial N connector	

LF CABLE

DOUBLE SHIELDED COAX., RG-58/U

length	25 m
impedance	53.5 Ω
capacitance	95 pF/m
BNC connector	

2. SIGNAL GENERATORS :

SHF SIGNAL GENERATOR, H/P 618C

frequency range	3.8 to 7.6 GHz

peak output power into 50Ω	0 to -127 dBm
	(224 to 0.0001 mV)
internal pulse modulation	
repetition rate	40 to 4000 Hz
pulse width	0.5 to 10 μs
synchronization pulse voltage	25 V
frequency accuracy	±1%
power accuracy	± 2 dBm

SHF SIGNAL GENERATOR, H/P 620A

frequency range	7 to 11 GHz
the other characteristics	
are like for h/p 618C above	

3. ANTENNAS :

HORN ANTENNA, DICO 10-849

frequency range	8 to 12.4 GHz
gain	16.5 dB at 9.5 GHz
-3 dB bandwidth	27°, 30°
aperture area	0.03 by 0.04 m^2

PYRAMIDAL ANTENNA, AEL APN 101B

frequency range	1 to 12.4 GHz
gain	8 dB
-3 dB bandwidth	60°, 60°

HORN ANTENNA, made according to AEL H 1458

frequency range	12 to 18 GHz
gain	14.5 to 18 dB
-3 dB bandwidth	32°, 22°
aperture area	0.054 by 0.041 m^2

4. DETECTORS :

COAXIAL CRYSTAL DETECTOR, H/P 420A

frequency range	0.01 to 12.4 GHz
low level sensitivity	> 0.15 mV/μW
max. input peak power	100 mW
N and BNC connectors	

WAVEGUIDE CRYSTAL DETECTOR, H/P X424A

frequency range	8.2 to 12.4 GHz
sensitivity for	
low (high) signal	0.4 (0.286) mV/μW
max. input peak power	100 mW
BNC connector, waveguide flange	

WAVEGUIDE CRYSTAL DETECTOR, H/P P421A

frequency range	12.4 to 18 GHz
no other data available	

5. AMPLIFIERS :

TWT AMPLIFIER, WJ-269

frequency range	2 to 4 GHz
gain	25 dB , min.
noise figure	5.5 dB , max.
power output, saturated	-10 dBm , min.

TWT AMPLIFIER, WJ-271

frequency range	4 to 8 GHz
gain	25 dB , min.
noise figure	6.5 dB , max.
power output, saturated	-5 dBm , min.

TWT AMPLIFIER, WJ-276-2

frequency range	7 to 11 GHz
gain	25 dB , min.
noise figure	8.5 dB , max.
power output, saturated	-5 dBm , min.

TWT AMPLIFIER, WJ-408

frequency range	8 to 12 GHz

no other data available

6. ADAPTERS :

ADAPTER WAVEGUIDE-COAXIAL, H/P P281B

frequency range	12 to 18 GHz

ADAPTER WAVEGUIDE-COAXIAL, H/P X281A

frequency range	8 to 12 GHz

7. ATTENUATOR :

ATTENUATOR, Aircraft Radio Co. Inc.

attenuation steps in dB	10, 20, 30, 40, 50
attenuation steps in dB	2, 4, 6, 8, 10
impedance	50 Ω

8. FILTER :

YIG FILTER, IM TMF-1800

tunable over frequency range	1 to 18 GHz
-3 dB bandwidth	15 to 70 GHz
selectivity	18 dB/octave
resonance isolation	70 to 80 dB
insertion loss	8 dB
limiting level (min.)	10 dBm
max. input power	30 dBm
connectors	SMA jack

YIG CONTROL UNIT

frequency accuracy	0.1% + 10 MHz
frequency resetability	10 MHz
operating modes	CW, SWEEP, EXT.
driving voltage in EXT. mode	0 to 10 V , external

9. OSCILLOSCOPE :

MAIN FRAME, TETRONIX 7904A

HORIZONTAL DEFLECTION SYSTEM, TETRONIX 7B85

horizontal deflection factor range	10 ns to 5 s
ext. trigger in	Vpk > 500 V , 1 MΩ

VERTICAL DEFLECTION SYSTEM, TETRONIX 7A22

vertical deflection factor range	10 μV to 10 V
bandwidth (HF -3 dB points)	100 Hz to 1 MHz
displayed noise	16 μV (or 0.1 div.)
input resistance (capacitance)	1 MΩ (47 pF)

10. POWER SUPPLY :

POWER SUPPLY, H/P 721A

metrer range	VDC 10, 30
	MA 300, 100, 30, 10

11. MOTOR :

AC MOTOR, HURST Mfg Corp. Princeton Ind. DA
(used for the bar)

supply	115 V , 60 Hz
speed	1 rpm

AC MOTOR, BODINE El. Co. NSH - 12 R
(used for the track)

supply	115 V , 60 Hz
speed	96 rpm

12. CURRENT METER :

SECONDARY EMISSION MONITOR, made in house

POWER supply, Varian associates 021-0006

13. ABSORBER :[17]

TABLE VIII

Absorber Efficiency

absorber thickness : 0.075 m

freq.(GHz)	V(mv) no abs.	V(mV) with abs.
7	10	0.07
"	5	0.03
"	2	0.00
"	1	0.00
8.56	10	0.03
"	5	0.01
"	2	0.00
"	1	0.00
11	10	0.00
"	1	0.00

[17]See section B 10 chapter 4 for absorber testing procedure. Obtained data for 'V' in Table VIII do not correspond to 'P' in Figures 4.7, 4.8 due to different attenuations.

14. LINAC :

TABLE IX

Linac Parameters

length	9.14 m
number of klystrons	3
peak output power per klystron	21 MW
operating frequency	2.8557 GHz
pulse repetition frequency	60 Hz
pulse width (Cerenkov pulse width)	1 μs
electron kinetic energy	100 MeV

TABLE X

MW Frequency Bands

band	freq. (GHz)
L	1 to 2
S	2 " 4
C	4 " 8
X	8 " 12
Ku	12 " 18
K	18 " 27
Ka	27 " 40

LIST OF REFERENCES

1. Jelley J. V., Cerenkov Radiation and its Applications, Pergam Press, 1958.

2. Panofsky W. K. H. and Phillips H., Classical Electricity and Magnetism, Addison-Weslay Publishing Company, 1962.

3. David, E. M., Cerenkov Radiation Produced by 100 MeV Electrons, M.S. Thesis, Naval Postgraduate School, Monterey, California, June 1981.

4. Leslie, J. B., Stimulated Cerenkov Radiation Produced by 100 MeV Electrons, M.S. Thesis, Naval Postgraduate School, Monterey, California, December 1981.

5. Buskirk R. F. and Neighbours R. J., "Cerenkov Radiation from Periodic Electron Bunches," Physical Review A, Volume 28, Number 3, page 1531, September 1983.

6. Naval Postgraduate School Report 61-83-010, Diffraction Effects in Cerenkov Radiation, by R. J. Neighbours and R. F. Buskirk, June 1983.

7. Buskirk R. F. Neighbours R. J. and Saglam A., "Cerenkov Radiation from a Finite Length Path in a Gas", Physical Review A, Volume 29, Number 6, page 246, June 1984.

8. Vujaklija, M., Lecture Notes, Cerenkov Radiation Course, Naval Postgraduate School, Monterey, California, Spring 1984.

9. Ahmet, S., Cerenkov Radiation, M.S. Thesis, Naval Postgraduate School, Monterey, California, December 1982.

10. Newton, A. L., Cerenkov Radiation Generated by Periodic Electron Bunches in a Finite Air Path, M.S. Thesis, Naval Postgraduate School, Monterey, California, December 1983.

11. Skolnik M. I., Introduction to Radar Systems, McGraw-Hill Book Company, 1980.

12. Chodorow, M. , et al., "Stanford High Energy Linear Electron Accelerator (Mark 3)," The Review of Scientific Instruments, Volume 26, Number 2, page 134, February 1955.

INITIAL DISTRIBUTION LIST

No.		Copies
1.	Professor F. R. Buskirk, Code 61Bs Department of Physics, Naval Postgraduate School, Monterey, California 93943	2
2.	Professor J. R. Neighbours, Code 61Nb Department of Physics, Naval Postgraduate School, Monterey, California 93943	5
3.	Professor X. K. Maruyama, Code 61Xa Department of Physics, Naval Postgraduate School, Monterey, California 93943	5
4.	Physics Library, Code 61 Department of Physics, Naval Postgraduate School, Monterey, California 93943	2
5.	Defense Technical Information Center, Cameron Station, Alexandria, Virginia 22314	2
6.	Superintendent, Attn: Library, Code 0142, Naval Postgraduate School, Monterey, California 93943	2
7.	Nacelnik, Attn: Biblioteka, Mornaricka Vojna Akademija, 58000 Split, Yugoslavia	2
8.	Lieutenant Milorad Vujaklija, Vojvodjanskih Brigada 74, 26300 Vrsac, Yugoslavia	5

END

5-87

DTIC